
Electronic Thesis and Dissertation Repository

9-16-2019 3:00 PM

Catalytic Conversion of 1,3,5 TIPB Over Y-Zeolite based Catalysts Catalyst/oil ratio(C/O) Effect and a Kinetic Model

Abdualkaber A. Alkhlel
The University of Western Ontario

Supervisor
de Lasa Hugo
The University of Western Ontario

Graduate Program in Chemical and Biochemical Engineering
A thesis submitted in partial fulfillment of the requirements for the degree in Doctor of
Philosophy
© Abdualkaber A. Alkhlel 2019

Follow this and additional works at: <https://ir.lib.uwo.ca/etd>

 Part of the [Engineering Commons](#)

Recommended Citation

Alkhlel, Abdualkaber A., "Catalytic Conversion of 1,3,5 TIPB Over Y-Zeolite based Catalysts Catalyst/oil ratio(C/O) Effect and a Kinetic Model" (2019). *Electronic Thesis and Dissertation Repository*. 6565.
<https://ir.lib.uwo.ca/etd/6565>

This Dissertation/Thesis is brought to you for free and open access by Scholarship@Western. It has been accepted for inclusion in Electronic Thesis and Dissertation Repository by an authorized administrator of Scholarship@Western. For more information, please contact wlsadmin@uwo.ca.

Abstract

A typical FCC unit involves the transport and rapid catalytic reaction of chemical species using 60-70 micron fluidizable catalyst particles. In FCC, hydrocarbon species evolve in the gas-phase are adsorbed on, and then react with the catalyst particles. In this case, large molecular weight hydrocarbons (vacuum gas oil) are converted into lighter products (gasoline). FCC also yields undesirable products such as light gases and coke. Coke promotes catalyst activity decay and as result, is detrimental to catalyst performance. Given the significance of coke as a catalyst decay agent in FCC, it is the objective of this PhD research to study catalyst deactivation by coke.

To accomplish this, three different Y-zeolite FCC catalysts, designated as CAT-A, CAT-B and CAT-C were employed in the present PhD study. Catalyst samples studied were characterized in terms of Crystallinity, Total Acidity, Specific Surface Area (SSA), Temperature Programmed Ammonia Desorption (NH₃-TPD) and Pyridine Chemisorption.

Catalytic cracking runs were carried out in a CREC Riser Simulator using a model hydrocarbon species (1,3,5-TIPB) as a hydrocarbon feedstock. This bench-scale mini-fluidized batch unit mimics the operating conditions of large-scale FCC units. Temperatures within the 510°C-550°C range and times ranging from 3s-7s were selected for catalyst evaluation. For every experiment, 0.2g of 1,3,5-TIPB was contacted with a catalyst amount ranging from 0.12g to 1g. This was done to achieve a C/O ratio in the range of 0.6 to 5.

Results obtained showed a consistent 1,3,5-TIPB conversion pattern for the three catalysts studied: increasing first, stabilizing later, and finally decreasing modestly. In spite of this, coke formation and undesirable benzene selectivity always rose. On this basis, a mechanism involving both single catalyst sites for cracking and two sites for coke formation was considered. In this respect, coke formation was postulated as an additive process involving coke precursor species, which are either adsorbed on two sites located in the same catalyst particle or adsorbed in two close sites in different catalyst particles.

Keywords

catalyst deactivation; FCC; coke formation; catalyst/feedstock (C/O) ratio; CREC Riser Simulator; 1,3,5-TIPB; kinetic modelling.

Summary for Lay Audience

Fluidized Catalytic Cracking (FCC) involves a rapid catalytic reaction and the transport of chemical species between two phases: a) hydrocarbons as gas phase species and b) particles as a discrete solid phase. During this process, heavy molecules (gas oil) are converted into a lighter product (gasoline). However, this approach is accompanied with the undesirable formation of C_1 - C_5 light gases and coke on the catalyst surface. Coke leads to catalyst decay and as result, is detrimental to catalyst performance. Given the significance of coke as a catalyst decay agent, the present PhD program is devoted to establishing a catalyst decay model suitable for the simulation of FCC in large scale riser and downer units.

To accomplish this, the present study pays special attention to various FCC operational parameters affecting coke formation and catalyst decay. To address these issues, runs were developed in a CREC fluidized Riser Simulator by varying: a) weight of the catalyst: 0.12g to 1g, b) Catalyst/ Oil ration (C/O ratio): 0.68 to 5, c) temperature: 510-550°C, d) contact time: 3 s to 7 s. The selected catalyst was an *ECat* FCC catalyst samples and the feedstock used was 1,3,5 tri-iso-propyl-benzene (1,3,5 TIPB).

Experiments findings in conjunction with advanced surface science techniques, allowed one to illustrate the influence of increasing the C/O ratio on 1,3,5-TIPB conversion, coke formation, and product selectivity. It was observed that a proper description of coke formation (e.g. Coke selectivity) and catalyst activity decay is required for an effective counting of Catalytic cracking with an ample range of C/O ratios (0.6–5 g-oil/g-cat).

Thus, it is anticipated that the postulated catalytic cracking reaction network influenced by catalyst density, affects both catalyst coking and deactivation, leads to an optimum C/O ratio, to accomplish maximum feedstock conversion, controlled coke-on-catalyst and gasoline benzene content. This is equivalent to a careful selection of both catalyst mass flow and hydrocarbon mass flow in large-scale risers or downers.

Dedication

This dissertation is dedicated to:

My father

For all the trust and encouragement, he has given me for which I'm forever
indebted

My mother,

Whose sincere prayers, sacrifice, and support made this dissertation possible.

My lovely wife,

Whose love, endurance, inspiration, and sacrifices made this dissertation
possible.

and

My darling kids

Whose love, inspiration made this dissertation possible.

Acknowledgments

In the name of All Mighty Allah, the Most Beneficent, the Most Merciful.

First and foremost, praise and gratitude are due to the Almighty, Allah, who has blessed me and gave me the opportunity, strength, courage and patience to finish my PhD study.

At first, I would like to express my endless gratitude to my advisor Dr. Hugo de Lasa, who provides me this unique opportunity to join his group and work on such an interesting and a challenging project at CREC center at UWO. His knowledge, encouragement, technical discussion, and hardworking highly motivated me to enrich my research journey.

My thanks go to all of my colleagues and friends at CREC. It has been a great pleasure to work with them. My sincere gratitude goes to Jose Muñoz and Pastor Solano from CREC, for their valuable technical support and giving me a helping hand always when needed. A very special thanks goes out to Imtiaz Ahmad and Sandra Lopes for their help in the Kinetic Modeling. I would also like to thank the CREC-Reaction Editor, Florencia de Lasa for her assistance in the editing of this manuscript.

During challenging days. profound gratitude goes to my parents, brothers, sisters and uncles especially uncle Ahmad, who has been a key part in this journey. Lastly, and most importantly, profound wishing goes to my lovely wife, not a single word can fully describe her whole support and love; my daughters (Balqes and Oswa), my sons (Asaedi, Anas, Sohail) just for being the reason and the love. To them, I would like to dedicate this thesis. May God bless them all.

Abdualkaber Alkhlel

August 2019

Contents

Abstract.....	i
Summary for Lay Audience	iii
Dedication.....	iv
Acknowledgments	v
List of Tables.....	x
List of Figures.....	xi
Chapter 1	1
1 Introduction.....	1
1.1 Problem Description and Motivation for this Research	1
1.2 Research Objectives	3
1.2.1 General Objectives:	3
1.2.2 Specific Objectives:	3
1.3 ORGANIZATION OF THE THESIS	4
1.4 Accomplishments of Research Objectives	5
Chapter 2	8
2 Literature Review	8
2.1 Introduction	8
2.2 Cracking Processes	8
2.3 Catalytic Cracking Mechanism over Zeolites	9
2.4 The Riser FCC Reactor and the Effect of Operating Parameters in the FCC Unit:13	
2.5 Modes of Catalyst Deactivation	16
2.6 Reversible and Irreversible Deactivation:	17
2.6.1 Coke and Deactivation:	17
2.6.2 Coke Characterization:	18

2.7	Diffusion and Adsorption-Desorption of Chemical Species	19
2.8	Estimation of Cracking Kinetics and Catalyst Activity Decay during 1,3,5-TIPB Cracking.	20
2.8.1	Introduction.	20
2.8.2	Catalyst Deactivation Functions.....	20
2.9	Conclusions	23
Chapter 3		25
3	Experimental Methodologies.....	25
3.1	Introduction	25
3.2	Materials and Methods	25
3.2.1	Feedstock and Catalysts	25
3.2.2	Catalytic Cracking with a Model Compound, and the Range of Operating Parameters Selected.....	26
3.2.3	Analytical Methods	27
3.3	Catalyst Characterization.....	28
3.3.1	X-Ray Diffraction (XRD).....	29
3.3.2	X-Ray Fluorescence (XRF).....	29
3.3.3	N ₂ Adsorption Isotherm (BET) and Pore Size Distribution PSD).....	29
3.3.4	Temperature Programmed Desorption (TPD).....	30
3.3.5	Fourier Transform Infrared Spectroscopy (FTIR).....	30
3.4	Catalytic Reactor System.....	31
3.4.1	Experimental Setup:	31
3.4.2	Experimental Procedures:.....	33
3.4.3	Thermal Runs	34
3.5	Gas Phase Sampling	34
3.6	Conclusions	35

Chapter 4	36
4 Cracking of 1,3,5-TIPB over CAT-A	36
4.1 Introduction	36
4.2 Catalyst Characterization.....	36
4.2.1 X- Ray Diffraction.....	36
4.2.2 NH ₃ -TPD (Temperature Programmed Desorption)	37
4.2.3 Nitrogen Adsorption and BET (Brunauer-Emmett-Taller)-Specific Surface Area.	38
4.2.4 FTIR Pyridine Adsorption (FTIR):	41
4.3 1,3,5-TIPB Conversion, and Product Selectivity on the Gas Phase.	43
4.4 Cracking Experiments:	45
4.4.1 Thermal Cracking Runs:.....	46
4.4.2 Catalytic Cracking Runs.....	47
4.5 Conclusions	57
Chapter 5	58
5 Catalytic Cracking of 1,3,5 TIPB Chemical Species using CAT-A, CAT-B, and CAT-C	58
5.1 Introduction:	58
5.2 Catalyst Characterization:	58
5.2.1 X- Ray Diffraction:.....	58
5.2.2 NH ₃ -TPD (Temperature Programmed Desorption).....	60
5.2.3 Pyridine-FTIR:	62
5.2.4 N ₂ Adsorption-Desorption Isotherms	63
5.3 Catalytic Cracking Runs:.....	67
5.3.1 Effect of Catalyst to Oil Ratio (Catoil C/O ratio) [g cat g feed ⁻¹] on Feed Conversion, Coke selectivity, Species distribution.	67
5.3.2 Coke Selectivity.....	68

5.3.3 Product Selectivity:	69
5.4 Coke Formation Mechanism:	70
5.5 Conclusions	74
Chapter 6	76
6 Kinetic Modeling of 1,3,5 TIPB over <i>E-CAT</i> base Y-Zeolite Catalysts.	76
6.1 Introduction:	76
6.2 Mechanistic of 1,3,5 TIPB Cracking Conversion and Coke formation:	76
6.3 Kinetic Development- Model-I	81
6.3.1 Kinetic Model Assumptions	81
6.3.2 Results Discussion - Model-I	82
6.4 Kinetic Development-Model II-Estimation of Reaction Step Intrinsic Parameters	86
6.5 Numerical Method Used.....	89
6.6 Discussion of Results-Model-II.....	90
6.6.1 Estimated Kinetic Parameters.....	90
6.7 Conclusions	95
CHAPTER 7	96
7 CONCLUSIONS AND RECOMMENDATIONS	96
7.1 Conclusions	96
7.2 Recommendations	97
References	98
Appendices	110
1 Curriculum Vitae	1

List of Tables

Table 3.1 Characteristics of 1, 3, 5-Tri-Iso-Propyl-Benzene. [111].....	26
Table 4.1: Characteristic XRD Diffraction Bands at Various 2θ Values for the CAT-A and for a NaY Zeolite as reported by Gianetto, A. 1993.	37
Table 4.2: Specific Surface Area [SSA] (m ² /g), Pore Volume [PV] (cm ³ /g), and Mesopore Volume (cm ³ /g) for CAT-A, Following Catalytic Cracking Runs at 550°C and 7 s, Using Different C/Os. SD on repeats: +/- 3 m ² /g.....	40
Table 4.3: Relative Brönsted /Lewis Acid Site Ratios using Pyridine FTIR. CAT-A samples with coke were analyzed following catalytic cracking runs at 550°C and 7 s.	43
Table 5.1: Properties of the Studied Catalysts.....	59
Table 5.2: NH ₃ -TPD for CAT- A, CAT- B and CAT- C Catalyst Samples.....	62
Table 5.3 Brönsted /Lewis Acid Site Ratios using Pyridine FTIR.....	63
Table 5.4: Specific Surface Areas and Pore Volumes of the Free of Coke Catalysts.....	65
Table 5.5: Specific Surface Areas [SSA] (m ² /g) and Pore Volumes [PV] (cm ³ /g) for CAT-B. Mesopore Volumes (cm ³ /g) for CAT-B were determined following catalytic cracking runs at 550°C and 7 s, using different C/O ratios. SD on repeats: +/- 3 m ² /g.	66
Table 6.1: Temperature Effect on $k_{10}' = \eta_A(k_{10} + k_{40}) K_A$	85
Table 6.2: Optimized Intrinsic Kinetic Parameters for Model II and Cross-Correlation Coefficients.....	92

List of Figures

<i>Figure 2.1 Schematic Diagram of Catalytic Cracking</i>	10
<i>Figure 2.2 Cracking Reaction of an Alkane Molecule (RH) Involving a Hydride Transfer to a Smaller Carbenium Ion (R1+) Followed by β-scission [63,64]</i>	11
<i>Figure 2.3 Haag–Dessau Cracking Mechanism for an Alkane Molecule (RH) involving a Carbonium Ion Transition State [63,64]</i>	11
<i>Figure 2.4 Comparison Showing the Similarity between Reaction Conditions in a Catalytic Downer Reactor and in the CREC Riser Simulator where C/O, Partial Pressures, Temperatures and Reaction Times are close in both units [Yira Aponte 2016 [86].</i>	15
<i>Figure 3.2 Sectional View of the CREC Riser Simulator Reactor with the Detailed Assembly of the Catalyst Basket and Impeller. The green line shows the gas flow path upon rotation of the impeller [124]</i>	31
<i>Figure 3.3 Schematic Diagram of the CREC Riser Simulator Experimental Setup [42]</i>	32
<i>Figure 4.1 NH₃-TPD Analyses for CAT-A. Notes: Continuous black line: FCC catalyst free of coke; Continuous red line: C/O= 0.6; Continuous blue line: C/O=1.25; Continuous violet line: C/O=2.5; continuous green line: C/O=5; Continuous blue line: experiment baseline...</i>	38
<i>Figure 4.2 Nitrogen Adsorption Plots affected at 77 K</i>	39
<i>Figure 4.3 Differential Pore Volume (dV/dD) as a Function of the Pore Diameter (D) Using the N₂-Adsorption Isotherm. (■) CAT-A free of coke; (●) CAT-A at C/O = 0.8g/g; (▲) CAT-A at C/O = 1.25g/g; (◄) CAT-A at C/O = 2.5g/g; (▼) CAT-A at C/O = 3.75g/g. CAT-A sample</i>	41
<i>Figure 4.4 Pyridine Desorption FTIR Spectra for CAT-A. The CAT-A "Free of Coke" is Represented by a Solid Line and the CAT-A "Deactivated by Coke "is Represented by a Dashed Line.</i>	42

<i>Figure 4.5 Reported Effect of the Vacuum Box Pressure on the 1,3,5 TIPB Conversion Using CAT-A. Notes: Contact times: 3s, 5s & 7s. Temperature: 550 oC. Reported data and standard deviations (vertical bars) represent average values from 3-5 repeat runs.</i>	44
<i>Figure 4.6 Molar Fractions of 1,3,5 TIPB and Propylene in the CREC Riser Simulator for: (i) Pressure in vacuum box=1.5 psi and (ii) Pressure in vacuum box=14.7 psia. Note: Reported values represent averages from at least 3 repeats.</i>	45
<i>Figure 4.7 Influence of Contact Times (3-7s) and Temperatures (510-550 °C) on 1,3,5-TIPB Thermal Cracking. Vertical bars represent standard deviations from at least 5 repeat runs.</i>	46
<i>Figure 4.8 Effects of Temperature and Reaction Time on the Conversion of 1,3,5 TIPB on CAT-A. The C/O was set to 2.5. Reported data and standard deviations (vertical bars) represent experimental data from at least 5 repeats.</i>	47
<i>Figure 4.9 Effects of Temperature and Reaction Time on the Coke Formation while Cracking 1,3,5-TIPB over CAT-A. The C/O was set to 2.5. Reported data and standard deviations (vertical bars) are from 4-7 repeat runs.</i>	48
<i>Figure 4.10 Influence of Contact Time and Temperature on the Propylene Selectivity-M during 1, 3, 5-TIPB Conversion using CAT-A. Reported data and standard deviations (vertical bars) represent average values from 4-7 repeat runs.</i>	49
<i>Figure 4.11a, 4.11b and 4.11c. Effects of Contact Time, and C/O Ratio on the 1,3,5-TIPB Conversion using CAT-A at 550 oC for Figure 11(a), 530 oC for Figure 11 (b) and 510 oC for Figure 11 (c). Contact times: 3s, 5s & 7s. Reported data and standard deviations (vertical bars) represent average values from at least 5 repeat runs.</i>	51
<i>Figure 4.12 Effect of Temperature on Propylene Selectivity at various C/O Ratios using Cat-A. Notes: Contact time: 7s. Reported data and standard deviations (vertical bars) represent average values from at least 5 repeat runs. Note: Propylene Selectivity-M is defined as the moles of propylene per mole of TIPB converted.</i>	52
<i>Figure 4.13 Changes of Product Selectivity-M with 1,3,5-TIPB Conversion at 550oC and 7s. Data is reported increasing the C/O ratio as indicated by the arrows: (1) C/O=0.6, (2)</i>	

C/O=0.8, (3) C/O=1.25, (4) C/O=2.5, (5) C/O=3.75, and (6) C/O=5. Reported data and standard deviations (vertical bars) represent average values from at least 5 repeat runs. 53

Figure 4.14 Effect of Temperature and C/O Ratio on Benzene Selectivity using a CAT-A at 7s. Reported data and standard deviations (vertical bars) represent average values from at least 5 repeat runs. 54

Figure 4.15 Changes of Moles of Coke (N_c) with Temperature (510oC, 530oC, 550oC) at Various C/O Ratios and 7 s Reaction Time. Reported data represent average values from at least 5 repeat runs. The vertical bars describe standard deviations of repeats. 54

Figure 4.16a, :4.17b, 4.16c. Effects of C/O Ratios on Coke Selectivity- W (weight-based coke selectivity) using a TIPB CAT-A. Operating Conditions: (a) 550°C, (b) 530°C, (c) 510°C. Reaction time: 3-7s Note: Coke Selectivity- W was determined as grams of of coke/ gr grams of 1, 3, 5 - TIPB converted..... 55

Figure 4.17 Effects of C/O Ratios on Coke Formed, for 1,3,5-TIPB Cracking using a CAT-A. The temperature was set to 550°C. Reported data represent average values from at least 5 repeat runs. 56

Figure 5.1: XRD Diffractograms for a CAT-B Sample of the Present Study Mixed with pure Silicon. Characteristic bands for silicon are shown at 28, 47 and 56 degrees in the 2θ scale. 59

Figure 5.2 NH₃-TPD Analyses for CAT-B. Notes: Continuous black line: FCC catalyst free of coke; continuous red line: C/O= 1.25; continuous blue line: C/O=2.5; continuous violet line: C/O=3.75; continuous green line: C/O=5; continuous blue line: experiment baseline. Samples with coke were analyzed following catalytic cracking runs at 550°C and 7 s. 61

Figure 5.3: FTIR Spectra Shows IR Band Peaks for the Catalysts A, B and C studied. The black solid line represents pyridine adsorbed on CAT- A; the red solid line denotes pyridine adsorbed on Cat-B; the blue solid line shows the pyridine adsorbed on CAT-C..... 63

Figure 5.4 BET-Nitrogen Adsorption Plot. N₂ Adsorption-Desorption Isotherms Obtained from Different Samples of CAT-B after a Run at 550°C and 7 s Contact Time. 64

Figure 5.5: Differential Pore Volume (dV/dD) as a Function of the Pore Diameter (D) Using the N_2 -Adsorption Isotherms. (■) CAT-B free of coke; (●) CAT-B at $C/O = 0.6g/g$; (▲) CAT-B at $C/O = 0.8g/g$; (▼) CAT-B at $C/O = 1.25g/g$; (◆) CAT-B at $C/O = 2.5g/g$; (◄) CAT-B at $C/O = 3.75g/g$. All samples were analyzed following catalytic cracking runs at $550^\circ C$ and 7 s..... 65

Figure 5.6 Changes of the 1,3,5-TIPB Conversion with the C/O Ratio in the CREC Riser Simulator for CAT-A, CAT-B, and CAT-C. Note: Reaction time: 7 s, Temperature: $550^\circ C$. Reported data and standard deviations (vertical bars) represent average values from at least 5 68

Figure 5.7 Effect of C/O on Coke Selectivity Using 1,3,5-TIPB and Cat-A, Cat-B & Cat-C Operating Conditions: $550^\circ C$ and 7s. Reported data and standard deviations (vertical bars) represent average values from at 5-7 repeat runs..... 69

Figure 5.8 Effect of C/O on the Product Selectivity Using 1,3,5-TIPB and CAT-B. The temperature and contact time were kept constant at $550^\circ C$ and 7s, respectively. Notes: a) The direction of the “arrows” represent increasing C/O ratios, b) Reported data and standard deviations (vertical bars) represent average values from at least 4-7 repeat runs..... 70

Figure 5.9 Changes of Species Mass Fractions for CAT-A. Note: Contact times are 3s, 5s & 7s; temperature: $550^\circ C$; the C/O : 2.5. The reported data and standard deviations (vertical bars) represent average values from at least 5 repeat runs. 71

Figure 5.10 Schematic Description of the Catalytic 1, 3, 5 TIPB Conversion Showing the Hypothesized Cracking Steps. 71

Figure 5.11: Schematic Representation of Coke Formation. Case (a) Coke is formed as a condensed species from two adsorbed coke precursors located in the sample particle. Case (b) Coke is formed as a condensed species from two adsorbed coke precursors located in two adjacent particles. 73

Figure 6.1 shows that the catalytic conversion of 1,3,5-TIPB encompasses a number of dealkylation steps, involving chemical and radical adsorbed..... 77

Figure 6.2: Schematic Representation of Coke Formation. Case (a) Coke is formed as a condensed species from two adsorbed coke precursors located in the sample particle. Case (b) Coke is formed as a condensed species from two adsorbed coke precursors located in two adsorbed coke precursors located in two adjacent particles. 79

Figure 6.3 Changes of TIPB Conversion with Reaction Time at 550°C for Different C/O Ratios. Reported data represent average values for at least 5 repeat runs. 84

Figure 6.4: Deactivated Parameter (α) as a function of catalyst to oil ratio in the 550°C-510°C and 3-7 s ranges..... 85

Figure 6.5 Parity Plot Comparison Theoretical Model Results with Experimental Data. Note: Relative Percentual Error: $\pm 6.5\%$ 86

Figure 6.6 Parity Plot Comparing Experimental Observed Chemical Species Concentrations with Model Predicted Concentrations in the 510- 550 oC and 3-7s ranges. Data: 270 average data points involved including at least 3-5 repeats per experimental condition..... 91

Figure 6.7 Comparison of Experimental and Model Predicted Chemical Species Concentrations during the 1,3,5-TIPB Catalytic Cracking. Operating Conditions: Contact times: 3-7s, C/O= 0.6-5, Temperature: 550 °C: Data: 270 average data points including at least 3-5 repeats. 93

Figure 6.8 Deactivated Parameter (α) as a Function of the Catalyst to Oil Ratio in the 510°C-550°C and 3-7 s Ranges 94

List of Appendices

Appendix A: Mass Balance Closure.....	107
Appendix B: Coke Formation $q_c (g_{coke} \setminus g_{cat})$	109
Appendix C: CAT-B and CAT-C Characterization	111
Appendix D: Product Selectivity	114
Appendix E: 1,3,5-TIPB Conversion Changes with Reaction Time at Various C/O...	115
Appendix F: Predicted Chemical Species Concentrations	117

List of Abbreviations

Nomenclatures

C_i	Volumetric concentration of species (A, B, C, D, and E) (mole/cm ³)
C_{coke}	Coke on catalyst (g _{coke} /g _{cat})
C_T	Catalyst site density (moles of sites/g _{cat})
D	Pore diameter (Å)
M_i	Number of moles of “i” species (moles) in the gas phase
M_{coke}	Number of moles of coke collected (moles)
k_i, k_j	Apparent kinetic rate constant ($\frac{m^3}{g_{cat} s}$)
k_{A0}	Frequency factor (1/s)
k'_{10}	$\eta_A(k_{10}+k_{40})$ KA group (1/s)
k_{11}	Coke formation kinetic constant (sites in the same particle) ($\frac{moles}{g_{cat} s}$)
k_{12}	Coke formation kinetic constant (sites in adjacent particles) ($\frac{moles}{g_{cat} s}$)
K_i	Adsorption equilibrium constants for “i” species (cm ³ /mole)
MW_{coke}	Molecular weight of the CH _{0.7} coke unit or 12.7 (g/mole coke)
N_i	Number of moles of “i” species (moles)
N_c	Total moles of coke
N_{coke}	Number of moles of coke collected (moles)
q_A	Concentration of “i” species adsorbed on catalyst surface (mole/g _{cat})
q_{coke}	Coke concentration on catalyst (g-coke/g-catalyst)
r_{Coke}	Rate of coke formation (moles coke /g _{cat} .s)
$r_{coke,sp}$	Rate of coke formation in sites placed in the same particle (moles coke /g _{cat} .s)
r_i	Rate of reaction for each species (moles of “i” /g _{cat} .s)
t	Reaction time (s)
T	Reaction temperature (K)
V	Pore Volume (cm ³ /g)
V. Box	Vacuum Box
V_T	Total CREC Riser Simulator volume (cm ³)

W_{cat}	Mass of catalyst (g_{cat})
W_{oil}	Total mass of hydrocarbons injected (g)

GREEK SYMBOLS

α	Deactivation parameter (g_{cat}/g_{coke})
γ	Rate of coke formation in close particles over the rate of coke formation in single particles (-)
η_i	The effectiveness factor for the “i” species (-)
θ_i	Fraction of “i” species occupied sites (-)

SUBSCRIPTS

i	Generic “i” species
o	Free of coke
A	1,3,5 TIPB (tri-iso-propyl-benzene)
B	DIBP (di-iso-propyl-benzene)
C	IPB (iso-propyl benzene) or Cumene
$Coke$	Coke
D	Benzene
E	Propylene

ACRONYMS

BAS	Brönsted Acid Sites
BET	Brunauer–Emmett–Teller
CAT-A	Catalyst A
CAT-B	Catalyst B
CAT-C	Catalyst C
Catoil (C/O)	Catalyst to Oil Ratio (g/g)

CREC	Chemical Reaction Engineering Center
DRIFTS	Diffuse Reflectance Infrared Fourier Transform Spectroscopy
FCC	Fluid Catalytic Cracking
FID	Flame Ionization Detector
FTIR	Fourier Transform Infrared Spectroscopy
GC	Gas Chromatography
LAS	Lewis Acid Sites
MSD	Mass Spectrometer Detector
PSD	Micropore Size Distribution
STP	Standard Temperature (0 °C) and pressure (1 atm)
PV	Pore Volume (cm ³ /g)
Selectivity-M	Moles of Product “i” Species/Moles of TIPB Converted
Selectivity-W	Grams of Coke /Grams of TIPB Converted.
SSA	Specific Surface Area (m ² /g)
TOC	Total Organic Coke (g-coke/g-cat.)
TPD	Temperature Programming of Desorption
UWO	The University of Western Ontario
VGO	Vacuum Gas Oil
XRD	X-Ray Diffraction
X-ray	Fluorescence XRF
4PV	4-port chromatographic valve
6PV	6-port chromatographic valve

Chapter 1

1 Introduction

1.1 Problem Description and Motivation for this Research

Fluidized catalytic cracking (FCC) is one of the most valuable processes in petroleum refineries [1–5] and the best example of the large-scale application of Y-zeolites. Every day, more than ten million barrels of gasoline are produced in FCC units throughout the world [6,7]. VGO or vacuum gas oil is the typical feedstock used in FCC units. The cracking of VGO hydrocarbons leads to desirable by-products such as gasoline, liquid petroleum gas as well as to undesirable ones such as light hydrocarbons and coke [8–11].

FCC involves a complex reaction network and uses a fluidizable catalyst [12–14]. The main component of the catalyst is usually a Y-zeolite embedded in a catalyst matrix. Y-zeolites catalyze cracking reactions given their acidic surface sites [15]. As well, and in addition to gasoline and light gases, coke is formed as a by-product; with coke formation being promoted at either higher temperatures or longer contact times. Coke formation also leads to a diminished catalyst activity with an undesirable drop in the overall rate of cracking [16].

Coke is composed of highly condensed aromatic rings. Coke may be deposited either on the dispersed outer Y zeolite surfaces embedded in the amorphous matrix or in the Y-zeolite micropores [17,18]. Coke has a very low volatility, remaining entrapped in the catalyst pore network [19,20]. The coke deactivated FCC catalyst can be reactivated via coke combustion. One should note however, that catalytic cracking is an endothermic reaction. Thus, the heat generated by coke combustion, is needed to achieve the thermal balance in the refinery. Thus, controlled amounts of coke are desirable.

Furthermore, by understanding coke formation, one can provide the basis for the development of kinetic models for FCC industrial risers and downers [12]. There is, in this respect, a significant interest in understanding and optimizing FCC operations. These optimizations may

enhance product selectivity, minimizing coke formation and reducing operational costs [21,22]. Given that nowadays FCC takes place in riser reactor units, and that in the future, it may potentially occur in downer units, one must establish reliable reaction rate equations, which adequately include catalyst activity decay [23].

The catalytic cracking of VGO (vacuum gas oil) and model compounds [21,24–27] has been developed through various kinetic studies. One should mention that, in particular, process factors affecting coke formation [28–30] need to be identified. Issues with coke are particularly relevant in FCC riser operation and for the simulation of large downflow reactor units [31–33].

Furthermore, and despite the anticipated importance of the C/O ratio on FCC performance, there is still a lack of proper understanding of its influence on FCC risers and downers. Few studies are recorded in the technical literature about the effect of the C/O ratio. Several authors [21,25,32-34] including Abul-Hamayel et al [34], claim that when the C/O ratio increases, this leads to enhanced catalytic cracking versus thermal cracking. Frequently, FCC units operate in the 6-12 C/O range. Thus, there is, in principle, the opportunity of using high C/O ratios for improving catalytic activity in industrial scale units. In keeping with this view, high C/O ratios could favor high feedstock conversion, limiting at the same time catalyst activity decay and coke formation. This reduced coke can be considered favorable given its anticipated influence on Sulphur oxide emissions. Sulfur species are entrapped in coke and can be released as SO_x in the FCC regenerator [35].

On this basis and given the high interest and value of this topic, it is the main goal of this PhD dissertation, to study catalyst deactivation by coke. As well, it is the objective of this research to address the critical effect of the C/O ratio on the hydrocarbon catalytic conversion using a rigorous methodology. With this end, 1,3,5 tri-iso-propyl-benzene (1,3,5-TIBP) with a good balance of paraffinic and aromatic functionalities was employed as a model compound during the experiments. This use of a representative model compound circumvents the analytical issue when using VGO feedstocks and simplifies the kinetic reaction network [36,37]. As well, this allows one to better understand the chemical reaction pathways. To accomplish this, 1,3,5-TIBP thermal and catalytic cracking were developed in a CREC Riser Simulator using Y-zeolite based

catalysts designated as CAT-A, CAT-B, and CAT-C. Experimental runs were adequately combined with catalyst characterization (XRD, XRF, NH₃-TPD, FTIR and BET) following cracking runs and catalyst regeneration.

1.2 Research Objectives

Based on the objectives stated above, the present study has been strategized to pay general and specific attention to the following objectives:

1.2.1 General Objectives:

The main objective of the current study is to shed light into the catalytic cracking reactions and catalyst deactivation by coke. To accomplish this, cracking of a 1,3,5 TIPB model compound over various catalysts with different activities, at different operating conditions relevant to FCC riser and downer reactors.

1.2.2 Specific Objectives:

1. To investigate the effects of reaction temperature, reaction time, and very specially C/O ratio on hydrocarbon thermal and catalytic conversion, product selectivity and catalyst deactivation by coke (particularly coke selectivity).
2. To perform a physicochemical characterization of both the regenerated and coked catalysts using advanced surface science techniques including NH₃-TPD, BET, and pyridine adsorption desorption. These technical runs allow us to examine the role of the acid sites and their changes with hydrocarbon conversion and product selectivity. This takes place with catalysts having different degrees of coke coverage.
3. To develop a new kinetic model for FCC, describing the effects of catalyst to oil ratio (C/O) on the coke formation selectivity. It is anticipated that the proposed model will be suitable for a wide range of operation conditions, different FCC riser and downer designs, and scales. This model should incorporate the catalyst activity changes as a function of the formed coke.

4. To estimate the kinetic parameters of the new kinetic model, including intrinsic kinetic constants and catalyst activity decay using model compounds.

To accomplish the above-described objectives, this dissertation includes seven Chapters. The contents of Chapters 2-7 are summarized in the next section.

1.3 ORGANIZATION OF THE THESIS

The contents of Chapter 2 to Chapter 7 of this PhD dissertation contribute to the present study as follows:

- Chapter 2. This chapter provides the background information on the fundamentals of catalytic cracking as well as a brief review of the effects of operating conditions such as reaction time, reaction temperature, and catalyst to oil ratio (C/O). The effects of these parameters on catalyst deactivation, hydrocarbon conversion, and product selectivity are considered. Furthermore, this chapter provides a review of the recent progress of catalyst deactivation models.
- Chapter 3. This chapter describes the experimental catalytic system and the model compounds used to perform catalytic and thermal runs in this PhD thesis. Moreover, in this chapter, various catalyst characterization techniques are described in detail. These techniques are applied to assess the catalyst physicochemical changes and its changes with coking. Furthermore, this chapter describes the experimental methodology considered, including the runs in the CREC Riser Simulator.
- Chapter 4. This chapter reports a detailed description of the experimental data obtained from catalytic cracking runs and thermal cracking runs in the CREC Riser Simulator. An FCC catalyst designated as CAT-A is used as the basis of the studies. First, there is a reported catalyst characterization based on crystallinity, total acidity, specific surface area, temperature-programmed ammonia desorption, pyridine desorption. Following this, a data

analysis based on 1,3,5 TIPB conversion, coke selectivity, and gas-phase hydrocarbon product selectivity at various operating conditions, is performed.

- Chapter 5. This chapter describes the C/O effect in a much broader context, using two additional FCC catalysts, designated as CAT-B and CAT-C. These two catalysts display different activities and acidities as compared with CAT-A. Following catalyst characterization (crystallinity, total acidity, specific surface area, and temperature-programmed ammonia desorption), 1,3,5, TIPB catalytic cracking runs in CREC Riser Simulator are reported. These runs show the same effect of the C/O ratio in terms of 1,3,5-TIPB conversion, coke selectivity, and product selectivity for the three catalysts studied (CAT-A, CAT-B and CAT-C).
- Chapter 6. This chapter reports a kinetic model of the catalytic cracking of 1,3,5 TIPB establish with CAT-A data. This mechanistic-based kinetics considers various gas-phase chemical species at different C/O ratios. The kinetic model is established using a numerical regression with various kinetic parameters reported with their 95% confidence interval parameters and their cross-correlation matrix.
- Chapter 7. This chapter provides the conclusions and recommendations of this PhD dissertation, highlighting the original aspects of this contribution.

1.4 Accomplishments of Research Objectives

The achievements of this PhD dissertation were reported in the following conference communication and published manuscripts:

- I. Conference Presentation 1: A. Alkhlel, H. de Lasa, “Catalytic Cracking of Hydrocarbons in a CREC Riser Simulator Using a Y-Zeolite Based Catalyst. Assessing the Catalyst/Oil(C/O) Ratio Effect”, CSCHE Conference Toronto, October 29, 2018.

- II. Manuscript 1: S. Lopez-Zamora, A. Alkhlel, H. de Lasa. Monitoring the progress of catalytic cracking for model compounds in the mid-infrared (MIR) 3200–2800cm⁻¹ range. *Chemical Engineering Science* 192 (2018) 788–802.

<https://doi.org/10.1016/j.ces.2018.08.021>

This manuscript addresses the application of Mid-Infrared (MIR) spectroscopy, to establish hydrocarbon species concentrations in the gas phase in riser and downer units. The proposal considers MIR monitoring chemical species at various reaction times. Catalytic cracking data of this PhD. Dissertation, obtained in the CREC Riser Simulator allows quantifying anticipated compositions differences between 1,3,5 TIPB total hydrocarbons concentrations and 1,3,5 TIPB concentrations in the gas phase. These differences were assigned to 1,3,5 TIPB intra-catalyst transport effects, as reported in CHAPTER 4 of this Dissertation.

- III. Manuscript 2: A. Alkhlel, H. de Lasa, “Catalytic Cracking of Hydrocarbons in a CREC Riser Simulator Using a Y-Zeolite Based Catalyst. Assessing the Catalyst/Oil(C/O) Ratio Effect”. *Industrial & Engineering Chemistry Research*. 2018, 57, 41, 13627-13638. <https://doi.org/10.1021/acs.iecr.8b02427>

Manuscript 2 investigates the effects of the changes of the catalyst to oil ratio (C/O) on FCC cracking using a Y-zeolite based catalyst designated as CAT-A. As well, it reports the influence of the C/O ratio on cracking conversion and catalyst decay. Detailed results are reported in CHAPTER 5 of this PhD Dissertation.

- IV. Manuscript 3: Abdulkaber Alkhlel, Hugo de Lasa, “Catalyst/Feedstock Ratio Effect on FCC Using Different Catalysts Samples”. *Catalysts* **2019**, 9(6), 542; <https://doi.org/10.3390/catal9060542>

This was an invited article to the *Catalysts* journal for a Special Issue on catalyst deactivation led by Prof. Pedro Castano, KAUST, Saudi Arabia. This manuscript reports the effects of the changes of the C/O ratio, using as the basis of the analysis,

two other catalytic cracking catalysts, CAT-B and CAT-C. Detailed results are reported in the CHAPTER 6 of this PhD Dissertation.

Chapter 2

2 Literature Review

2.1 Introduction

Fluidized Catalytic Cracking (FCC) is one of the most important vacuum gas oil (VGO) feedstock conversion methods in oil refineries. FCC is a major contributor to the production of gasoline [2,12,35]. This technology is in many aspects, a relatively simple process, readily adaptable to several feedstocks [12]. However, FCC is still being researched and developed. Today, there are still some aspects of FCC that require further study, such as the catalytic cracking chemistry, the kinetics and the operating conditions [37]. On this basis, a considerable number of researchers have been investigating catalytic cracking [38,39]. More specifically, this involves the modelling of coke formation over acid zeolites such as Y-zeolites [40]. Coke formation affects chemical species adsorption, diffusion and catalytic reactions and requires further analysis. These issues will be reviewed in the upcoming sections of this literature review.

2.2 Cracking Processes

Gasoline is a main product from a petroleum refinery [41]. About 75-80 % of the VGO converted products are gasoline and the remaining are light gases and diesel [42]. However, the current FCC product breaks down; it may not satisfy the future market demand for low molecular weight olefins (e.g. ethylene and propylene). Thus, it is anticipated that LCO (light cycle oil), HCO (heavy cycle oil) and unconverted VGO should be further converted into low molecular weight hydrocarbons as stated in [43,44]

Concerning the FCC processes, both thermal cracking and catalytic cracking have been used in refineries. However, the use of catalytic hydrocarbons over zeolite catalysts at 500°C, and under slightly above atmospheric pressure, with low contact times is a preferred option [45,46]. In thermal cracking, ethylene together with large amounts of C₁ and C₂ are formed [12]. In catalytic cracking however, there is a reduced light gas fraction [10], with higher yields of C₃-C₄ olefins [47]. This difference in product composition is due to the different reaction mechanisms, with

free radicals being dominant for thermal cracking, and carbonium ions having a major role in catalytic cracking [41,48]. Additionally, catalytic cracking, produces higher aromatic fractions [43,48], with these aromatic species condensing as coke precursors [49].

2.3 Catalytic Cracking Mechanism over Zeolites

The catalytic cracking of hydrocarbons over FCC zeolite catalysts is a process dominated by endothermic reactions [50]. These reactions are accompanied with the undesirable formation of C₂-C₅ light gases and coke. Coke leads to catalytic activity decay and selectivity changes with catalyst time-on-stream [51,52]. Furthermore, catalyst reactivation through coke combustion involves an exothermic reaction, which is a critical contributor to the thermal balance of the refinery [53,54].

A typical FCC unit involves the transport and rapid catalytic reaction of chemical species on solid fluidizable particles as follows: a) hydrocarbons evolving in the gas phase are adsorbed on the catalyst, and b) adsorbed hydrocarbon species react on the catalyst particles. At riser outlet adsorbed hydrocarbons are stripped from the catalyst using steam [55]. This complex reaction encompasses both monomolecular and bimolecular reaction steps [56].

Catalytic cracking relies on intermediate carbocation ions [57]. Carbocations can be divided into two types: a) Trivalent carbenium ions (e.g. CR₃), and b) Penta or Tetra- coordinated (e.g. CR₅ or C₂R₅) carbonium ions[58]. Others also argue on the role of di-coordinated and tri-coordinated carbonium ions [59,60].

Thus, final hydrocarbon product compositions are strongly influenced by carbonium ion intermediates, as well as by the accessibility of hydrocarbon species to the reactive catalyst sites inside the zeolite crystallite micropores [60,61].

Typical FCC feedstock is comprised of a combination of hydrocarbons, with these being mainly aromatic and polyaromatic, paraffinic, and naphthenic species. These hydrocarbons are cracked through various primary processes, including isomerization, dealkylation of aromatic species, polymerization, condensation and dehydrogenation [48]. Primary cracking species are exposed

to secondary reactions which can involve intra/or intermolecular reactive hydrogen transfer [62]. Under these conditions, the formation of aromatic species can occur [60]. However, some of these reactions, including isomerization, and the dealkylation of aromatic species, can be beneficial for the desired product chemical structure [12,48,60].

The catalytic cracking reaction can be considered a cyclic process as described in Figure 2.1, with the following being involved as in Wojciechowski, B. W [56]:

- Reactant species being adsorbed on acid sites, forming surface ions.
- These intermediate surface ion species undergoing both bimolecular and monomolecular surface reactions.
- Products desorbing from catalytic sites, leaving them free of adsorbed species.

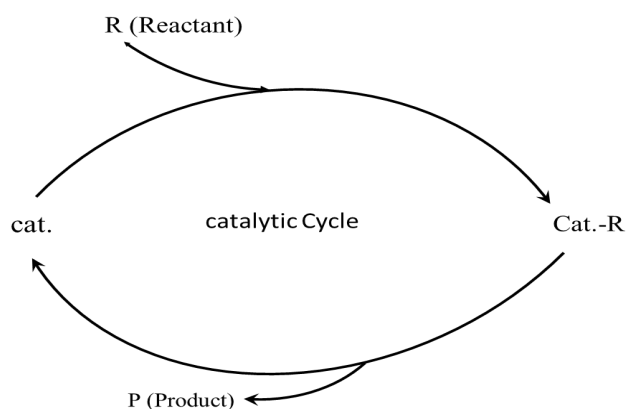


Figure 2.1 Schematic Diagram of Catalytic Cracking

Figure 2.1 describes the intrinsic catalytic cracking steps in more detail, including: a) reaction initiation, b) reaction chain propagation, c) reaction termination.

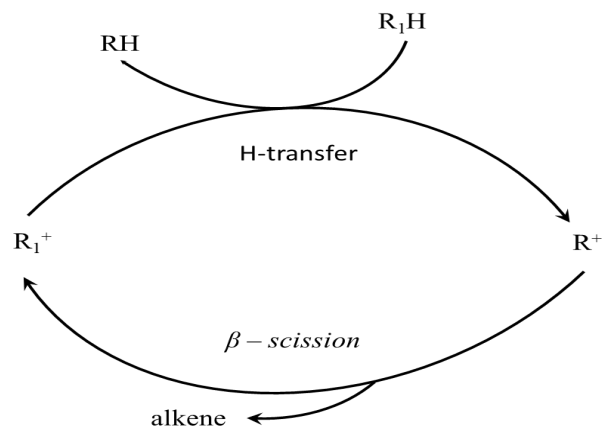


Figure 2.2 Cracking Reaction of an Alkane Molecule (RH) Involving a Hydride Transfer to a Smaller Carbenium Ion (R_1^+) Followed by β -scission [63,64].

In this regard, one can envision a first step, encompassing carbenium ion formation at an active catalyst site. This may be followed by hydride ion abstraction from other chemical species, with hydride ions being transferred to adsorbed carbenium ions. This leads to carbonium ion formation. Carbonium ions can crack, at the C-C bond, placed at β position of the trivalent positively charged carbon atom. The cycle is completed via a termination step which involves the desorption of observed product species (e.g. alkenes) [63–65].

Figure 2.3 describes the 1984 Haag-Dessau mechanism involving activated alkenes. This mechanism is, widely accepted and frequently considered as a landmark in catalysis [63,64,66].

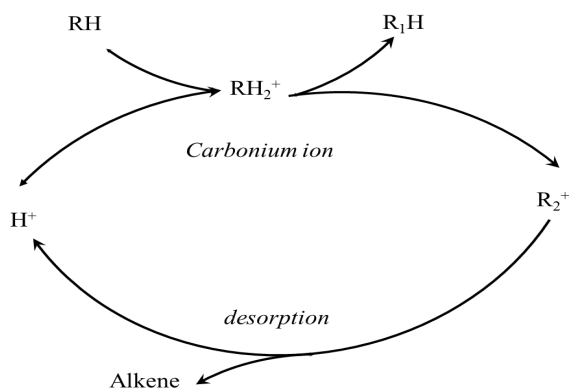


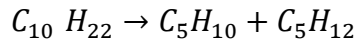
Figure 2.3 Haag–Dessau Cracking Mechanism for an Alkane Molecule (RH) involving a Carbonium Ion Transition State [63,64].

The Haag-Dessau mechanism involves carbenium ions being formed through hydride abstraction or through the protonation of alkenes (e.g. olefin). Hydride abstraction can be hypothesized as originating from paraffins on Lewis acid sites (trivalent or tri-coordinated aluminum). As well, the protonation of olefins can take place concurrently on the strong Bronsted acid sites (penta- or tetra-coordinated carbocation) [56,59]. The outcome is an alkene formation with a donation of a proton to a zeolite site while freeing an active site [64,67].

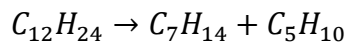
Regarding carbocation catalytic cracking, based on an acid–base reaction, carbonium ions concentration depend on acid site strength [56]. This explains the higher cracking reactivity on the catalyst with higher Bronsted acid sites over Lewis acid sites ratio [56,59]. Carbocation ion chemistry can also explain product isomerization. This is given the carbocation tendency of forming more stable ions [12,60,68].

Together with catalytic reaction mechanism understanding, insights into the catalytic cracking chemistry are imperative to further enhance the performance of FCC units [45]. One can in this respect, postulate a stoichiometry of the main catalytic cracking reactions as follows [48,68]:

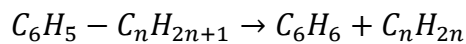
1. Paraffins are cracked to yield olefins and smaller paraffins:



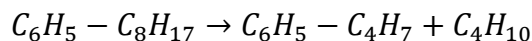
2. Olefins are cracked to give smaller olefins:



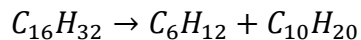
3. Alkyl aromatics undergo dealkylation:



4. Aromatics can also undergo side-chain scission:



5. Naphthenes are cracked to obtain olefins:



2.4 The Riser FCC Reactor and the Effect of Operating Parameters in the FCC Unit:

The FCC process unit is configured with two main sections: a riser reactor and a catalyst regenerator. It is in the riser reactor where the catalytic cracking occurs, with the reaction being promoted in 60-70-micron pellets: Y-zeolite crystallites dispersed in silica-alumina matrix pellets. The FCC riser reactor operation can also determine coke formation. Hydrocarbon conversion, gasoline selectivity and coke formation, are all FCC operating parameters that are affected by reaction temperature, reaction time, feedstock composition, catalyst properties, hydrocarbon partial pressure and catalyst/oil ratios (C/O) [27,32,44,69,70].

Coke formed in the riser is combusted in the regenerator where the catalyst activity is recovered [54,71]. Coke formation is also important given it provides the heat balance to the riser-regenerator [10,50,72] and secures an outlet riser temperature in the 510-545 °C range, in order to maintain product yields at anticipated values [43,47].

The effect of these parameters on the FCC catalyst performance has been widely studied in several catalytic reactors, with different design configurations. This has been done to optimize the conditions of existing commercial FCC risers and downers, in order to enhance the product selectivities, and to minimize the cost [22,73,74]

With this end, kinetic descriptions of catalytic cracking reactions with different degrees of simplifications have been considered for both the cracking of VGO (vacuum gas oil) and model compound [7,21,26,75]. Micro Activity Units (MAT), Confined Fluid Bed Reactors (CFBRs) (e.g. Advanced Cracking Evaluation ACE), and pilot plant riser units (e.g. ARCO)[30,76] [27,77] have also been employed in these studies [24,27]. The MAT (Micro Activity Test) has been more frequently been used [21,69,78]. The MAT is operated using a set amount of catalyst in both fixed bed and fluidized bed configurations. A hydrocarbon flow contacts the catalyst particles continuously, for a set period of time (e.g. 1 min.). Thus, in these units, the C/O ratio is established based on a cumulative C/O or a claimed equivalent cumulative parameter (W/F_{HC}

t). In the MAT, W represents the total amount of catalyst in grams, F_{HC} denotes the hydrocarbon mass flow in grams per second and t is the time-on-steam in seconds.

Based on the open technical literature, it has become imperative to assess and develop available laboratory reactors to provide technical support to petroleum refineries for both catalyst and feed selection [27]. In this regard, since 1992, significant research efforts have been made to clarify the kinetics of the catalytic cracking of hydrocarbons using both VGO and model compounds and a new experimental device designated as the CREC Riser Simulator [30,79–82]

The CREC Riser Simulator is a unique experimental batch bench-scale reactor, which mimics the reaction conditions of an FCC industrial circulating fluidized bed unit [83]. The reaction conditions are temperature, partial pressures of hydrocarbons, and contact time [3,76,84]. In the CREC Riser Simulator, C/O ratios are established on a sound basis: the ratio of the weight of the catalyst over the weight of hydrocarbon feedstock fed is determined. The Riser Simulator not only to emulate operating conditions in an industrial fluidized bed unit, but also provides a close mathematical analogy of continuous risers and downers. In the CREC Riser Simulator, the C/O is set at a value close to the catalyst mass flow over the hydrocarbon mass flow fed ratio in a riser unit, as shown in Figure 2.4.

In recent years, the application of the CREC Riser Simulator has allowed researchers in various laboratories around the world [85], to obtain kinetic data under short contact times (less than 10 seconds), for a diversity of catalytic reactions.

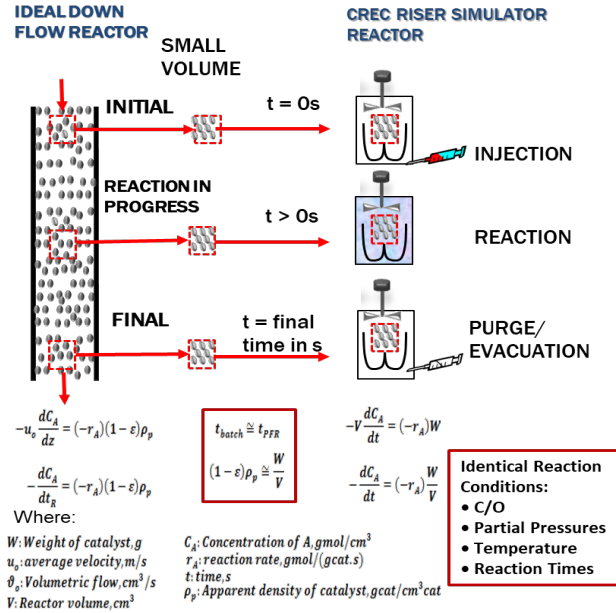


Figure 2.4 Comparison Showing the Similarity between Reaction Conditions in a Catalytic Downer Reactor and in the CREC Riser Simulator where C/O, Partial Pressures, Temperatures and Reaction Times are close in both units [Yira Aponte 2016 [86].

The C/O ratio is a parameter of potential significant importance in FCC units [87]. Changes of C/O ratio in a continuous FCC riser, can be achieved if one modifies the amount of catalyst recirculated from the regenerator to FCC riser reactor[43]. In this respect, one can notice evaluations of FCC operational parameters importance [27], have been consistently overlooked the C/O ratio.

Regarding the C/O influence on FCC, the following observations are provided in the technical literature: a) S. Ng (2001)[88] and Corma. A. (2013) assert that at higher C/O ratios, higher temperatures, and shorter contact times, diesel fractions (C₉-C₁₅) are favored. This is consistent with enhanced hydrocarbon cracking and hydrogen transfer [81,89], b) Sip Chin (2014) [90], and Corma, A. (2013) state that catalytic cracking at higher temperatures, longer contact times and higher C/O ratios favor undesirable dry gas yields and coke formation.

Additional interesting data are reported by Xiaohong Li, et al. (2007) who investigated the effect of mild temperatures and C/O ratios, in the 550-560°C range and in the 5-8 g/g range,

respectively. These authors postulate that increasing the C/O ratio augments the light gas yields. On the other hand, Maya Yescas (2005) claimed that higher C/O ratios lead to higher gasoline yields (about 50%) and this in the C/O 9.5-10.5 range.

To be able to address these issue, Yakubu M et. al. (2017) conducted an FCC unit simulation by varying the C/O in the 1.7-2.4 range, using units with 1-1.6-meter diameter. It was found that the higher the C/O ratios and temperatures, the lower the gasoline yields, and coke formed.

Given these conflicting results, it is the goal of this PhD dissertation to consider the effect of C/O ratio on FCC unit performance. These experiments to be developed in the CREC Riser Simulator, will allow establishing the C/O ratio effect on both feed conversion, product selectivity and coke formation.

2.5 Modes of Catalyst Deactivation

FCC catalysts may be deactivated by coke. This is a major issue in FCC. Coke can be formed in the zeolite micropores [80,91], or alternatively in the catalyst particle matrix [76]. Deactivation may in fact, involve two concurrent phenomena: a) physical deactivation and b) chemical deactivation. Physical deactivation refers to pore blockage. Coke precursors may deposit on catalyst surfaces blocking pores. Thus, reactants are not able to diffuse and reach active sites [17]. Jimenez et al [79] describe VGO reaching mesopores (outer surface of the zeolites) where coke precursors and coke form. Chemical deactivation on the other hand, takes place when highly condensed aromatics deposit on catalyst micropore acid sites.

In regard to coke formation, one can notice that spent catalysts display a dark grey color. This visible dark grey color can be associated to the coke formed on the outer FCC particle surfaces [43]. Thus, the coke formed on the matrix of the catalyst and on the Y-zeolites appears to be significant.

While both physical and chemical deactivation may contribute to lower catalytic activity, there may be discrepancies in the interpretation of deactivation events. For instance, it may be considered that:

- a) Coke precursors are formed first, in the intracrystallite pores, or
- b) Coke precursors overflow to the catalyst matrix cavities forming coke (polyaromatic molecules) and in some cases blocking pores [92].

In addition, it can be envisioned that coke forms on the catalyst matrix first (e.g. VGO is precracked in the matrix). Additional coke can be formed later as gasoline and light cycle oil crack in the Y- zeolites. This second coke formation mechanism appears to be the one more likely to occur when FCC catalysts with active catalytic matrices crack heavy VGOs.

2.6 Reversible and Irreversible Deactivation:

2.6.1 Coke and Deactivation:

Coke is comprised of highly condensed aromatic molecules that deposit on catalyst active sites and/or block the catalyst pores [70]. Coke formation is affected by several factors including the “pore structure” zeolite topology, the reaction temperature as well as the feedstock impurities. These parameters affect the observed rates of chemical reactions.

The term “coke” has been used to designate carbonaceous materials left on the catalyst matrix or in the zeolite micropores after the FCC reaction. Wang [85] argues that coke is not a single species “per se”, but rather a complex combination of strongly adsorbed high molecular weight by-products. On this basis, a general formula for coke is considered as follows: CH_n where “n” decreases with the extent of aromatic species condensation [93]

Coke formation is a complex phenomenon [92] that may be affected by operating conditions [94] such as: a) temperature, b) C/O ratio, c) reaction time, d) catalyst properties and e) feed composition [95]. At high temperatures, unwanted polyaromatics are formed causing catalyst

deactivation. Precursors of the undesired polymers may already be present in the feed or may be formed in the product species.

On this basis, coke formed on FCC catalysts can be classified as follows:

- Catalytic coke. This coke is formed as a by-product of catalytic cracking. It is deposited on the acid sites, mainly located in the micropores of the zeolite crystallites.
- Thermal coke. This coke is formed because of thermal cracking and is deposited on the matrices of the catalyst particles. The maximum expected thermal coke can be approximated with the Conradson Carbon Residue (CCR) of the feedstock [85].
- Contaminant coke. This coke is produced because of the dehydrogenating activity of Ni, Cu, V or Fe feedstock contaminants.
- Additive coke. This coke is produced by the impurities of the feedstock (from heavy molecules already present in the feed) [85,95].
- Catalyst to oil coke. This coke is formed by hydrocarbons trapped in the small FCC catalyst pores, which frequently show difficulties to be removed in the FCC stripper [17].

However, irreversible catalyst deactivation can be caused by factors other than coke. For instance, catalysts subjected to severe hydrothermal operations may lead to losses of crystallinity [96,97]. As well, FCC samples can be poisoned by undesirable elements, such as nickel, and/or vanadium [25,98]. Vanadium deactivates the active sites and form vanadic acid, while nickel increases undesirable products [99–101]

Given the significance of coke on FCC and the influence of C/O this PhD Dissertation, addresses catalytic coke and its effects on catalyst activity decay.

2.6.2 Coke Characterization:

Catalyst deactivation by coke has been under active research for more than 60 years [95,102]. Coke formation may be affected by chemical species catalytic cracking and diffusional transport

[17,80]. Coke can be characterized in terms of elemental composition, using carbon and hydrogen elemental analysis as determined by TOC (total organic carbon) analysis.

One should note that the catalyst sampling in FCC industrial riser units is limited to the unit exit. Thus, one is confined to look for alternatives. An option is to perform TOC coke analysis on catalyst samples obtained from FCC simulators such as the CREC Riser Simulator at various reaction times and temperatures.

2.7 Diffusion and Adsorption-Desorption of Chemical Species

Hydrocarbon diffusion and adsorption play a major role in catalytic cracking. For catalytic cracking to take place, reactants must be adsorbed on the catalyst matrix or on the micropore crystallites (zeolites). [92,102]. Hydrocarbon species diffusion may affect the overall catalytic reaction, and this may be the case when cracking occurs more quickly than in diffusional transport [92]. While diffusion in the catalyst matrix may belong to the molecular or Knudsen diffusivity regime, diffusion in the Y intracrystallite spaces may take place using the “configurational” regime [30,92,102].

2.8 Estimation of Cracking Kinetics and Catalyst Activity Decay during 1,3,5-TIPB Cracking.

2.8.1 Introduction.

Catalytic reactions lead to coke formation as a by-product [27]. It is well known that most of the active sites exist in an intracrystallite “zeolite pore structure” [15,20,103]. Thus, for the reaction to advance, molecules of reactants must diffuse within the network of micropores. Thus, the transport of hydrocarbon molecules through the zeolite micropores is highly dependent on the kinetic hydrocarbon reactant species molecular diameter [55]. Thus, catalytic cracking and diffusional steps, may both affect the overall extent of catalytic cracking [27,44,104].

2.8.2 Catalyst Deactivation Functions

Coke effects on catalyst activity can be described using several available deactivation models [26]. These models link catalytic activity decay to time-on-stream (TOS) [105] and the coke-on-catalyst (q_c) [106] variables.

In this respect, Voorhies 1945 [107] proposed a model where coke formation was primarily a function of the residence time (t):

$$q_c = \varepsilon t^m \quad (2.1)$$

with q_c represents the coke weight fraction and ε and m are adjustable parameters.

Voltz et al [108] confirmed that the Voorhies equation can be employed with different feedstocks. Later, Yates [109] discussed the inadequacy of Voorhies equation. These authors mentioned that this equation does not account for reactant composition, extent of conversion and hydrocarbon space velocity.

On the other hand, Levenspiel [46] considered an exponential catalyst decay function in terms of the catalyst time-on-stream (TOS or t_c):

$$\phi = \exp(-\alpha t_c) \quad (2.2)$$

with t_c representing the catalyst time-on-stream.

One should note that Eq. (2.2) does not consider the hydrocarbon concentration and/or the fraction of available active sites on the catalyst surface. Despite this, this empirical model has been used extensively in industrial refineries[110].

Furthermore, Levenspiel 1968 [46] argued that a catalyst activity decay function should include the rate of active site changes as follows:

$$-\frac{d\phi}{dt} = k_d \phi^m \quad (2.3)$$

with $\phi = 1$ at $t=0$

Or alternatively Eq. (2.3) can be expressed in the integrated form as follows:

$$\phi = [1 + k_d(m - 1)t_c^{-1/m-1}]^{-1/m} \text{ for } m \neq 1 \quad (2.4)$$

Eq. (2.4) becomes in fact Eq. (2.2), at $m=1$, or $\phi = \exp.(-k_d t_c)$

Regarding Eq. (2.4), and when considered it at long time-on-stream (TOS) or t_c , the $k_d(m - 1)$ term becomes larger than 1 with the following being obtained [12]:

$$\phi = Dt^n \quad \text{where } D = [(n - 1)K_d]^{-n} \quad (2.5)$$

Eq. (2.3) can also be expressed by including both the fraction of active sites and the feedstock concentration as follows:

$$-\frac{d\phi}{dt} = k_d C_A^2 \phi^m \quad (2.6)$$

where ϕ is the fraction of the active sites, t represents the TOS, k_d denotes the deactivation constant and m stands for the order of catalyst activity decay.

One should note that the above described models require the joint evaluation of k_d and n [110].

Bischoff (1968), and Froment and Bischoff [89], proposed as an alternative, an exponential decay function of coke concentration [108] as follows:

$$a = a_0 \exp(-\alpha q_c) \quad \text{or} \quad \phi = \exp.(-\alpha q_c) \quad (2.7)$$

with α being a decay constant.

Finally, Corella [44] suggested a decay model based on q_c or T-O-S (time-on-stream) as independent variable instead of C-O-C (coke-on-catalyst)

$$\text{or} \quad \phi = \exp.(-\alpha R) \quad (2.8)$$

Where α represents a crackability factor to be fitted experimentally (empirical parameter) and R corresponds to a TOS (time-on-stream) variable.

In summary, the modelling of catalyst deactivation has gone through significant changes since 1945. Empirically based functions such as exponential decay functions expressed in terms of TOS or q_c , have been considered to represent catalyst activity decay. Modifications of these functions such as the ones using the crackability factor appear to be inadequate [43].

Jimenez et al [79] recently proposed to represent catalyst activity using an effectiveness factor as shown below:

$$a_i = a_0 \eta_{Gs} \quad (2.9)$$

with a_i being the observed catalyst activity and a_0 being the initial value of activity at zero reaction time, η_{Gs} is a dimensionless overall effectiveness factor for spherical particles.

Jimenez et al[79] argued that the calculation of η_{Gs} or effectiveness factor should involve both internal and external transport processes. Furthermore, and regarding the coke deposited on the zeolite, one should evaluate the η_{Gs} (applicable to species diffusion-controlled transport) using the following equation:

$$\eta_{Gij} = \frac{1}{\phi_{ij}} \quad (2.10)$$

with ϕ_{ij} being the Thiele modulus of the j reaction and i chemical species

Furthermore, if coke is deposited on the catalyst inner particle surfaces, catalyst activity may change with reaction time.

Thus, it is anticipated that, as coke is deposited, the effectiveness factor decreases as the effective diffusivity given, shown below:

$$\frac{\eta_{G_{ij}}}{\eta_{G_{ij}}^{Ecat}} = \left(\frac{D_{effi}}{D_{effij}^{Ecat}} \right)^{0.5} \quad (2.11)$$

with D_{effi} representing the effective diffusivity for an individual (i) compound (m^2/s),

It is therefore expected, that the η_{Gs} will change with the variation of the pore volume fraction, resulting in coke deposition as follows:

$$\frac{\eta_{G_{ij}}}{\eta_{G_{ij}}^{Ecat}} = \left(\frac{\varepsilon_p}{\varepsilon_p^{Ecat}} \right)^{0.5} \quad (2.12)$$

Where ε is the internal void fraction of the catalyst ($\frac{m^3_{micropore}}{m^3_{particle}}$).

Thus, when this model is used, the observed catalytic activity is expected to diminish with the porosity or pore volume. One can anticipate, however, that the mathematical activity decay model as originally formulated by Jimenez et al [79], would require re-analysis using the species balances in the crystallites instead of using the FCC particle size.

2.9 Conclusions

The following are the main conclusion of the present chapter:

- a) Fluidized bed catalytic cracking modeling should consider the influence of temperature, reaction time and C/O ratio and its effect on coke formation, hydrocarbon conversion, and product selectivity. While these topics are well understood, there is still significant

uncertainty regarding the effect of C/O ratios and the needed catalyst decay models accounting for coke formation.

- b) Coke effect on catalyst decay has evolved over the years from empirical equations to more fundamentally based models. These fundamentally based kinetics are critical to describe catalytic activity decay and coke selectivity in FCC units.
- c) Establishing this kinetics including the critical influence of the C/O ratio is one of the main aims of the present PhD Thesis. With this end, experiments are developed in CREC Riser Simulator. This is the first experimental study showing the effect of coke selectivity via the changes of C/O ratio. These runs were developed progressively increasing catalyst loading in the CREC Riser Simulator as reported and discussed in CHAPTER 4, and CHAPTER 5.

Chapter 3

3 Experimental Methodologies

3.1 Introduction

This chapter reports the experimental equipment and procedures used in this PhD dissertation. The first section describes the properties of the materials employed. In addition, this chapter reports the various characterization techniques utilized to assess the effect of coke formation on the FCC Y-zeolite based catalyst.

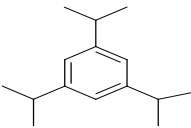
Following this first section, this chapter provides details of the mini-fluidized bed CREC Riser Simulator reactor system along with its various auxiliary components. This reactor was used in all the catalytic runs of this PhD dissertation.

3.2 Materials and Methods

3.2.1 Feedstock and Catalysts

In this study, the 1,3,5-TIPB chemical species was chosen as a model compound feedstock to evaluate the catalytic cracking of a Y-zeolite based catalyst. The 1,3,5-TIPB was selected as a model compound, given its special combination of aromatic and iso-paraffin functionalities [111,112]. Additionally, the 1,3,5-TIPB is considered a valuable chemical species given its 9.4 Å critical molecular diameter, which allows combined diffusional and catalytic effects in the Y zeolites to be evaluated [97,113–115]. All products from the 1,3,5-TIPB conversion were identified and quantified using GC-MS analyses as described in upcoming section 3.2.3. The main properties of the feedstock are outlined in Table 3.1 as follows:

Table 3.1 Characteristics of 1, 3, 5-Tri-Iso-Propyl-Benzene. [111]

Structure	Empirical Formulae	Molecular Weight/(Da)	Boiling Point/(°C)	Molecular Diameter/ Nanometer
	C ₁₅ H ₂₄	204.4	232-236	0.94

Regarding the FCC catalysts employed, three commercial equilibrium FCC Y-zeolite fluidizable catalysts with a 60–70-micron average particle size, were employed in this PhD thesis. These three catalysts were designated as CAT-A, CAT-B, and CAT-C, with their properties reported in Chapter 5 (section 5.2.1). These catalysts were characterized using XRD, XRF, NH₃ ammonia adsorption desorption, pyridine desorption and BET, as described in upcoming Section 3.3.

3.2.2 Catalytic Cracking with a Model Compound, and the Range of Operating Parameters Selected.

The 1,3,5-tri-iso-propyl-benzene (TIPB) has been widely employed as a model compound to evaluate and characterize catalyst activity and kinetic modelling in FCC [66,116]. The 1,3,5-TIPB cracking reaction is relatively easy to follow, given that one can identify and quantify various reaction products. With this information, rigorous kinetic modelling can be developed and catalyst deactivation by coke be determined. [54,70,71].

With this goal in mind, 1,3,5-TIPB catalytic cracking runs were developed in the CREC Riser Simulator, using the commercial catalysts denoted as CAT-A, CAT-B and CAT-C. Both thermal and catalytic runs were conducted under the following conditions: a) temperatures: 510, 530 and 550°C, b) contact times: 3, 5 and 7 seconds, c) catalyst-to-oil ratios (C/O ratio): 0.6,

0.8, 1.25, 2.5, 3.75 and 5. For every experiment, 0.2g of 1,3,5-TIPB was contacted with 0.12g, 0.16, 0.25, 0.5, 0.75, and 1g of catalyst amount. This was done, to achieve a C/O ratio in the range of 0.6 to 5.

Regarding the runs, they were developed under operating conditions that closely resemble those in FCC riser and downer units. This was required to validate the proposed coke formation mechanism model (refer to Chapter 4), and to provide adequate and reliable data for kinetic modelling (refer to Chapter 6). With this end and in the context of the present PhD studies, in excess to 670 runs were performed in the CREC Riser Simulator. This included thermal and catalytic cracking, with at least 5 repeats per experimental condition. This was carried out, to ensure the consistency, the reproducibility and the statistical significance of experimental results.

3.2.3 Analytical Methods

An Agilent Varian 6890 gas chromatograph unit (Santa Clara, CA, USA) was used to quantify various chemical species formed. This unit was equipped with a flame ionization detector (FID) and a 0.25 μm ID and 30 m length HP1 capillary column. During this analysis, the FID detector temperature was set to 320 $^{\circ}\text{C}$, while the column temperature was augmented at a rate of 5 $^{\circ}\text{C}/\text{min}$ starting from 35 $^{\circ}\text{C}$, up to 350 $^{\circ}\text{C}$. The 320 $^{\circ}\text{C}$ temperature was maintained for 22 min. Additionally, an Agilent 5973N mass selective detector (MSD) was employed for the identification of various chemical product species, with the help of the MSD Chemstation software library.

On this basis, gas phase detectable products were comprised of propylene, benzene, cumene and DIPB (di-isopropyl-benzene). These observed cracking products can be used to establish the 1,3,5 TIPB catalytic cracking network as described in Chapter 6.

Thus, given the above, the following 1,3,5 TIPB conversion and product selectivity parameters can be established using the following equation:

$$1,3,5 \text{ TIPB Conversion (\%)} = \frac{(M_{propylene} + M_{DIPB} + M_{cumene} + M_{benzene} + M_{coke})}{M_{1,3,5 \text{ TIPB}}} \times 100 \quad (3.1)$$

$$\text{Product Selectivity} - M = \frac{\text{Moles}_{i, \text{product}}}{\text{Moles of } 1,3,5 \text{ TIPB Converted}} \quad (3.2)$$

$$\text{Coke Selectivity} - W = \frac{M_{coke}}{M_{1,3,5 \text{ TIPB Converted}}} \quad (3.3)$$

Where M_i are the moles of “i” species (moles) in the gas phase, M_{coke} are the moles of coke formed on the catalyst, Selectivity-M are the moles of product “i” species per mole of 1,3,5-TIPB converted, and Selectivity-W are the grams of coke per gram of TIPB converted.

3.3 Catalyst Characterization

The various FCC catalysts used were characterized prior to and after catalytic cracking runs using the 1,3,5 TIPB model compound with the following methods:

- X-ray Diffraction (XRD)
- X-Ray Fluorescence (XRF) was used to establish the Ni, AL, Si, and V metal content.
- The N₂ Adsorption Isotherm (BET and pore size distribution PSD).
- The Temperature Programmed Desorption (TPD).
- Fourier Transform Infrared Spectroscopy (FTIR).

3.3.1 X-Ray Diffraction (XRD)

Powder X-ray diffraction (XRD) patterns of the catalysts of the present study were obtained by Ni-filtered Cu K α radiation ($\lambda = 0.15406$ nm). XRD diffractograms cover the 5–90° degrees of the 2 θ scale. The crystallinity and unit cell size per catalyst were determined by using the ASTM D-3942-85 method. High purity silicon powder (99%) was employed as an internal calibration standard. Unit cell size and crystallinity were calculated using XRD diffractograms as illustrated in CHAPTER 5.

3.3.2 X-Ray Fluorescence (XRF)

XRF was used to determine the metal content (Ni, Al, Si, Fe, Ca, and V) of the FCC catalysts studied. Metals can contribute to irreversible catalyst deactivation [102,117,118]. Metals on the catalyst can be traced to VGO impurities (e.g. Ni, V containing species [98,119]. Deposited metals may also affect catalytic activity and selectivity. This is the case for vanadium reacting with zeolite framework, forming vanadic acid as well as for nickel, depositing in the zeolites and increasing undesirable hydrogen formation [120]. Observed metals content of different catalysts are reported in appendix C2.

3.3.3 N₂ Adsorption Isotherm (BET) and Pore Size Distribution PSD)

The FCC catalyst can be affected by hydrothermal aging (dealumination) with a loss of surface area. [23,121,122]. Thus, for each catalyst studied, the specific surface area, the pore volume, and the pore size distribution (PSD) were determined by using an ASAP 2010 Analyzer BET for nitrogen adsorption (Norcross, GA, USA) at 77K. Samples were degassed at 200 °C for 4 hours, prior to analysis. The pore size distribution (PSD) was established by plotting the dV/dD (the differential pore volume) as a function of the pore diameter (D) [123]. The integration of the differential pore volume function provided the total pore volume (PV). Furthermore, the consideration of the PSD allowed us to determine micropores (7Å-12Å) and mesopores (>12Å) [76].

3.3.4 Temperature Programmed Desorption (TPD)

NH₃-TPD was employed to determine the total acidity of the catalysts studied. This was achieved by measuring the amount of ammonia desorbed while heating catalyst samples (up to 550 °C), using a 15 °C/min heating ramp. For each TPD, a 0.1–0.2 g of catalyst sample was first pretreated for 1 h at 650 °C while in contact with a 50 mL/min helium carrier. Following this, the catalyst sample was cooled down to 100 °C and was contacted with a 5% NH₃/He gas mixture for 1 h. Then, the catalyst sample was heated progressively at a rate of 15 °C/min under a 50 mL/min helium flow. Heating continued until 650 °C was reached. Due to the progressive heating, ammonia was gradually desorbed from the catalyst and measured with a thermal conductivity detector (TCD).

3.3.5 Fourier Transform Infrared Spectroscopy (FTIR)

FTIR spectroscopy was also employed in conjunction with pyridine desorption to quantify the ratio of Brønsted and Lewis acid sites. Pyridine analysis was conducted in a Bruker FTIR (Billerica, MA, USA). Prior to measurements, the zeolite samples were first dried in a furnace tube under nitrogen flow, at 550 °C for 2 h. Then, a pyridine/nitrogen gas mixture was contacted with the catalyst at 100 °C for 1 h. Following this, with the temperature at 100 °C, a nitrogen flow was introduced into the furnace tube to remove weakly adsorbed pyridine species. After this stage, the catalyst sample was placed on a sodium chloride wafer with the pyridine FTIR spectrum of adsorbed species being recorded using a diffuse reflectance Fourier-transform Infrared Spectrometer (DRIFTS). The catalyst sample was dispersed in a KBr wafer and analyzed by using the FTIR technique. The details of the spectral ranges and the IR bands of the pyridine adsorption detected are described in Chapter 4.

3.4 Catalytic Reactor System

3.4.1 Experimental Setup:

The design and assembly of the CREC Riser Simulator is described in Figure 3.2. The CREC Riser Simulator is constituted by two main sections, an upper and a lower reactor shell. The lower shell holds a catalyst basket. The two shells allow easy access to the reactor basket for the loading and unloading of the catalyst. Two grids placed at the top and bottom of the basket constrain catalyst mobility inside the basket. Additionally, the reactor is equipped with an impeller located in the upper reactor section. Rotation of the impeller at 5700 rpm facilitates particle fluidization and hydrocarbon species recirculation. This forced movement of the gases causes FCC particles to be fluidized.

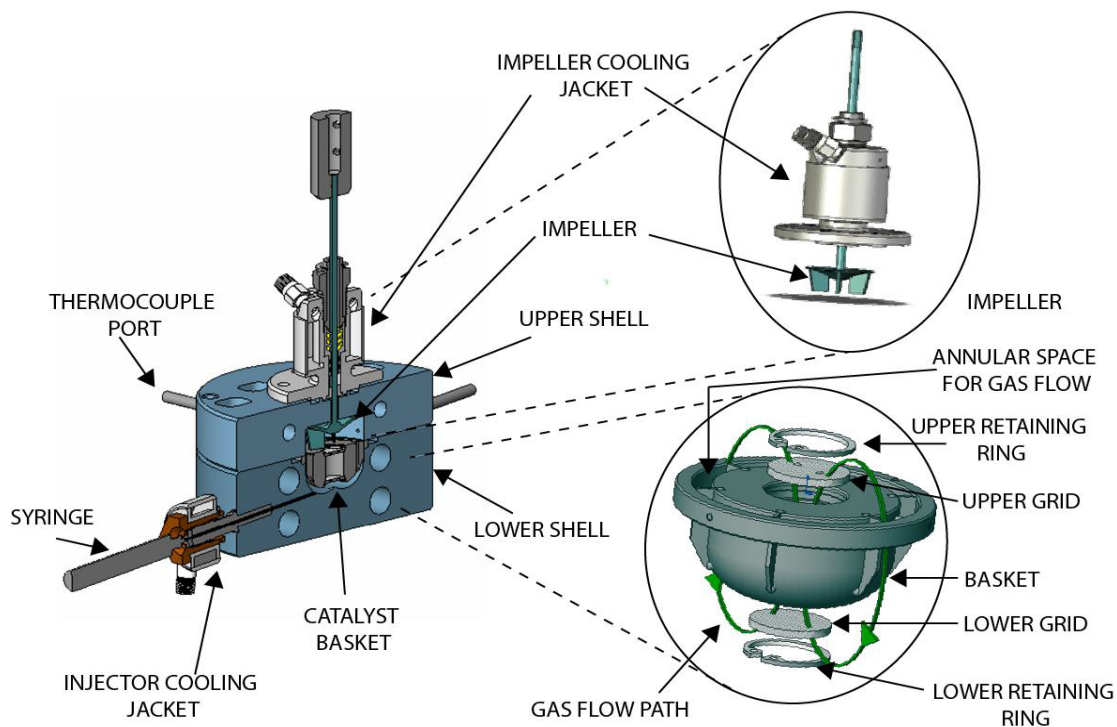


Figure 3.1 Sectional View of the CREC Riser Simulator Reactor with the Detailed Assembly of the Catalyst Basket and Impeller. The green line shows the gas flow path upon rotation of the impeller [124]

The CREC Riser Simulator operates in association with other accessories, such as a vacuum box, a gas chromatograph (GC), a series of sampling valves, a timer, two pressure transducers and two temperature controllers. A schematic diagram of the CREC Riser Simulator, along with the major accessories is illustrated in Figure 3.3. The vacuum box, which is a stainless-steel cylinder is connected to the reactor by a four-port valve that enables the connection-isolation of the reactor and the vacuum box. A timer is connected to an actuator, which operates the four-port valve. This timer is used to set the reaction time for every experimental run.

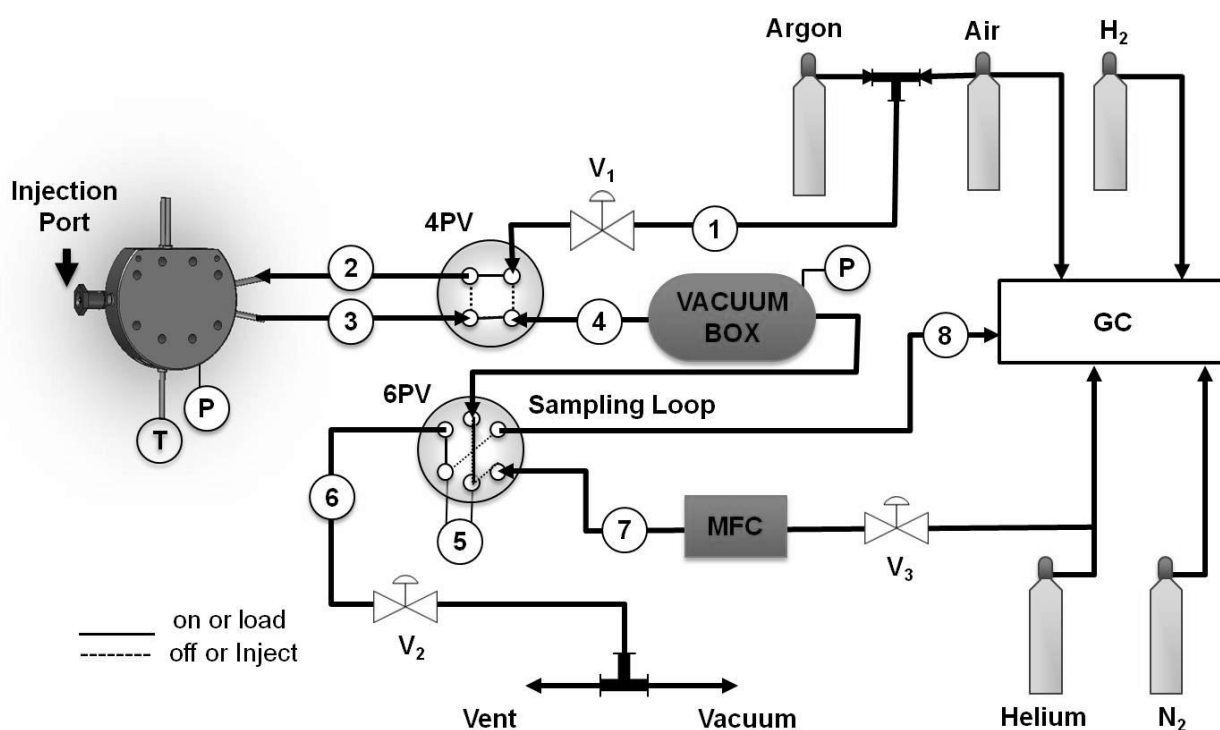


Figure 3.2 Schematic Diagram of the CREC Riser Simulator Experimental Setup [42]

3.4.2 Experimental Procedures:

All thermal and catalytic runs were conducted in CREC Riser Simulator as described in the former Section 3.4.1. Various amounts of catalyst, from 0.12 to 1g, were loaded into the catalyst basket. Following this, the reactor unit was sealed and heated to 650°C. Then, air was circulated in the reactor for a 20-minute period. This was done to combust the coke formed on catalyst. Following this, the reactor was cooled down to reach the selected reaction temperature (e.g. 550°C) with argon being circulated for 10 min. This allowed air to be completely purged from the reactor system. Once the desired pre-set reactor temperature was achieved, the vacuum box at typically 300°C, was also brought to 1.5 psi of vacuum pressure. Then, the impeller of the reactor was rotated at 5500rpm. This was done to fluidize the catalyst sample contained in between the two basket grids [83].

At this stage, the reactor system was considered ready to start a run. In fact, a run was initiated immediately once the 0.2 g of TIPB (feed) was injected in the reactor via the injection port. Once this was accomplished, the hydrocarbon sample was vaporized almost instantaneously. The run continued for a pre-set reaction time (e.g. 5 s.) with the hydrocarbon species and the fluidized catalyst being in close contact. Once the pre-set reaction time was attained, the reactor contents were evacuated to the vacuum box through a 4PV (four-port valve). The evacuation of the reactor contents was quick. This was the case given the pressure difference between the reactor and the vacuum box. In this manner and given that all the catalyst remained in the reactor basket, it was considered that all cracking reactions were essentially arrested at this time.

Once the reactor contents were completed, the hydrocarbon sample was transferred to a GC-MS for analysis through a transfer line. The GC-MS analysis allowed identification and quantification of all hydrocarbon species, and calculation of both hydrocarbon conversion and product selectivity.

Following this, the FCC catalyst was removed from the catalyst basket. A TOC (Total Organic Carbon) analysis on the catalyst was performed using a TOC-V_{CPH} Analyzer from Shimadzu (Kyoto, Japan). In the TOC analyzer, an infrared detector measured the total moles of CO₂ formed by coke combustion. With this information, the moles of coke formed were calculated

and the coke-on-catalyst (COC) was established as a weight fraction. Coke was burned under air flow at 900°C. A thermal conductivity detector (TCD) measured the total moles of CO₂ formed by combustion. With this information, the moles of coke were calculated and the weight fraction of the coke-on-the catalyst (COC) was established.

3.4.3 Thermal Runs

Preliminary studies included thermal cracking runs developed in the CREC Riser Simulator using an empty reactor: no catalyst was loaded in the basket. This allowed assessing the effects of thermal conversion on the overall 1,3,5-TIPB conversion. Furthermore, and to confirm the minor influence of thermal cracking, runs were also developed using a reactor basket loaded with an inert solid (hydroxyapatite), with no detectable acidity. These thermal cracking runs were developed at the three reaction temperatures and the three reaction times of the catalytic runs (refer section 3.2.2)

3.5 Gas Phase Sampling

One important feature of the CREC Riser Simulator reactor is its capability to shed light into the potential influence of hydrocarbon intra-catalyst diffusional effects [125]. This is the case, given that it can be operated with two possible sampling modes:

- a) *Sampling Mode 1*: Reactor at Quasi Total Evacuation. This is in fact the sampling mode described in Section 3.4.2. In this case, once the selected reaction time was reached, almost the entire hydrocarbon species reactor contents were transferred to the vacuum box for further GC-MS analysis. It was found that the GC-MS data can be used to accurately and reliably establish the total amount of hydrocarbon species present and the overall TIPB hydrocarbon conversion. This mode of operation was in fact, the mode of operation considered in most of experimental runs of this PhD dissertation.
- b) *Sampling Mode 2*: In this sampling mode, while all run preparation steps were identical to the ones of Mode 1, the vacuum box was set at a total pressure of close to atmospheric pressure (13.5-14.7psia). Thus, in this case, only the hydrocarbon species in the reactor gas

phase was transferred to the vacuum box. The data resulting from this sampling mode was used to assess potential inaccuracies in the overall TIPB conversion as a result of 1,3,5-TIPB intraparticle diffusional effects.

3.6 Conclusions

This present chapter describes the various methods successfully studied in this PhD Dissertation.

- a) The BET specific surface area, the N₂-adsorption isotherm, and the particle size distribution methods were used successfully to establish the structural and physicochemical properties of the catalysts.
- b) The XRD was utilized with advantage to establish the crystallinity and the unit cell size of the Y zeolites of the FCC catalyst used.
- c) The NH₃-TPD and pyridine desorption was valuable to determine catalyst total acidity, and Brönsted and Lewis acid site ratios, respectively.
- d) The fluidized CREC Riser Simulator reactor, proved to be a reliable device to evaluate the hydrocarbon conversion, as well the product selectivity of the 1.3.5-TIPB model compound.

Chapter 4

4 Cracking of 1,3,5-TIPB over CAT-A

4.1 Introduction

This chapter aims to report the experimental results obtained from thermal cracking and catalytic cracking using 1,3,5-TIPB over a commercial FCC catalyst designated as CAT-A. A detailed description of these trends in terms of 1,3,5-TIPB conversion, coke selectivity, product selectivity, along with catalyst characterization data, is also provided in the subsequent sections of this chapter.

4.2 Catalyst Characterization

4.2.1 X-Ray Diffraction

X-ray diffraction was used to identify the Y zeolite structure in the catalyst. This was done given the observed Y zeolite characteristic diffraction bands of the CAT-A particles as reported in Table 4.1. Table 4.1 shows a comparison of the characteristic XRD bands for the CAT-A and the ones reported for the Y zeolites [Gianetto, A. 1993 [126]]. One can notice the similarity of the observed bands obtained from the CAT-A and those from the cited reference. As a result, it was confirmed that the zeolites embedded in the matrix were of the Y type.

Table 4.1: Characteristic XRD Diffraction Bands at Various 2θ Values for the CAT-A and for a NaY Zeolite as reported by Gianetto, A. 1993.

<i>Peak</i>	<i>NaY Zeolite</i>	<i>Cat-A</i>
1	6.24	6.28
2	7.16	7.11
3	11.47	10.88
4	13.78	12.05
5	14.92	15.02
6	18.16	19.11
7	20.84	20.83
8	24.22	24.12
9	26.5	26.16
10	27.5	27.42
11	30.2	30.08
12	31.00	31.02
13	31.5	31.4
14	32.36	32.90
15	35.42	35.41
16	36.62	36.35
17	37.96	37.61
18	38.5	38.71
19	39.7	39.80
20	41.54	41.58
21	43.44	43.36

4.2.2 NH₃-TPD (Temperature Programmed Desorption)

Figure 4.1 reports the NH₃-TPD analyses for four CAT-A samples as follows: a) Continuous black line: FCC catalyst free of coke, b) Continuous blue line: FCC catalyst with 0.193 wt.% of coke, c) Continuous red line: FCC catalyst with 0.178 wt.% of coke, d) Continuous violet line: FCC catalyst with 0.236 wt.% of coke, and e) Continuous green line: FCC catalyst with 0.263 wt.% of coke, f) Continuous blue line: represents experiment baseline.

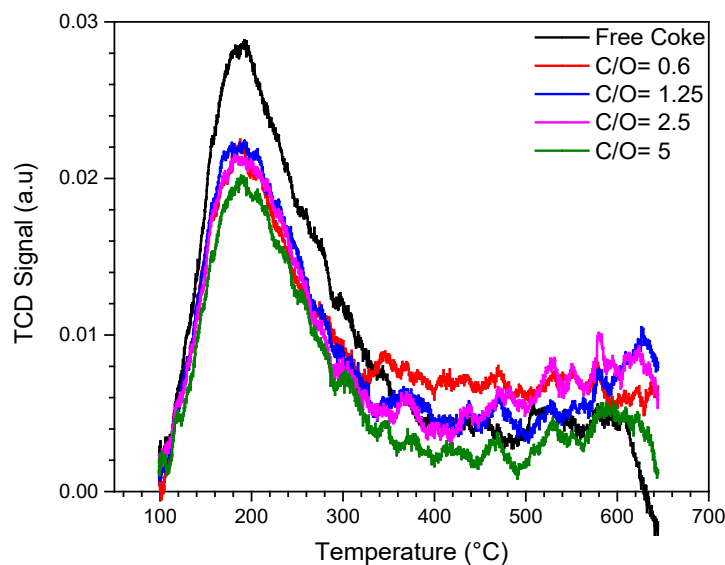


Figure 4.1 NH_3 -TPD Analyses for CAT-A. Notes: Continuous black line: FCC catalyst free of coke; Continuous red line: C/O= 0.6; Continuous blue line: C/O=1.25; Continuous violet line: C/O=2.5; continuous green line: C/O=5; Continuous blue line: experiment baseline.

One can observe as shown in Figure 4.1, that there is a reduction in catalyst acidity, with this being particularly noticeable when the catalyst to oil ratio was increased from 2.5 to 5. In this case, the NH_3 adsorbed as recorded by TPD decreased from 78 to 67 cm^3 STP/g NH_3 -TPD.

4.2.3 Nitrogen Adsorption and BET (Brunauer-Emmett-Taller)-Specific Surface Area.

The catalyst specific surface area, pore volume and pore size distribution of the CAT-A samples were determined using ASAP 2010 Analyzer. Figure 4.2 reports the nitrogen adsorption isotherms effected at 77 K for the following catalyst samples: a) A regenerated CAT-A free of coke, b) A coked CAT-A catalyst following runs at 550 °C and 7s, using 0.8, 1.25, 2.5, 3.75, and 5 C/O ratios:

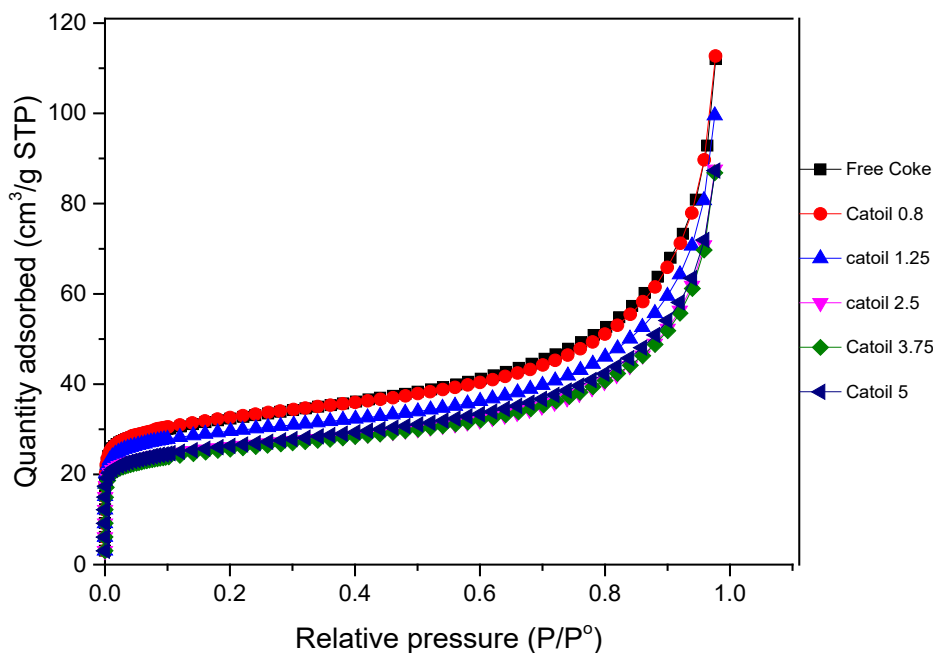


Figure 4.2 Nitrogen Adsorption Plots affected at 77 K.

Table 4.2 summarizes the catalyst specific surface area (SSA) and catalyst pore volume (PV) that were calculated based on the data reported in Figure 4.2. One can notice a progressive reduction in both the SSA and PV with the increasing catalyst/oil ratio (C/O): from 99.6 m²/g and 0.1586 cm³/g to 78.5 m²/g and 0.123 cm³/g, respectively. To ascertain these changes using the selected samples, up to three repeats were performed. A 3% standard deviation for specific surface areas was noticed.

Table 4.2: Specific Surface Area [SSA] (m²/g), Pore Volume [PV] (cm³/g), and Mesopore Volume (cm³/g) for CAT-A, Following Catalytic Cracking Runs at 550°C and 7 s, Using Different C/Os. SD on repeats: +/- 3 m²/g.

CAT-A Catalyst Samples						
	Free Coke	C/O= 0.8	C/O=1.25	C/O=2.5	C/O=3.75	C/O=5
BET (SSA)	99.6	99.0	86.9	85.75	80.4	78.5
Pore Volume (PV)	0.158	0.158	0.141	0.135	0.122	0.123
Mesopore Volume	0.112	0.111	0.0983	0.0941	0.0840	0.085
Micropore Volume	0.0468	0.047	0.0421	0.0409	0.0379	0.038

Thus, the reduction of both the SSA and the PV at higher C/O ratios, suggests that higher C/Os lead to increased coke per unit weight of catalyst. However, and to fully characterize the extent of pore deactivation by coke, one should consider the CAT-A micropore volume in the 7-20 Å range [80].

Table 4.2 and Figure 4.3 both report the micropore volume of the regenerated *CAT-A* (free of coke) and the micropore volume of *CAT-A* after runs at 7s, 550°C and C/O=5. It is shown that increased C/Os lead to considerably diminished macropore and micropore volumes, decreasing from 0.112 cm³/g to 0.085cm³/g and from 0.0468 cm³/g to 0.038 cm³/g, respectively. This is consistent with an augmented coke formed per unit weight of catalyst, which is the case for higher C/Os. This diminish activities are in the line with other finding [129].

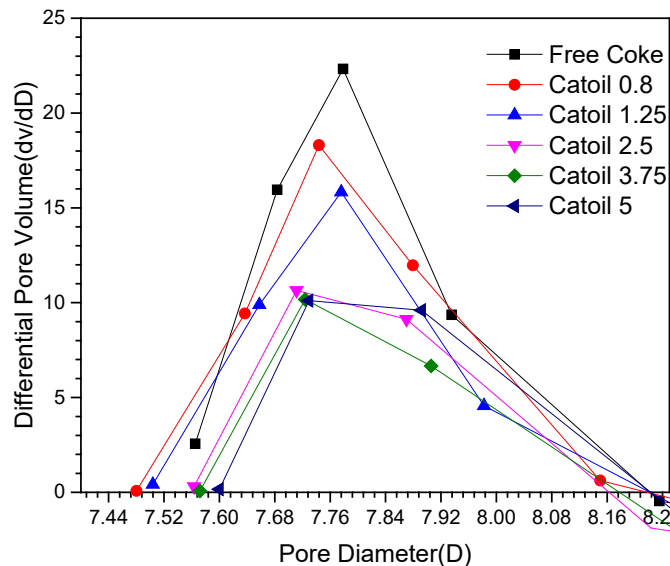


Figure 4.3 Differential Pore Volume (dV/dD) as a Function of the Pore Diameter (D) Using the N_2 -Adsorption Isotherm. (■) CAT-A free of coke; (●) CAT-A at $C/O = 0.8g/g$; (▲) CAT-A at $C/O = 1.25g/g$; (◄) CAT-A at $C/O = 2.5g/g$; (▼) CAT-A at $C/O = 3.75g/g$. CAT-A sample

4.2.4 FTIR Pyridine Adsorption (FTIR):

Figure 4.4 reports the pyridine desorption FTIR spectra for CAT-A, for both the free of coke as well as the coke deactivated catalyst samples.

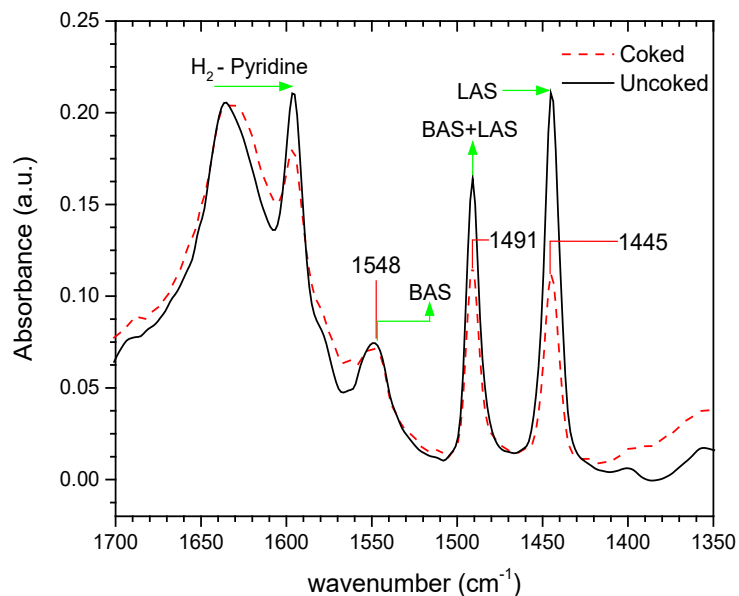


Figure 4.4 Pyridine Desorption FTIR Spectra for CAT-A. The CAT-A "Free of Coke" is Represented by a Solid Line and the CAT-A "Deactivated by Coke" is Represented by a Dashed Line.

To characterize the acid sites covered by coke, a recommended FTIR spectral range between 1700 and 1350 cm^{-1} [30,125,127,128] was selected. Within this range, four IR bands of pyridine adsorption were recorded. From these bands, the 1548 cm^{-1} and 1445 cm^{-1} bands were assigned to Brönsted acid sites (BAS) and Lewis acid sites (LAS), respectively. Furthermore, the 1491 cm^{-1} peak was considered as a Brönsted and Lewis acid site combined band. Finally, the 1600 cm^{-1} band was assigned to hydrogen-bonded pyridine [30,125]

On this basis and by examining the 1445 cm^{-1} and 1548 cm^{-1} band areas of a "free of coke" and of a "coked" CAT-A, respectively, one was able to notice a higher Lewis site density (LAS) for the "free of coke" catalyst, while the Brönsted acid site (BAS) density remained essentially unchanged.

Table 4.3 reports the relative acid strengths of the Brönsted /Lewis ratios of CAT-A prior to and after being exposed to a hydrocarbon mixture. This led to a Brönsted/Lewis site density ratio being increased from 0.30 to 0.38 comparing, with this showing that most of coke was formed on the weak Lewis acid sites (LAS) instead of on the Brönsted sites (BAS).

Table 4.3: Relative Brönsted /Lewis Acid Site Ratios using Pyridine FTIR. CAT-A samples with coke were analyzed following catalytic cracking runs at 550°C and 7 s.

Catalyst Samples	Brönsted /Lewis acid sites
<i>CAT-A</i> [free Coke]	0.30
<i>CAT-A</i> [Coked]	0.38

4.3 1,3,5-TIPB Conversion, and Product Selectivity on the Gas Phase.

Preliminary hydrocarbon catalytic cracking runs were carried out over the catalyst denoted as CAT-A. All runs were developed in the CREC Riser Simulator at 550°C and contact times of 3, 5, and 7s. In every experiment, 0.2g of 1,3,5-TIPB were contacted with 1g of fluidized catalyst. Thus, a catalyst/oil ratio of 5 g-cat/g-oil was established.

Data obtained from these experiments was analyzed using the two modes of sampling described in Section 3.6. These two modes of sampling allowed one to establish the significance of transport processes in the FCC catalyst (intracrystallite transport influence) [125] using the CREC Riser Simulator.

Figure 4.5 reports the 1, 3, 5 TIPB conversion using the two modes of sampling: a) with the vacuum box pressure set at 1.5 psia, b) With the vacuum box pressure set at 13.7 psia.

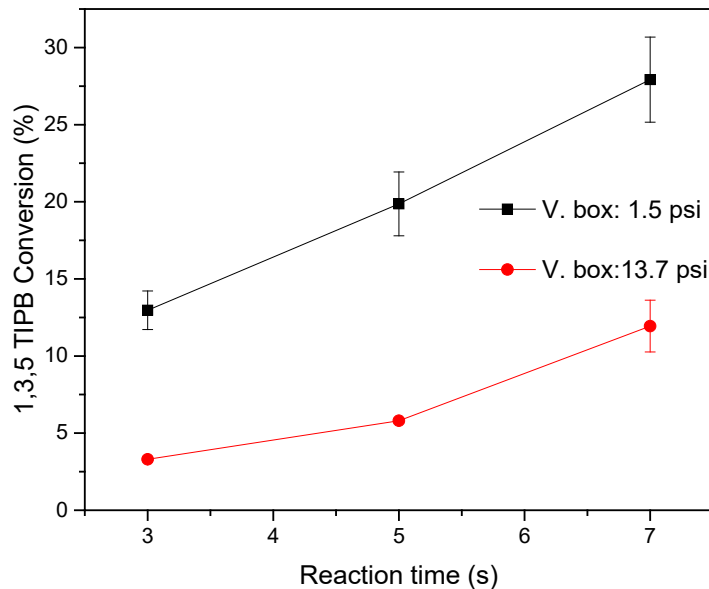


Figure 4.5 Reported Effect of the Vacuum Box Pressure on the 1,3,5 TIPB Conversion Using CAT-A. Notes: Contact times: 3s, 5s & 7s. Temperature: 550 oC. Reported data and standard deviations (vertical bars) represent average values from 3-5 repeat runs.

One can thus see, that the 1,3,5 TIPB conversion calculated with the entire reactor contents, using a 1.5 psia vacuum box pressure was significantly higher than the one with the vacuum box at 13.7 psia. This result means that the 1,3,5 TIPB may have been diffusionaly hindered while being evacuated and that the 1,3,5 TIPB conversion was incorrectly established. Thus, limiting the vacuum box pressure to 1.5 psia or a Mode 1 of sampling, provides a better representation of all chemical species present at a particular reaction time.

Figure 4.6 establishes the observed molar fractions for both 1,3,5 TIPB and propylene using the two modes of sampling. Mode 1 provides the more reliable definition of the chemical species present in the reactor unit.

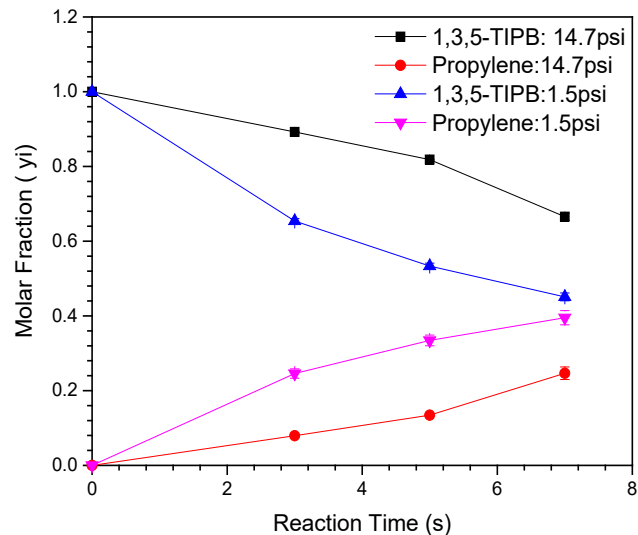


Figure 4.6 Molar Fractions of 1,3,5 TIPB and Propylene in the CREC Riser Simulator for: (i) Pressure in vacuum box=1.5 psi and (ii) Pressure in vacuum box=14.7 psia. Note: Reported values represent averages from at least 3 repeats.

On this basis, all the data reported in this PhD Dissertation was established using the Sampling Mode 1. This was done to be able to adequately assess all chemical species molar fractions at various reaction times.

4.4 Cracking Experiments:

The operation of FCC units calls for a better understanding of the catalyst/oil ratio effects on unit performance [1]. The likely anticipated results are to achieve the following at higher C/Os: a) higher 1,3,5 TIPB conversions at set contact times, or alternatively b) close 1,3,5-TIPB conversions with shorter reaction times. Proving these assumptions is an important goal of the present PhD dissertation.

Catalytic cracking runs of 1,3,5-TIPB were developed in the CREC Riser Simulator, using a commercial catalyst (CAT-A). Both, thermal and catalytic runs were conducted under the following conditions: a) 510, 530 and 550°C temperatures, b) contact times: 3, 5 and 7 seconds, c) 0.6, 0.8, 1.25, 2.5, 3.75 and 5 catalyst-to-oil ratios (C/O ratio).

Given that one of the main objectives of the current study, was to clarify the effect of the catalyst-to-oil ratio (C/O), the TIPB amount fed was kept constant while catalyst loading was increased. As a result, catalytic cracking experiments were developed by varying the C/O parameter widely. This was required to validate the proposed coke formation mechanism model to be discussed in upcoming sections.

To accomplish this, 475 runs were conducted in total. This included thermal and catalytic cracking runs, with at least 5 repeats per experimental condition. Run repeats ensured reproducibility and the statistical significance of experimental results.

4.4.1 Thermal Cracking Runs:

Preliminary studies included thermal cracking runs in the CREC Riser Simulator with a reactor loaded with an inert solid (hydroxyapatite) only. Various reaction times and temperatures were considered.

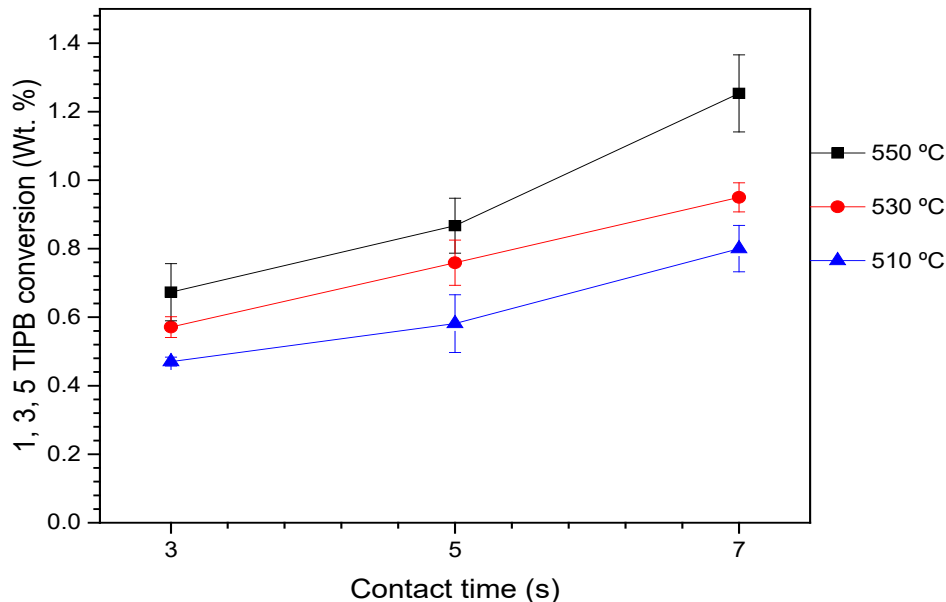


Figure 4.7 Influence of Contact Times (3-7s) and Temperatures (510-550 °C) on 1,3,5-TIPB Thermal Cracking. Vertical bars represent standard deviations from at least 5 repeat runs.

One can observe that all thermal conversions were below 2% with ethylene, propylene and coke being the main products. In this respect, one should emphasize that 7 seconds was the longest anticipated reaction time and 550°C was the highest predicted temperature. It was on this basis assumed, that thermal cracking effects on 1,3,5-TIPB catalytic conversion were negligible. [7,36]

4.4.2 Catalytic Cracking Runs

4.4.2.1 Effect of Operating Conditions on 1,3,5-TIPB Conversion, Coke Formation, and Product Selectivity at C/O=2.5

A first series of systematic catalytic runs was developed with the CAT-A loaded in the CREC Riser Simulator basket, using a set C/O ratio of 2.5. Figure 4.8 reports a progressive increase of TIPB conversion with an augmentation both in temperature and in reaction time. One should notice that these results are in line with the ones already reported in the technical literature by others [30,36,42,79,129] using the CREC Riser Simulator.

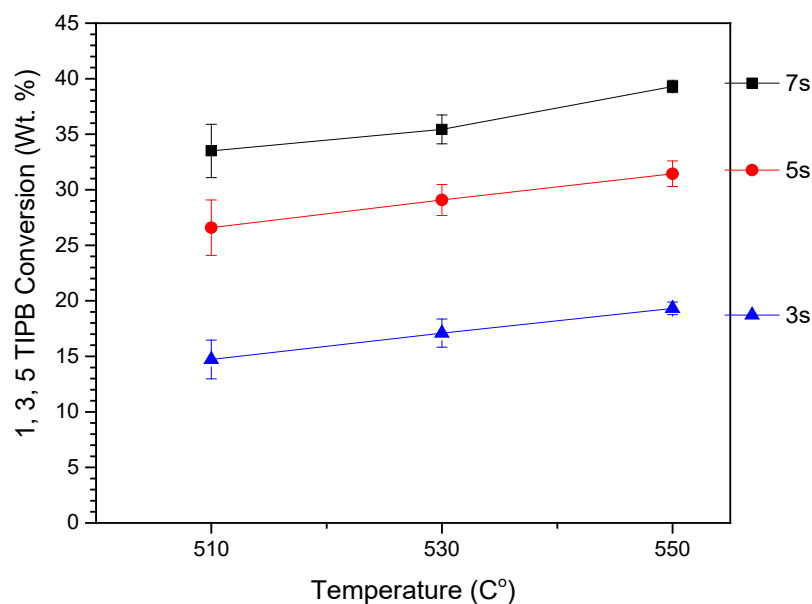


Figure 4.8 Effects of Temperature and Reaction Time on the Conversion of 1,3,5 TIPB on CAT-A. The C/O was set to 2.5. Reported data and standard deviations (vertical bars) represent experimental data from at least 5 repeats.

Moreover, Figure 4.9 describes the changes of $q_c \times 100$ (percentual coke concentration in g coke/catalyst $\times 100$). Figure 4.8 reports the expected increase of q_c with both temperature and reaction time.

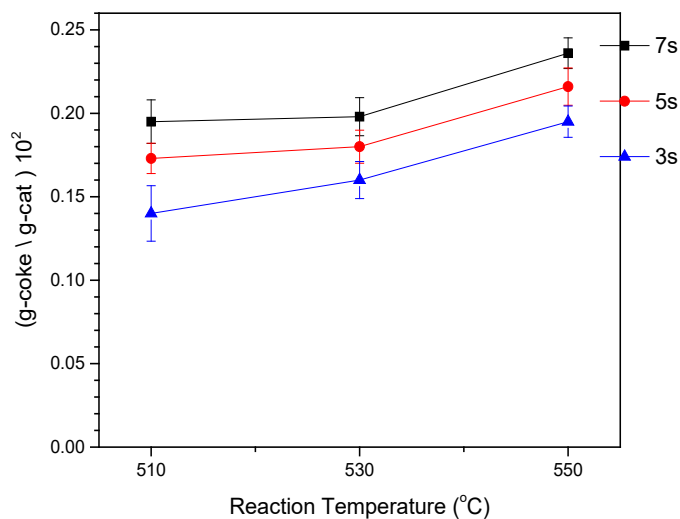


Figure 4.9 Effects of Temperature and Reaction Time on the Coke Formation while Cracking 1,3,5-TIPB over CAT-A. The C/O was set to 2.5. Reported data and standard deviations (vertical bars) are from 4-7 repeat runs.

Finally, Figure 4.10 describes the changes of propylene selectivity (moles of propylene formed / moles of 1,3,5 TIP converted). One can notice an increase of propylene selectivity with a rise in temperature, as well as with an increase in reaction time (3-7). This can be assigned to the more dominant effect of thermal cracking at the higher temperatures.

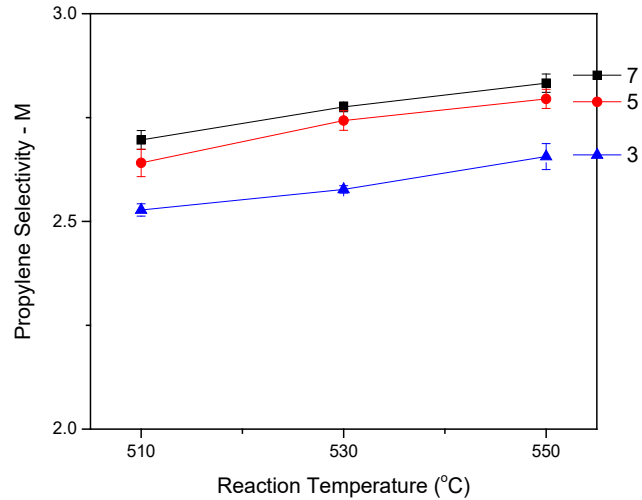


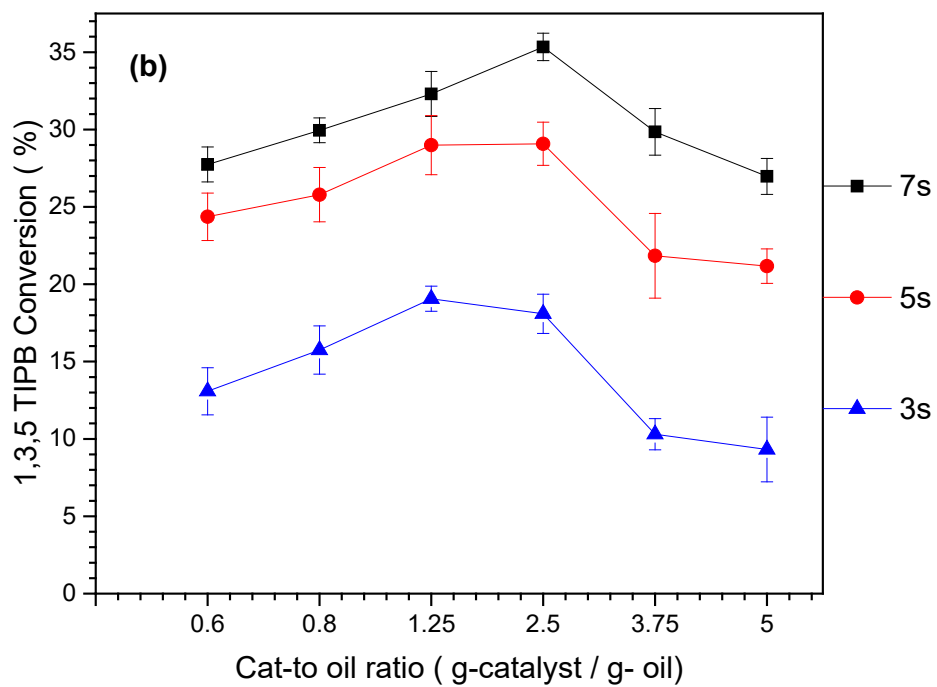
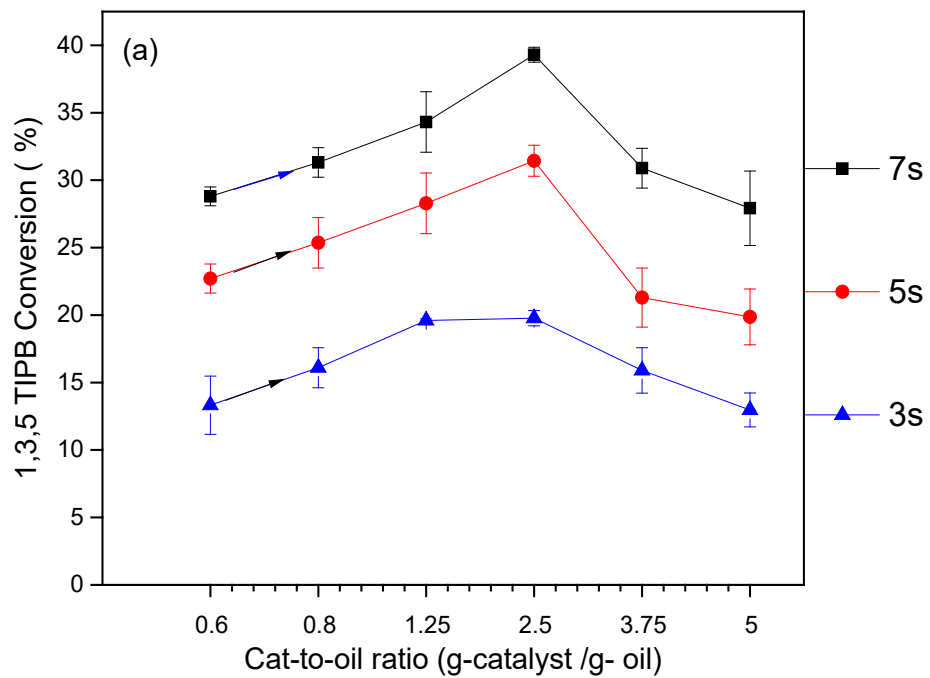
Figure 4.10 Influence of Contact Time and Temperature on the Propylene Selectivity-M during 1, 3, 5-TIPB Conversion using CAT-A. Reported data and standard deviations (vertical bars) represent average values from 4-7 repeat runs.

In summary, the observed changes of 1,3,5-TIPB conversion, product selectivity, and coke concentration seen at C/O=2.5 are in line with anticipated trends. These experiments help to support and validate the results obtained in the CREC Riser Simulator and to demonstrate that the results of this PhD study are in line with data obtained by others in the CREC Riser Simulator [79–81,111,130]

4.4.2.2 Effect of C/O Ratio [g cat g feed⁻¹] in the 0.6 to 5 Range on 1, 3, 5, TIPB Conversion, Coke Formation, and Product Selectivity.

4.4.2.2.1 1,3,5-TIPB Conversion:

Figures 4.11a, 4.11b and 4.11c report the changes of 1,3,5 TIPB conversion with C/O ratio at various thermal levels and reactions times.



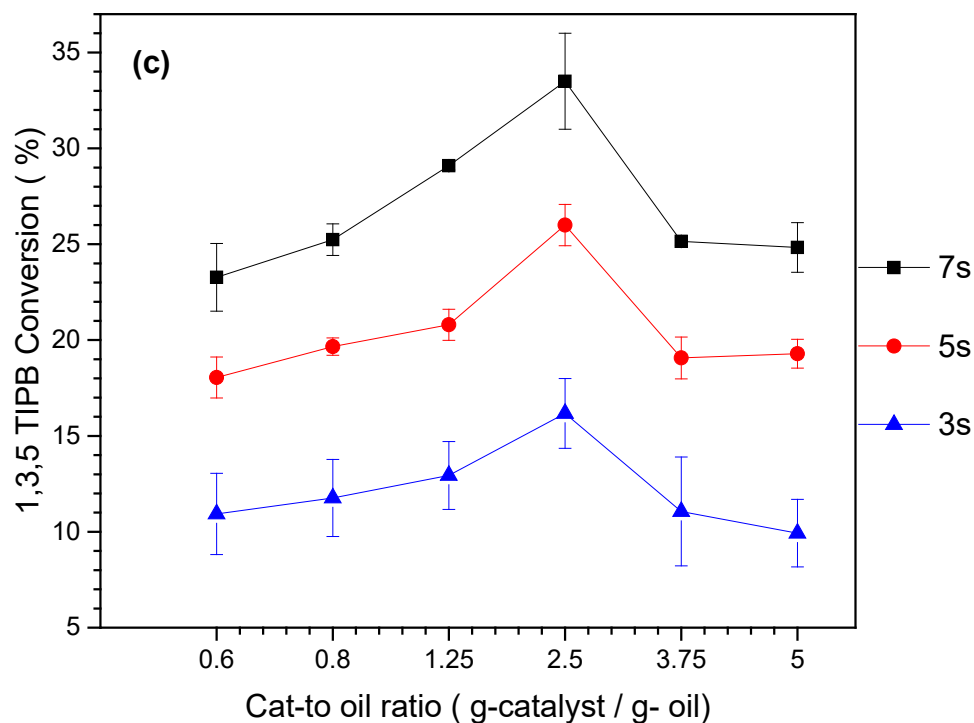


Figure 4.11a, 4.11b and 4.11c. Effects of Contact Time, and C/O Ratio on the 1,3,5-TIPB Conversion using CAT-A at 550 oC for Figure 11(a), 530 oC for Figure 11 (b) and 510 oC for Figure 11 (c). Contact times: 3s, 5s & 7s. Reported data and standard deviations (vertical bars) represent average values from at least 5 repeat runs.

One can thus see, that consistently and for 510, 530 and 550 °C and 3, 5 and 7 seconds, higher C/Os lead to higher 1,3,5-TIPB conversions first, with 1, 3, 5 TIPB conversions stabilizing at C/Os in the range of 2.5. However, when the 2.5 C/O ratio is surpassed, the 1,3,5-TIPB conversion is not increased but reduced instead.

In this respect, Figure 4.10a reports 1,3,5-TIPB conversions of 13.3%, 22.7% and 28.8 % at a C/O ratio of 0.6, a temperature of 550°C and 3s, 5s, and 7s contact times, respectively. Furthermore, it can also be observed in Figure 4.10a that at the C/O ratio of 2.5, at a temperature of 550 °C and contact times of 3s, 5s, and 7s, the 1, 3, 5-TIPB conversions reached 19.7, 31.4 and 39.3 %, respectively. Similar trends were observed at 530°C and 510 °C, as illustrated in Figures 4.10b and 4.10c, with however, at C/O ratios higher than 2.5, a consistent reduction in 1,3,5-TIPB conversions.

Moreover, Figure 4.11 reports that despite the potential changes in 1,3,5-TIPB and in coke formation with the C/O ratio, propylene selectivity remains consistently in the 1.7-2.7 range. This is below the expected stoichiometric value of 3 for complete conversion of the 1,3,5-TIPB into benzene. One can also notice in Figure 4.12, that the highest propylene selectivity value of 2.7 is attained consistently at the highest C/O ratios.

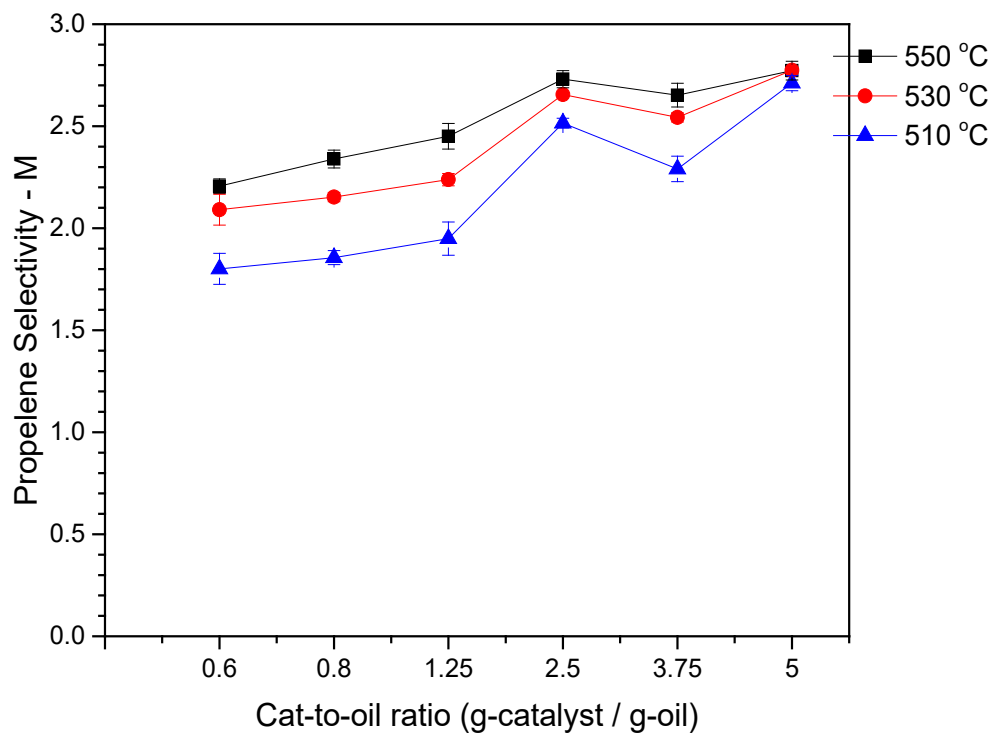


Figure 4.12 Effect of Temperature on Propylene Selectivity at various C/O Ratios using Cat-A. Notes: Contact time: 7s. Reported data and standard deviations (vertical bars) represent average values from at least 5 repeat runs. Note: Propylene Selectivity-M is defined as the moles of propylene per mole of TIPB converted.

Furthermore, Figure 4.13 describes the selectivity changes of various dealkylation products as a function of the 1,3,5-TIPB conversion. This figure shows that by increasing the C/O ratio, equivalent to the directions shown with arrows, this leads to benzene selectivity augmenting steadily as a final cracking product.

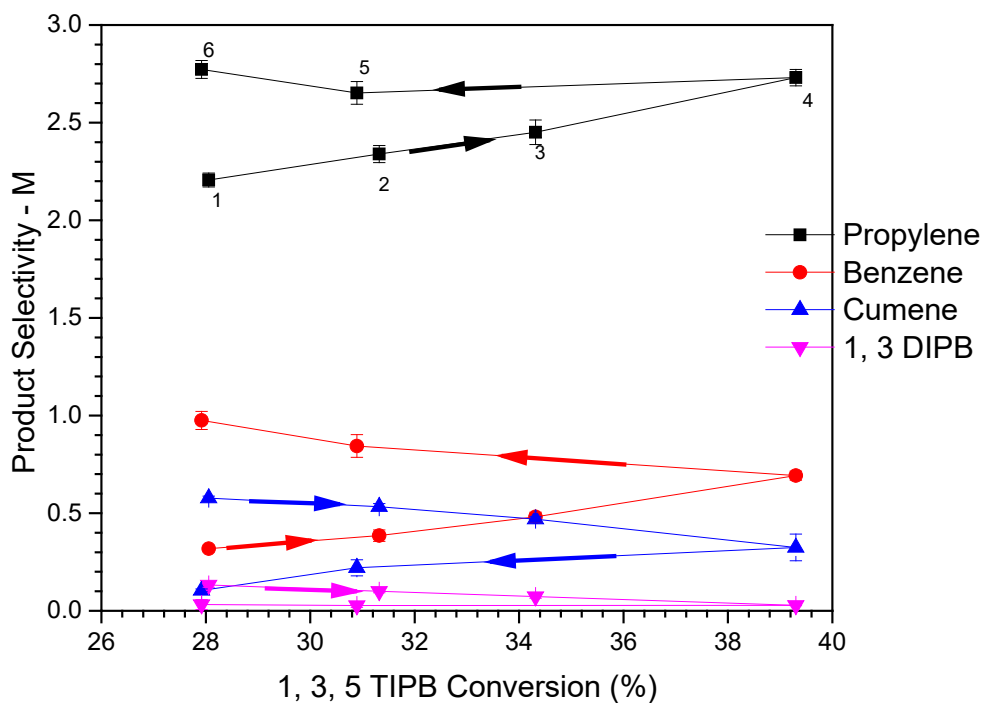


Figure 4.13 Changes of Product Selectivity-M with 1,3,5-TIPB Conversion at 550oC and 7s. Data is reported increasing the C/O ratio as indicated by the arrows: (1) C/O=0.6, (2) C/O=0.8, (3) C/O=1.25, (4) C/O=2.5, (5) C/O=3.75, and (6) C/O=5. Reported data and standard deviations (vertical bars) represent average values from at least 5 repeat runs.

Note: The selectivity-M is defined as the moles of a product per mole of TIPB converted.

In addition, Figure 4.14 reports the effect of temperature and C/O ratio on benzene selectivity for CAT-A at 7s. One can observe the consistent increase of benzene selectivity with increasing temperature and C/O ratio. This shows the importance of controlling the C/O ratio to keep benzene content at acceptable low levels. This is given the fact that benzene is a carcinogenic chemical species that one would like to limit in gasoline as much as possible. Benzene selectivity augments steadily, with an increasing C/O ratio, which points higher C/O ratios favouring dealkylation of aromatic species. Therefore, C/Os higher than 2.5, leading to higher benzene content are not recommended.

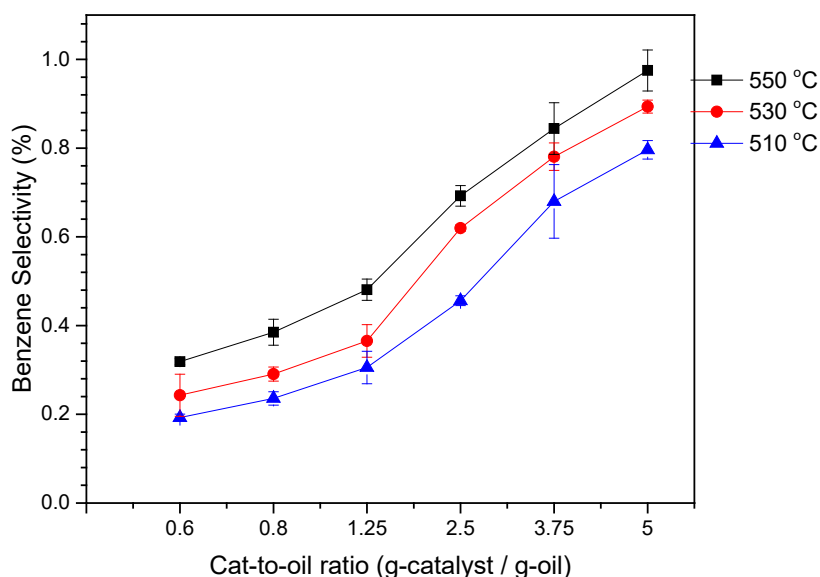


Figure 4.14 Effect of Temperature and C/O Ratio on Benzene Selectivity using a CAT-A at 7s. Reported data and standard deviations (vertical bars) represent average values from at least 5 repeat runs.

4.4.2.2.2 Coke Formation

Figure 4.15 reports the effect of the C/O ratio and thermal levels on N_c (total moles of coke). Based on this, one can conclude that the N_c increases with C/O ratio almost linearly, with temperature level for the run being of less significance.

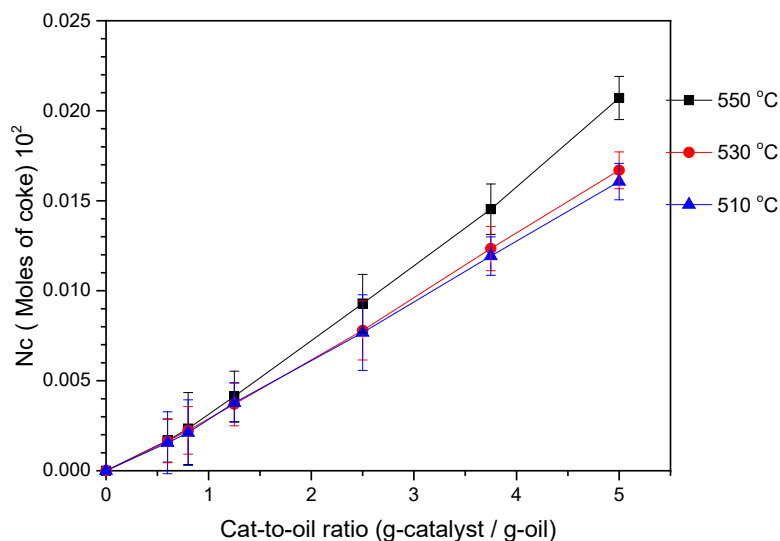


Figure 4.15 Changes of Moles of Coke (N_c) with Temperature (510oC, 530oC, 550oC) at Various C/O Ratios and 7 s Reaction Time. Reported data represent average values from at least 5 repeat runs. The vertical bars describe standard deviations of repeats.

Figures 4.16a, 4.16b and 4.16c report a steady and consistent increase in the weight-based coke selectivity (Coke Selectivity-W) at the higher C/O ratios and reaction times. These increased C/Os with a set amount of 1,3,5-TIPB and various catalyst amounts enhance coke selectivity.

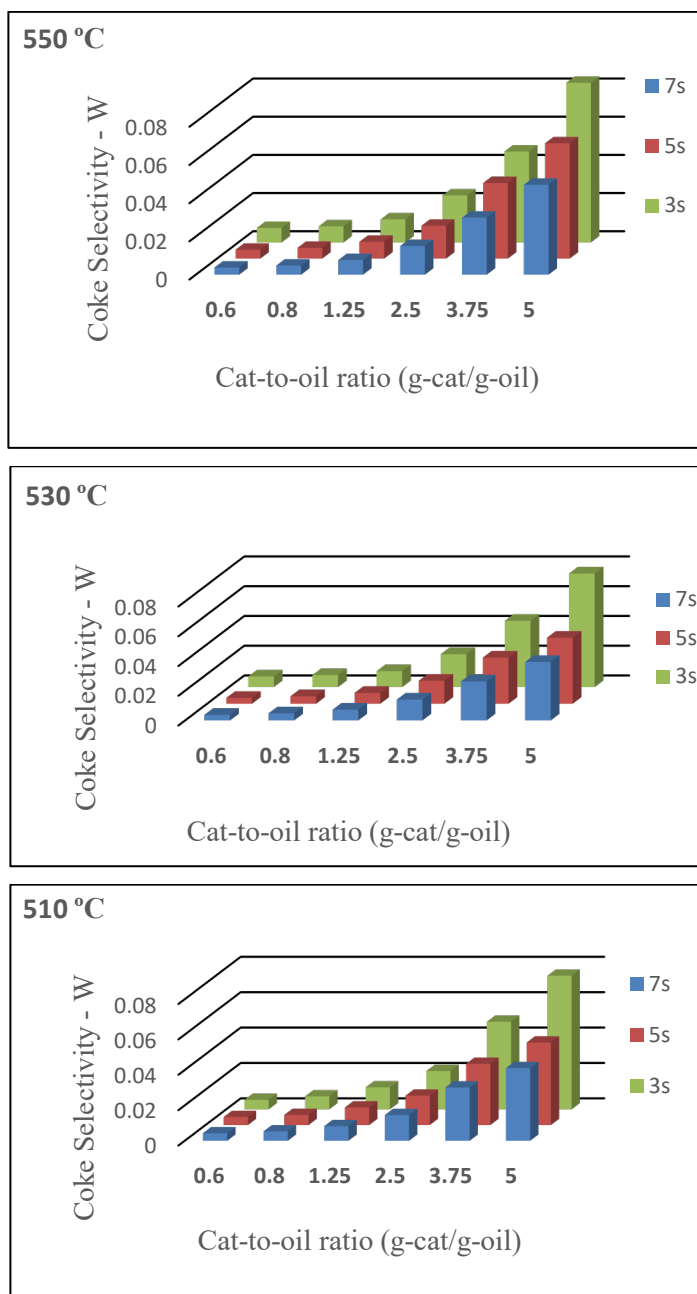


Figure 4.16a, :4.17b, 4.16c. Effects of C/O Ratios on Coke Selectivity-W (weight-based coke selectivity) using a TIPB CAT-A. Operating Conditions: (a) 550°C, (b) 530°C, (c) 510°C. Reaction time: 3-7s Note: Coke Selectivity-W was determined as grams of of coke/ gr grams of 1, 3, 5 - TIPB converted

Thus, it appears that higher catalyst densities in the CREC Riser Simulator favour coke formation, with this being a consistent trend for all runs developed.

Furthermore, and to be able to better understand coke formation, it is valuable to consider the changes of the percentual coke-on-catalyst (q_{coke}) with C/O ratios. Figure 4.17 reports, in this respect, a moderately increasing coke-on-catalyst at higher C/O ratios. Thus, it appears that augmenting the catalyst density (grams catalyst per unit reactor volume) in the CREC Riser Simulator favours higher q_c with this being more apparent at 550 °C. It has to be mentioned that this finding on coke-on-catalyst increasing with C/O was also found for the runs conducted at 530 °C and 510 °C, as reported in Appendix B1 and B2, respectively.

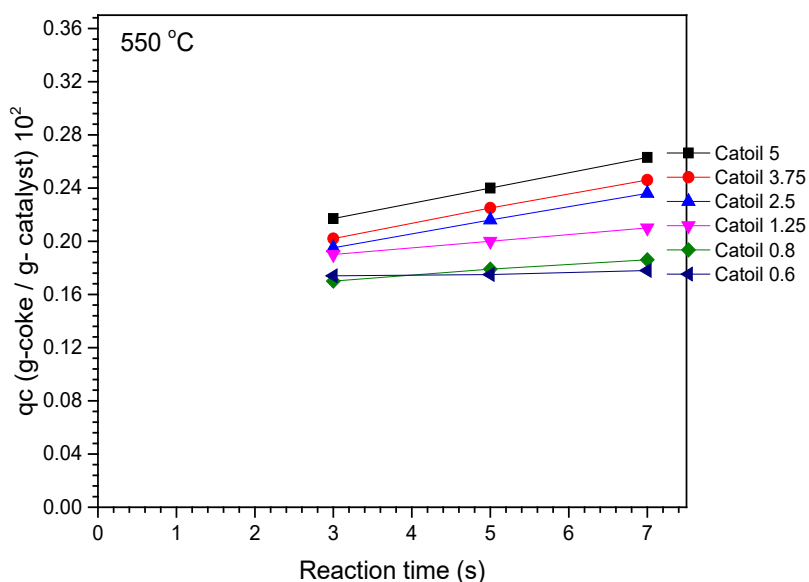


Figure 4.17 Effects of C/O Ratios on Coke Formed, for 1,3,5-TIPB Cracking using a CAT-A. The temperature was set to 550°C. Reported data represent average values from at least 5 repeat runs.

To summarize, the reported experimental results obtained with CAT-A by changing the C/O ratio, a critical FCC operating parameter, one can influence the 1,3,5-TIPB catalytic conversion, as well as propylene, DIPB, IPB and benzene and coke selectivities. As well, one can observe that the highest recorded coke-on-catalyst values were found at the highest C/Os and reaction times.

4.5 Conclusions

- a) It is shown that 1,3,5-TIPB cracking in a CREC Riser Simulator provides critical information to establish riser/downer performance. This is achieved by changing the C/O ratio (0.6 to 5), the temperature (510-550 °C) and the reaction time (3-7s).
- b) It is observed that the dominant cracking products detected were propylene, benzene, Cumene, 1,3-DIPB and coke. It was also noticed that C/O ratios higher than 2.5 led to undesirable high benzene content.
- c) It is demonstrated that the 1,3,5-TIPB conversion displays a maximum value at a C/O ratio of 2.5, decreasing progressively at higher C/O ratios. This trend was consistently observed at various temperatures and reaction times.
- d) It is observed that coke-on-catalyst selectivity steadily increases as C/O ratios increase. These findings are in agreement with the physicochemical changes observed in catalyst acidity, specific surface area, macro and micropore pore volume.

Chapter 5

5 Catalytic Cracking of 1,3,5 TIPB Chemical Species using CAT-A, CAT-B, and CAT-C

5.1 Introduction:

This chapter is a follow-up to Chapter 4. Given the originality of the reported results in Chapter 4, regarding the effect of the C/O ratio on catalytic cracking activity and catalyst deactivation, it was decided to consider this effect using two additional catalysts designated as CAT-B and CAT-C.

Thus, the aim of this chapter is to reconsider the C/O effect in a much broader context, using other catalysts than CAT-A, with these catalysts displaying different activities and acidities. The two additional selected catalysts were characterized as well in terms of crystallinity, total acidity, specific surface area, and temperature-programmed ammonia desorption.

One should notice that various results for CAT-A, in terms of catalyst characterization as well as of catalytic cracking are frequently reported in this chapter again as a basis for comparison.

5.2 Catalyst Characterization:

5.2.1 X-Ray Diffraction:

Powder X-Ray Diffraction (XRD) patterns of the catalysts were obtained by Ni-filtered Cu K α radiation ($\lambda = 0.15406$ nm). XRD diffractometry was used in the 5° to 90°, 2 θ scale. The crystallinity and unit cell size per catalyst were determined by following the ASTM D-3906-85 method. High purity of silicon powder (99%) was used as a calibration standard. Table 5.1 reports both the relative crystallinity and unit cell size observed for the three catalysts used in this PhD Dissertation.

Table 5.1: Properties of the Studied Catalysts

Samples	Particle SiO ₂ /Al ₂ O ₃ (mol/mol)	Unit cell size (Å ^o)	Crystallinity
CAT- A	0.86	24.30	0.094
CAT- B	0.72	24.30	0.077
CAT- C	0.92	24.29	0.078

XRD was used to identify and determine the Y zeolite crystal structure, involving zeolite unit cell size and crystallinity. An example of XRD diffractograms is reported in Figure 5.1 for Catalyst B. XRD for CAT-A sample was already reported in Chapter 4, while for CAT-C is given in Appendix C1.

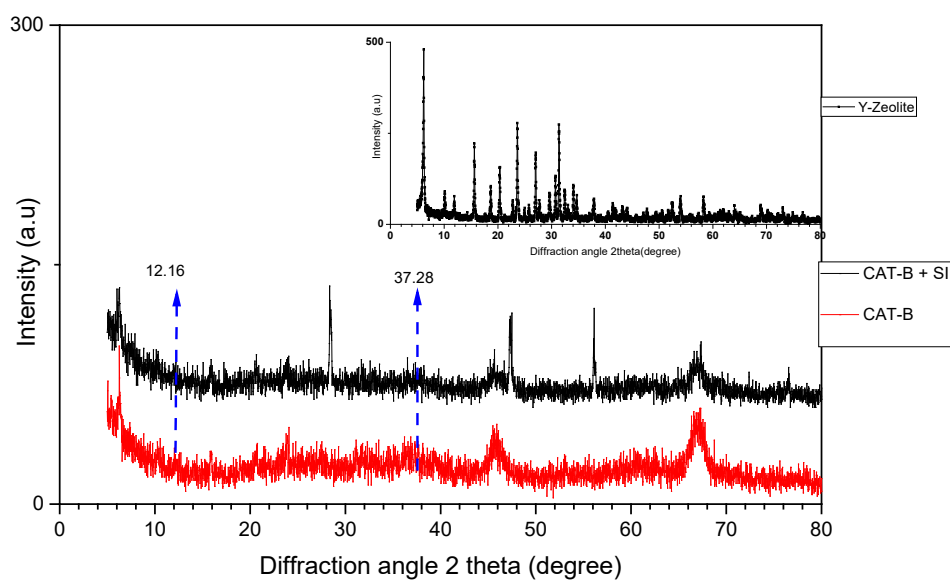


Figure 5.1: XRD Diffractograms for a CAT-B Sample of the Present Study Mixed with pure Silicon. Characteristic bands for silicon are shown at 28, 47 and 56 degrees in the 2θ scale.

5.2.1.1 Calculation of the Unit Cell Size (UCS)

XRD allows one to establish the unit cell size following the ASTM method ASTM. D-3942.85 as well as to determine the relative crystallinity. The XRD calculation procedures consistently applied to CAT-A, CAT-B and CAT-C were as follows:

- I. 1 gram of solid catalyst sample was placed in a drying oven at 110° C for 1hr.
- II. This 1-gram dried sample was blended with about 0.05g of silicon in mortar and was grounded until it was intimately mixed.
- III. Following this, the mixed sample was placed in the hydrator for 16 hrs. The hydrator was packed in the diffractometer mount.
- IV. Finally, the X-ray diffraction was determined in the range of 5° to 90°, 2θ scale.

The peaks considered for the XRD calculation were located in the range of d- spacing values of about 3.7, 3.2, 2.8 as shown in the Figure 5.1.

The formula used in the calculation of the unit cell size was as follows:

$$a = [(d_{hkl})^2 * (h^2 + k^2 + l^2)]^{1/2} \quad (5.1)$$

Where a = unit cell size A

d_{hkl} = distance between reflecting planes

$h^2 + k^2 + l^2$ = respective zeolite reflections

5.2.2 NH₃-TPD (Temperature Programmed Desorption)

NH₃-TPD spectra were determined for CAT-A, CAT-B and CAT-C. Figure 5.2 reports the NH₃-TPD for the CAT-B sample. Figure 5.2 reports that increasing the C/O ratio leads to a consistent reduction of total acidity, pointing towards a progressive catalyst deactivation [34]. The NH₃-TPD for the CAT-A sample was already reported in Chapter 4, while NH₃-TPD for CAT-C is given in Appendix C3.

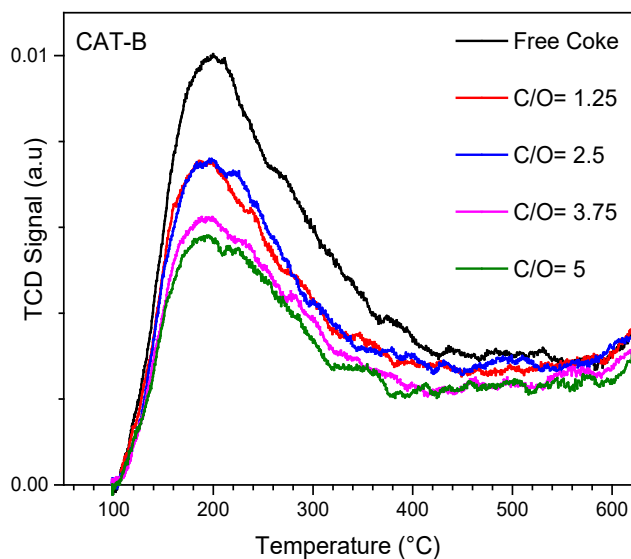


Figure 5.2 NH₃-TPD Analyses for CAT-B. Notes: Continuous black line: FCC catalyst free of coke; continuous red line: C/O= 1.25; continuous blue line: C/O=2.5; continuous violet line: C/O=3.75; continuous green line: C/O=5; continuous blue line: experiment baseline. Samples with coke were analyzed following catalytic cracking runs at 550°C and 7 s.

Table 5.2 reports that CAT-A displays the highest acidity as measured by ammonia TPD at free of coke conditions: 3.37 cm³ NH₃ STP/g in comparison with 1.73 cm³ NH₃ STP/g and 1.47 cm³ NH₃ STP/g for CAT-B and CAT-C, respectively. Thus, and on this basis, one can anticipate similar trends in the 1,3,5-TIPB conversion and in coke formation.

Table 5.2: NH₃-TPD for CAT- A, CAT- B and CAT- C Catalyst Samples

Samples	CAT. A NH ₃ uptake (cm ³ STP/g)	CAT. B NH ₃ uptake (cm ³ STP/g)	CAT. C NH ₃ uptake (cm ³ STP/g)
Free of Coke	3.36	1.73	1.47
Catoil=1.25	2.48	1.24	1.14
Catoil=2.5	2.31	1.24	1.13
Catoil=3.75	2.24	1.04	0.94
Catoil=5	2.23	0.95	0.84

Table 5.2 also shows a consistent behavior for the three catalysts, with higher C/Os leading to a steady reduction in acidity as shown by NH₃-TPD. These findings are in line with a progressive reduction of catalyst acidity with increased coke deposition, as will be later reported in the upcoming sections.

5.2.3 Pyridine-FTIR:

The FTIR analysis of chemisorbed pyridine was used to assess both Brönsted and Lewis acidities for the catalysts studied, under free of coke conditions. Figure 5.3 displays the pyridine FTIR for CAT-A, CAT-B, and CAT-C, with the characteristic Brönsted and Lewis acid site peaks identified at 1445cm⁻¹ and 1545cm⁻¹ wavenumbers. On this basis, Brönsted/Lewis acid strength ratios were calculated, with Table 5.3 showing that CAT-C displays the highest ratio followed by CAT-B and CAT-A.

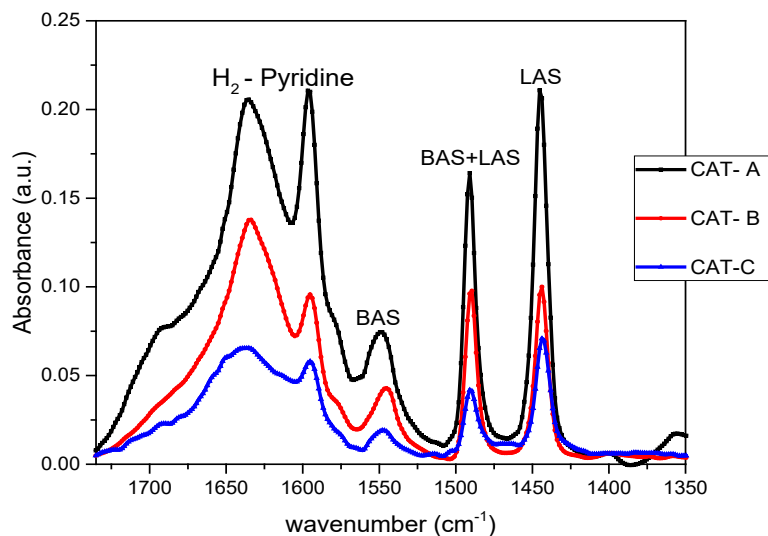


Figure 5.3: FTIR Spectra Shows IR Band Peaks for the Catalysts A, B and C studied. The black solid line represents pyridine adsorbed on CAT- A; the red solid line denotes pyridine adsorbed on Cat-B; the blue solid line shows the pyridine adsorbed on CAT-C.

Table 5.3 Brönsted /Lewis Acid Site Ratios using Pyridine FTIR

Sample Catalyst	Brönsted/Lewis Acid Sites Ratio
CAT-A	0.298
CAT-B	0.334
CAT-C	0.321

5.2.4 N₂ Adsorption-Desorption Isotherms

Figure 5.4 reports the N₂ adsorption desorption isotherms for CAT-B at various C/O ratios (0.8, 1.25, 2.5, 3.75, 5) and compares them with those of the free of coke catalyst. N₂ adsorption desorption isotherms for CAT-A were already reported in Chapter 4, while the N₂ adsorption isotherms for CAT-C are given in Appendix C4.1. One can then see, that there is a significant

isotherm shape change with increased C/O ratios. This is consistent with an increased coke amount, as will be reported later in this manuscript.

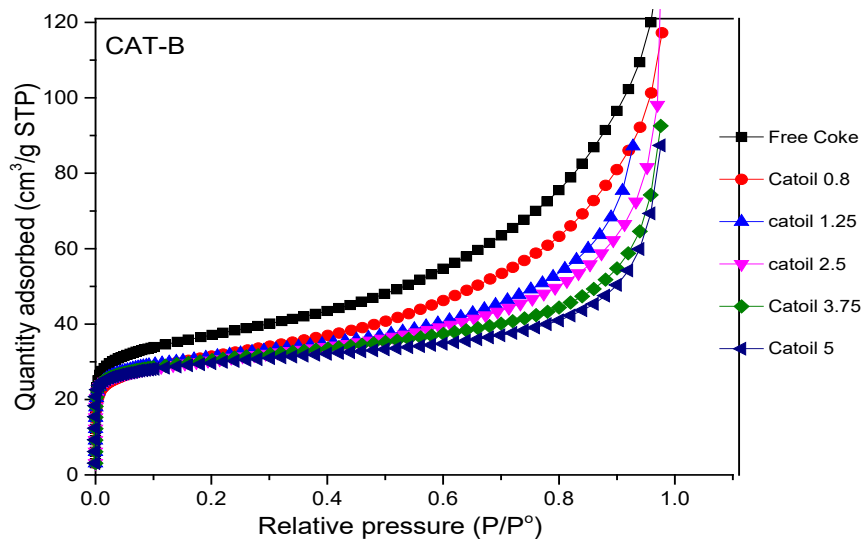


Figure 5.4 BET-Nitrogen Adsorption Plot. N₂ Adsorption-Desorption Isotherms Obtained from Different Samples of CAT-B after a Run at 550°C and 7 s Contact Time.

Table 5.4 summarizes the specific surface areas of CAT-A, CAT-B and CAT-C, which were established using the BET method. Table 5.4 also gives the total pore volumes showing the differences between mesopores and micropores.

Table 5.4: Specific Surface Areas and Pore Volumes of the Free of Coke Catalysts.

	CAT- A	CAT- B	CAT- C
BET (SSA)	99.6	118.5	102
Pore Volume (PV) (cm ³ /g)	0.158	0.196	0.140
Mesopores Volume (cm ³ /g)	0.112	0.142	0.0916
Micropores Volume(cm ³ /g)	0.0468	0.0540	0.0491

Figure 5.5 and Table 5.5 also show the influence of the C/O ratio on the micropores of CAT-B. Similar results were already reported in Chapter 4. For CAT-C, results are given in Appendix C4.2. One can thus see, that the catalyst micropore volume after every run is reduced, with this being more pronounced at the higher C/O ratios.

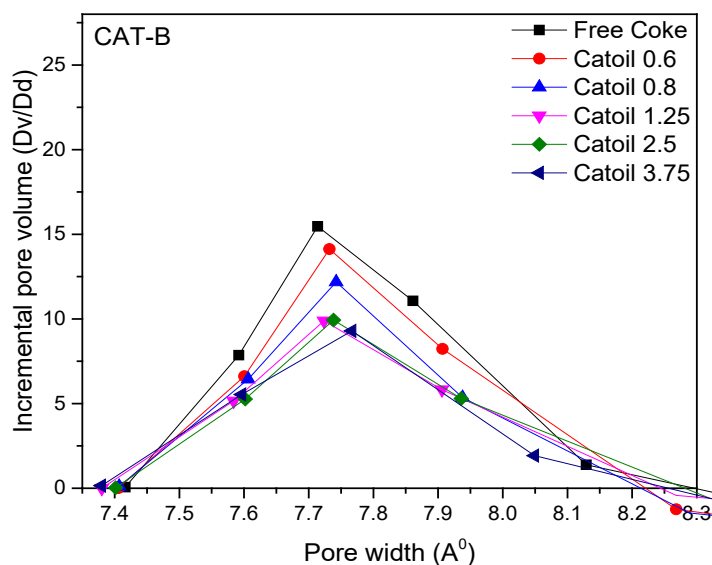


Figure 5.5: Differential Pore Volume (dV/dD) as a Function of the Pore Diameter (D) Using the N_2 -Adsorption Isotherms. (■) CAT-B free of coke; (●) CAT-B at C/O = 0.6g/g; (▲) CAT-B at C/O = 0.8g/g; (▼) CAT-B at C/O = 1.25g/g; (◆) CAT-B at C/O = 2.5g/g; (◄) CAT-B at C/O = 3.75g/g.. All samples were analyzed following catalytic cracking runs at 550°C and 7

s.

Table 5.5: Specific Surface Areas [SSA] (m²/g) and Pore Volumes [PV] (cm³/g) for CAT-B. Mesopore Volumes (cm³/g) for CAT-B were determined following catalytic cracking runs at 550°C and 7 s, using different C/O ratios. SD on repeats: +/- 3 m²/g.

	CAT- B Catalyst Samples					
	Free Coke	C/O= 0.6	C/O=0.8	C/O=1.25	C/O=2.5	C/O=3.75
BET (SSA)	102	93.37	91.88	89.18	88.92	81.56
Pore Volume (PV) cm ³ /g	0.140	0.129	0.137	0.121	0.122	0.120
Mesopores- Macropores Volume, cm ³ /g	0.0916	0.0864	0.0936	0.0785	0.0795	0.0815
Micropores Volume cm ³ /g	0.0491	0.0435	0.0439	0.0430	0.0425	0.0390

Based on the above observations, the following conclusions for the CAT-A, the CAT-B and the CAT-C catalysts of this study were reached:

- a) FCC catalysts when being used together with cracking products, form coke. Coke alters both the structure and physicochemical properties of the catalyst, particularly the specific surface area, the micropore volume and the acidity. Thus, catalyst regeneration with air is needed for the FCC catalysts to regain catalytic activity.

- b) However, changes of the catalyst structural and physicochemical properties (specific surface area, micropore volume, acidity) are increased at higher C/O ratios. This is given the fact that higher C/O ratios lead to higher amounts of coke deposited, as is shown in the upcoming sections of this manuscript.

5.3 Catalytic Cracking Runs:

In this section of study, a total of 146 catalytic runs are reported including at least 5 repeats. All these runs were conducted in the CREC Riser Simulator including at least 5 repeats per run. This allowed establishing conversions and selectivities with their required statistical indicators (e.g. standard deviations). Furthermore, and based on the detected propylene, DIPB, cumene, and benzene product species and their changes with reaction time, a series-parallel network was established as is described later in Section 5.4.

5.3.1 Effect of Catalyst to Oil Ratio (C/O ratio) [g cat g feed⁻¹] on Feed Conversion, Coke selectivity, Species distribution.

Given the value of the results reported using CAT-A in Chapter 4, regarding the influence of the C/O ratios, or the equivalent of the apparent catalyst bed density (mass of catalyst per unit reactor volume), two additional catalysts (CAT B and CAT C) were studied. In every run, the 1, 3, 5 TIPB conversion, the coke formed, and the selectivities of various product chemical species were determined. With this end, runs were developed using set amounts of 0.2g of feedstock, while changing the catalyst load from 0.12g to 1g. Furthermore, the catalyst to oil ratio “C/O” employed was set to 0.6, 0.8, 1.25, 2.5, 3.75 and 5, during the runs.

Figures 5.6, 5.7, and 5.8 report the changes in 1,3,5-TIPB conversion, product selectivity and coke content using CAT-A, CAT-B and CAT-C catalysts at various C/Os. In particular, Figure 5.6 shows a comparison of 1,3,5-TIPB conversions between CAT-A, CAT-B and CAT-C catalysts at various C/O ratios. It is apparent that CAT-A, with higher acidity and crystallinity, showed the highest 1,3,5-TIPB conversions. CAT-B and CAT-C on the other hand, displayed comparable lower levels of 1,3,5-TIPB conversions. These differences in catalytic activity are consistent with differences of crystallinity, total acidity as well as density of stronger acid sites as reported in Sections 5.2.1, 5.2.3, and 5.2.4.

In spite of these differences and as shown in Figure 5.6, a common trend emerges when the changes in the 1,3,5-TIPB conversions with C/O ratios are examined. The 1,3,5-TIPB conversion increases first at a range of 0.6-1.25 C/Os, leveling off at the 2.5 intermediate C/O and decreasing later at the higher range of 3.75-5 C/O values.

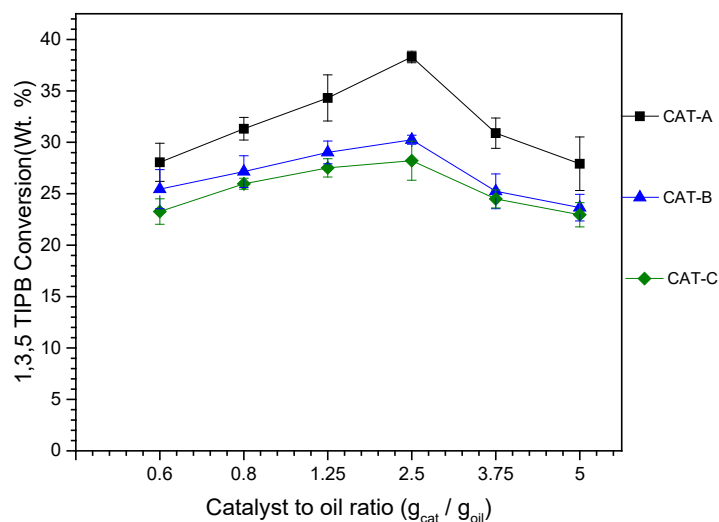


Figure 5.6 Changes of the 1,3,5-TIPB Conversion with the C/O Ratio in the CREC Riser Simulator for CAT-A, CAT-B, and CAT-C. Note: Reaction time: 7 s, Temperature: 550oC. Reported data and standard deviations (vertical bars) represent average values from at least

5

In order to be able to explain this behaviour, one should consider coke formation at various conditions, including C/O changes as will be reported in the subsequent section.

5.3.2 Coke Selectivity

Figure 5.7 reports a comparison of coke selectivities (g coke/ g of 1,3,5-TIPB converted) for the three catalyst (CAT-A, CAT-B and CAT-C) at various C/O ratios. Figure 5.7 shows how coke selectivity augments steadily with C/O ratio, with this being true in all cases and for the three catalyst samples. One can thus see, a significant contrast of coke formation increases with C/O ratios versus the 1,3,5-TIPB conversion tendencies with C/O reported in Figure 5.6.

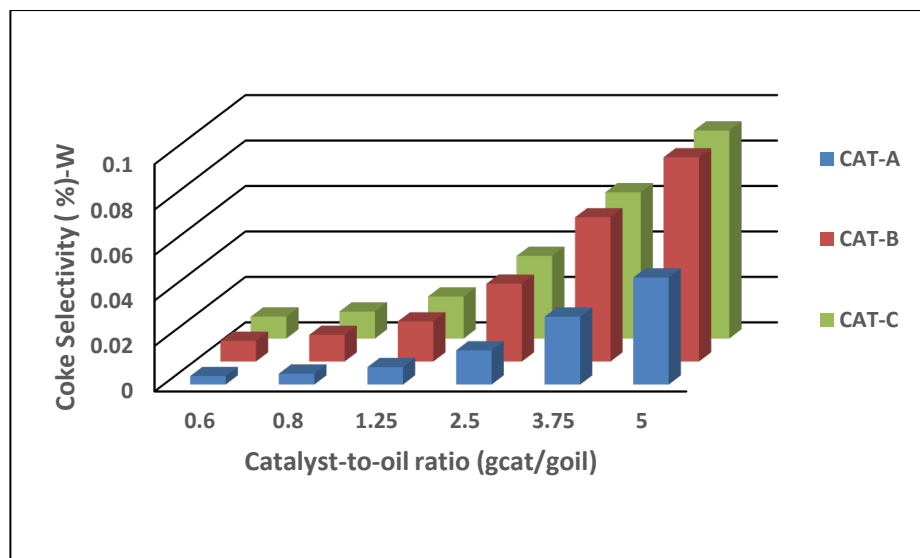


Figure 5.7 Effect of C/O on Coke Selectivity Using 1,3,5-TIPB and Cat-A, Cat-B & Cat-C Operating Conditions: 550 oC and 7s. Reported data and standard deviations (vertical bars) represent average values from at 5-7 repeat runs.

Thus, and to be able to explain these consistent trends applicable to the three catalysts studied, one can claim a reaction mechanism as analysed in upcoming section 5.4 (Fig. 5.10, and 5.11). Increases in C/Os leads to higher catalyst densities and as a result, an increased interaction of particles with adsorbed hydrocarbon species. It is thus, speculated that higher C/Os provide increased opportunities for bimolecular condensation reactions and as a result, enhanced coke formation [115,134].

5.3.3 Product Selectivity:

Given the value of establishing the influence of C/O ratios on FCC, one should also consider their effect on product selectivity. Figure 5.8 reports the changes of product selectivity for the main cracking products. In this figure, product selectivity is quantified as a function of 1,3,5-TIPB conversion and C/O using CAT-B at 550 °C and 7s. Furthermore, the increasing C/O ratios in successive runs (range of 0.6 to 5), are represented with the “arrow” directions.

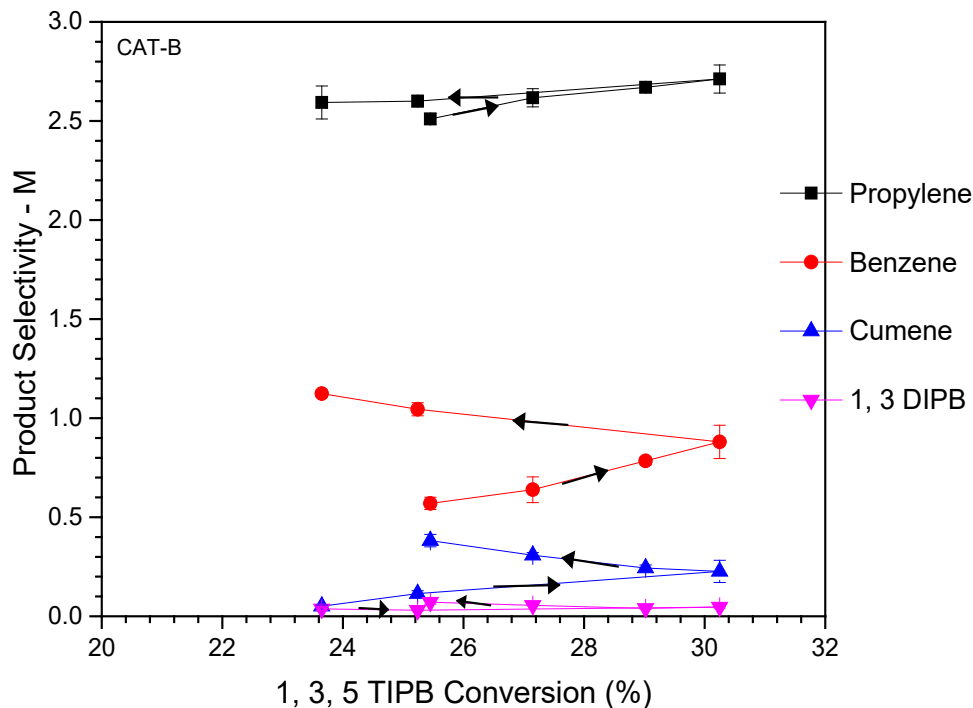


Figure 5.8 Effect of C/O on the Product Selectivity Using 1,3,5-TIPB and CAT-B. The temperature and contact time were kept constant at 550oC and 7s, respectively. Notes: a) The direction of the “arrows” represent increasing C/O ratios, b) Reported data and standard deviations (vertical bars) represent average values from at least 4-7 repeat runs.

Thus, Figure 5.8 shows, that 1,3-Di-isopropyl-benzene, cumene and benzene selectivities, always consistently increase with C/O ratio. In contrast, propylene remains at essentially constant levels. Thus, aromatic product species display a consistent maximum at the highest C/O of 5. This trend is especially noticeable for benzene, which is a non-desirable terminal catalytic cracking product. In this respect, one can see that product selectivity for the CAT-B catalyst, is consistent with data reported in Chapter 4 for CAT-A, and in agreement with data reported in Appendix D1 for CAT-C.

5.4 Coke Formation Mechanism:

In order to provide a comprehensive understanding of the coke formation mechanism, it is valuable to consider each one of the cracking hydrocarbon species as shown in Figure 5.9. One

can note in this respect, that after 7 seconds, there is a modest gain in the TIPB conversion with the formation of various product species remaining essentially unchanged.

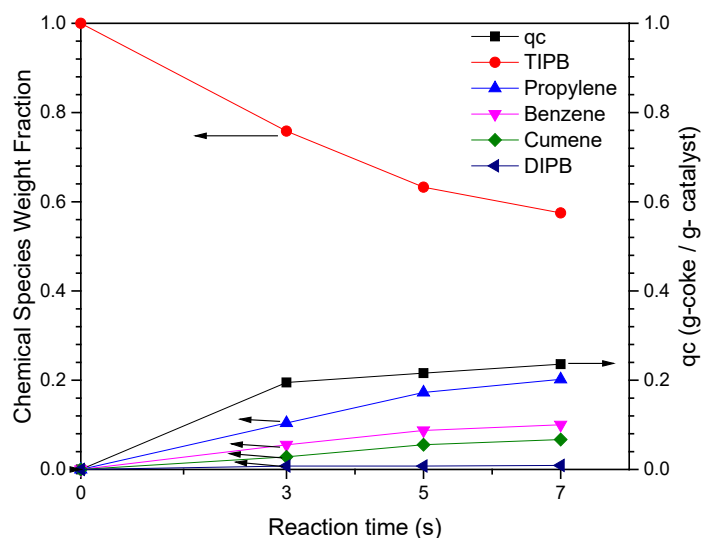


Figure 5.9 Changes of Species Mass Fractions for CAT-A. Note: Contact times are 3s, 5s & 7s; temperature: 550 °C; the C/O: 2.5. The reported data and standard deviations (vertical bars) represent average values from at least 5 repeat runs.

Therefore, and on this basis, one can consider a reaction mechanism as outlined in Figure 5.10. The catalytic conversion of 1,3,5-TIPB encompasses a number of dealkylation steps, involving chemical and radical adsorbed species.

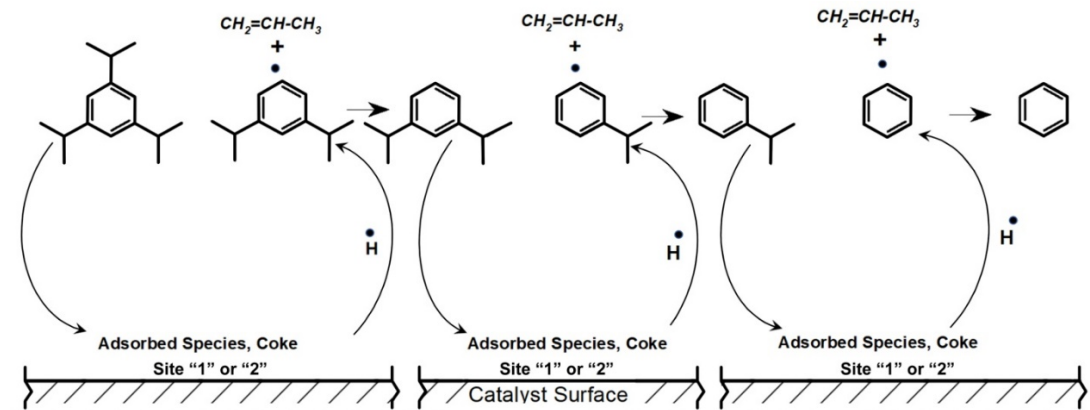


Figure 5.10 Schematic Description of the Catalytic 1, 3, 5 TIPB Conversion Showing the Hypothesized Cracking Steps.

Notes: a) Sites Type 1 are sites located in the same particle, b) Sites 1 and 2 are sites placed in different particles.

Thus, one can postulate as in Figure 5.10, that the catalytic cracking of 1,3,5-TIPB leads to the progressive removal of propyl radicals as follows: a) *Step 1*: involves the removal of a first propyl radical, b) *Step 2*: encompasses the abstraction of a second propyl, and c) *Step 3*: includes the removal of the last propyl radical left in the aromatic ring. Therefore, one can see that every elementary reaction step also leads to the formation of an aromatic radical. Aromatic radicals may however, be stabilized via catalyst H-transfer forming DIPB, cumene and benzene with the potential of evolving later in the gas phase. As well, aromatic radicals may alternatively condense with other aromatic radicals on the catalyst surface forming coke.

Therefore, while the 1,3,5-TIPB catalytic cracking is a single site driven reaction with the rate of change being proportional to the catalyst density, coke formation involves instead, at least two catalyst sites located in either the same or a close but different particle. Thus, a higher C/O proportionally increases coke formation, with being the case when the 2.5 C/O is surpassed. As a result, the catalytic cracking of 1,3,5-TIPB with higher C/Os or higher catalyst densities in the CREC Riser Simulator, consistently displays the following, as shown for three FCC catalysts:

- It leads to higher coke selectivities,
- It promotes the formation of undesirable final cracking products such as benzene,
- It yields 1,3,5-TIPB conversions that increase first and later decrease at the higher C/Os.

Based on these observations, one is capable of setting an optimum C/O ratio for FCC unit operation.

As a result, and given these findings, coke formation can be viewed as shown in Figure 5.11, as a bimolecular reaction involving adsorbed coke precursor species in adjacent S1 and S2 sites. These sites can however, be located either in the same particle or in close particles.

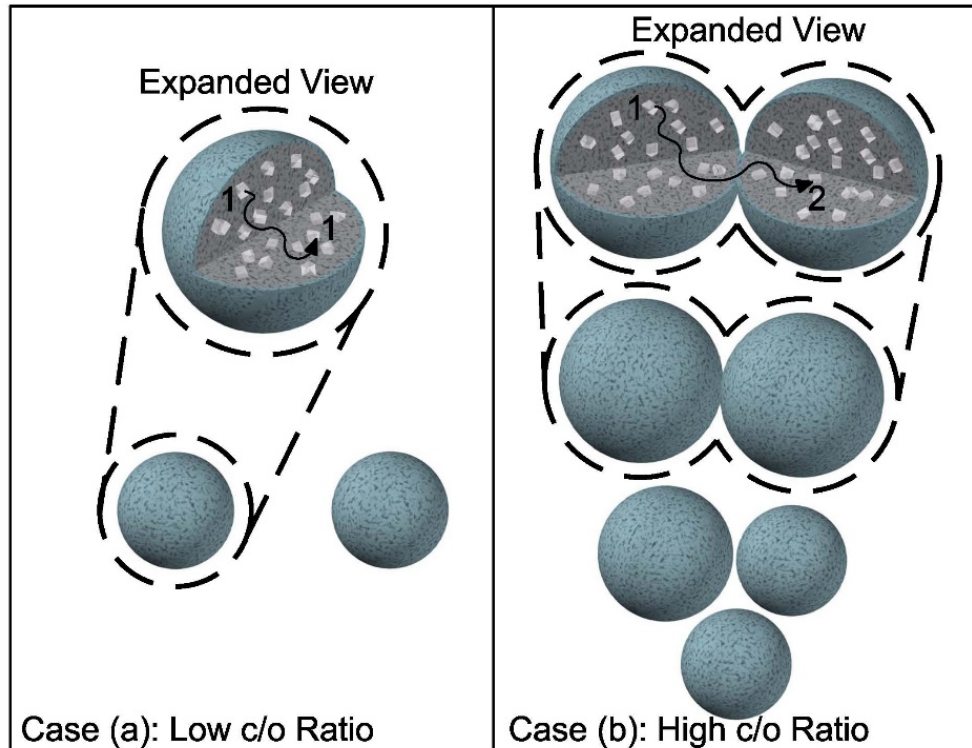


Figure 5.11: Schematic Representation of Coke Formation. Case (a) Coke is formed as a condensed species from two adsorbed coke precursors located in the sample particle. Case (b) Coke is formed as a condensed species from two adsorbed coke precursors located in two adjacent particles.

On this basis, and as per the proposed coke formation mechanism described in Chapter 6, coke formation in the CREC Riser Simulator can be envisioned as a combination of two events:

- I. Case (a) or 1-1 Sites as in Figure 5.11. This is the dominant coke formation step at low C/O ratios or the equivalent low catalyst densities ($C/O < 2.5$). This case represents coke formation occurring as condensed species through two adsorbed coke precursors located in the same particle.
- II. Case (b) or Sites 1-2 as in Figure 5.11. This becomes a significant coke formation effect at higher C/O ratios or at the equivalent higher catalyst densities ($C/O > 2.5$). This case describes that coke is formed as condensed species through two adsorbed coke precursors located in two adjacent particles.

One should note that this coke formation mechanism leads to increased coke selectivity at higher C/O ratios as reported consistently in the Figures 4.15a, 4.15b, 4.15c and 5.7. This proposed coke formation mechanism is consistent with the view that higher amounts of catalyst (elevated C/O values) or the equivalent higher catalyst densities in the CREC Riser Simulator not only promote the cracking of hydrocarbon species, but also increase the interaction of adsorbed species with adjacent particles. In this respect, the 1,3,5-TIPB conversion and coke yields results reported here are also supported by the significantly reduced acidity and diminished micropore volume at higher C/O s (refer to Section 5.2.2 and 5.2.4).

Thus, and based on the results obtained, one should consider the operation of an FCC unit, as requiring the optimization of C/O ratios. This is equivalent to a careful selection of both catalyst mass flow and hydrocarbon mass flow in large-scale risers or downers. This optimum C/O ratio should be considered to achieve maximum feedstock 1,3,5 -TIPB conversion, controlled coke-on-catalyst and low benzene yields.

To summarize and based on these findings, coke formation in the CREC Riser Simulator becomes the additive contribution of two events. It involves sites in close particles versus those in the same particle.

5.5 Conclusions

- e) It is shown that 1,3,5-TIPB catalytic cracking displays common activity trends at increasing C/O ratios. This is shown using three based Y-zeolite catalysts (CAT-A, CAT-B and CAT-C) with different acidities and crystallinities.
- f) It is proven that the 1,3,5-TIPB catalytic cracking for these three catalysts show consistently a maximum 1,3,5-TIPB conversions at C/O ratios of 2.5.
- g) It is observed that 1,3,5-TIPB cracking product selectivities show the highest coke and undesirable benzene selectivity at the highest studied C/O of 5.

- h) It is thus anticipated that catalyst density, a main parameter in the setting of the C/O ratio, plays a critical role in achieving the highest 1,3,5-TIPB conversions. This phenomenon is of significant importance for the operation of scaled FCC units.
- i) It is shown that a coke formation mechanism involving two coke precursors adsorbed species both on the same particle sites and on two adjacent particles sites can be justified.

Chapter 6

6 Kinetic Modeling of 1,3,5 TIPB over *E-CAT* base Y-Zeolite Catalysts.

6.1 Introduction:

This chapter covers both 1,3,5-TIPB conversion, various intermediate chemical species and coke kinetics for the CAT-A catalyst. The first section of this chapter considers a postulated 1,3,5 TIPB mechanism reaction network and the associated kinetics, with various model assumption being justified as applicable the CREC Riser Simulator. Furthermore, and to be able to analyze the proposed kinetics, catalytic runs developed with CAT-A were considered. These runs included variation of reaction conditions as follows: a) temperatures: 510, 530 and 550°C, b) contact times: 3, 5 and 7 seconds, c) catalyst-to-oil ratios (C/O ratio): 0.6, 0.8, 1.25, 2.5, 3.75 and 5.

Following this, two stages of model simulation were considered solving via non-linear regression the model differential equation, involving 5 and 5 independent intrinsic kinetic parameters and activation energies, respectively. These various kinetic parameters were estimated through within a 95% confidence interval and small cross correlation coefficients. To complete this analysis the adequacy of the estimated kinetic parameters was confirmed using 45 degrees parity plots.

6.2 Mechanistic of 1,3,5 TIPB Cracking Conversion and Coke formation:

Catalytic cracking of hydrocarbon species such is the case of catalytic cracking of 1,3,5-TIPB involves coke formation. Coke having noticeable effects on the physical and chemical catalyst properties. In particular, the C/O ratio have a specific influence of coke formation and catalyst decay as described in the Chapter 4 and Chapter 5 of this dissertation. Thus, C/O shall be also accounted in catalyst deactivation.

Given a mechanistic based model for the 1,3,5-TIPB catalytic conversion has to be based on experimental observations, as per of the results reported in CHAPTER 4 and 5 the following can be considered:

- a) *Issue 1: 1,3,5-TIPB Conversion.* The 1,3,5-TIPB conversion increases with C/O ratio until a maximum value at 2.5 C/O ratio is reached. Then it decreases progressively. This is an unexpected result given that when C/O augments (more catalyst is added per unit volume) one would assume in principle, a smooth and always increasing 1,3,5-TIPB conversion.
- b) *Issue 2: Propylene Selectivity.* Propylene selectivity is consistently below the maximum stoichiometric value of 3. One can notice that propylene selectivity increases first and stabilizes later. This is an unanticipated result as well. One would expect a propylene selectivity steadily increasing towards the value 3 with higher C/O ratios, given the larger catalyst density at higher C/O ratios.
- c) *Issue 3: Coke Formation and Coke selectivity.* The amount of coke formed increases with C/O ratio even at C/O values higher than 2.5. This in sharp contrast with a declining 1,3,5-TIPB conversion under these conditions.

On the basis of the above described results one can consider the catalytic cracking of 1,3,5-TIPB as a series-parallel reaction network as outlined in Figure 6.1.

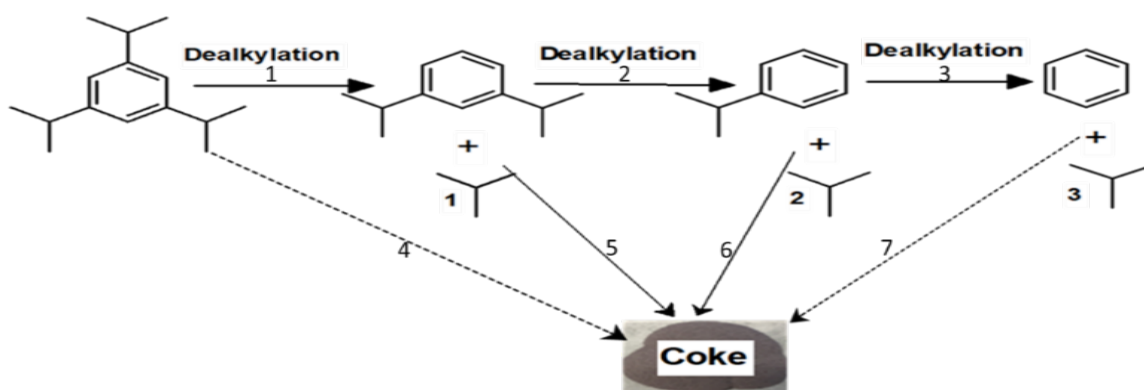


Figure 6.1 shows that the catalytic conversion of 1,3,5-TIPB encompasses a number of dealkylation steps, involving chemical and radical adsorbed

In this respect, Figure 6.1 describes a TIPB cracking reaction network with 1,3,5-TIPB first forming DIPB and propylene. Following this, the DIPB may be further converted, yielding IPB\cumene and propylene. Finally, the cumene can be further converted, producing benzene and propylene. Together with this, and while various aromatic chemical species are formed, both aromatic and olefin radicals may concurrently contribute to coke formation.

In order to establish a thorough understanding of the reaction network, in addition to the 1,3,5-TIPB conversion, it is of paramount importance to consider the 1,3-DIPB, cumene, benzene, propylene and coke selectivities at various C/O ratios as described in the former CHAPTER 4 and CHAPTER 5.

Thus, and on this basis, one can consider the 1,3,5 -TIPB catalytic cracking as a single site driven reaction with the rate of change being proportional to catalyst density. On the other hand, coke formation involves instead, at least two catalyst sites located in either the same or a close but different particle. Thus, a higher C/O proportionally increases coke formation, and this is the case when a given C/O (e.g. C/O=2.5) value is surpassed.

As a result, the catalytic cracking of 1, 3, 5 TIPB at higher C/Os or higher catalyst densities in the CREC Riser Simulator, consistently displays as shown for three FCC catalysts, the following:

- a) It leads to higher coke selectivities,
- b) It promotes the formation of undesirable final cracking products such as benzene,
- c) It yields 1, 3, 5-TIPB conversions increasing first and later decreasing at the higher C/Os.

Thus, coke formation can be viewed as shown in Figure 6.2, as a bimolecular reaction involving adsorbed coke precursor species in adjacent S1 and S2 sites. These sites can however, be located either in the same particle or in close particles.

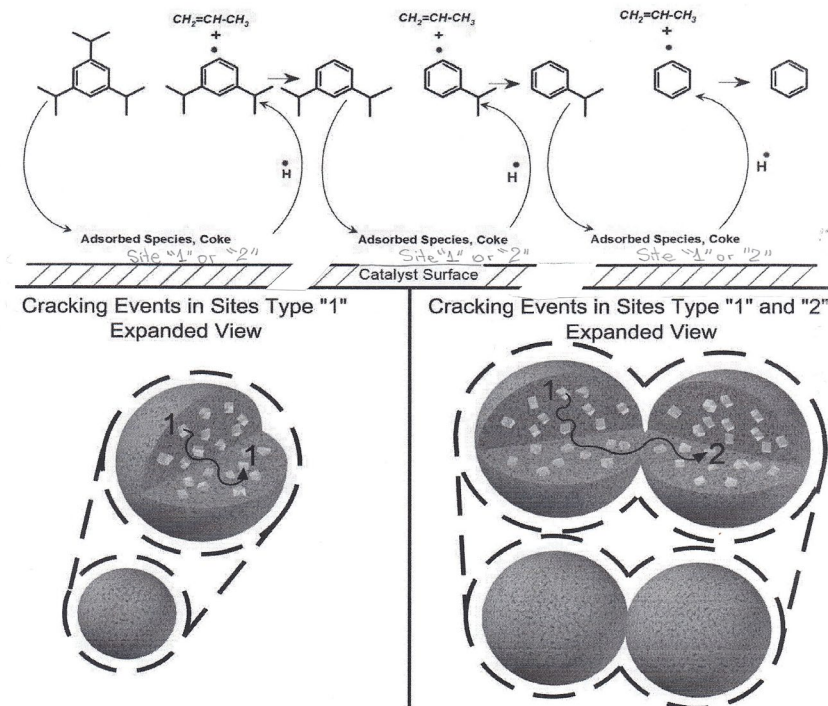


Figure 6.2: Schematic Representation of Coke Formation. Case (a) Coke is formed as a condensed species from two adsorbed coke precursors located in the sample particle. Case (b) Coke is formed as a condensed species from two adsorbed coke precursors located in two adsorbed coke precursors located in two adjacent particles.

Thus, and to address these three critical issues, a new kinetic model has to be postulated. In this new kinetic model, a role has to be assigned to incremental of coke selectivity via incremental particle density.

It is interesting to note that coke selectivity role passed unnoticed, as far as we are aware of in previous studies in the technical literature. It is in fact, thanks to the ability of the CREC Riser Simulator allowing changes of the amount of catalyst at a set feedstock partial pressure, equivalent to C/O ratio changes, this critical reaction-engineering phenomenon is unveiled.

On this basis, coke formation in the CREC Riser Simulator becomes the additive contribution of two events:

$$r_{coke} = \sum_1^n k_{11} \theta_{i1} \theta_{j1} + \sum_1^n k_{12} \theta_{i1} \theta_{j2} \quad (6.1)$$

with k_{11} being the kinetic constant for coke formation from sites in the same particle and k_{12} being the kinetic constant for coke formation from sites in close particles.

As a result,

$$\frac{dN_{coke}}{dt} = r_{coke,sp}(1 + \gamma)W \quad (6.2)$$

with $r_{coke,sp}$ representing the coke formation rate in single particles. $\gamma = \frac{\sum_1^n k_{12} \theta_{i1} \theta_{j2}}{\sum_1^n k_{11} \theta_{i1} \theta_{j1}}$ describe the relative role of coke formation involving sites in close particles versus those in the same particle. The γ parameter is hypothesized to be a function of the total weight of catalyst W or the equivalent catalyst density.

Thus, the rate of coke-on-catalyst can be expressed as:

$$\frac{dq_{coke}}{dt} = r_{coke,sp}(1 + \gamma)MW_{coke} \quad (6.3)$$

and the total coke-on-catalyst formed as:

$$q_{coke} = ((1 + \gamma) MW_{coke} \int_0^t r_{coke,sp} dt \quad (6.4)$$

with q_c representing the cumulative coke-on-catalyst at a given total reaction time.

As a result, coke formation as per eqs (6.3) and (6.4), can be considered the combined addition of:

- a) Case (a) or 1-1 Sites as in Figure 6.2. This is the dominant coke formation step at low C/O ratios or the equivalent low catalyst densities ($C/O < 2.5$).
- b) Case (b) or Sites 1-2 as in Figure 6.2. This becomes a significant coke formation effect at higher C/O ratios or at the equivalent higher catalyst densities ($C/O > 2.5$).

Thus, coke formation can be viewed as shown in Figure 6.2, as a bimolecular reaction involving two adsorbed coke precursor species in adjacent S1 and S2 sites. These two sites can however, be located either in the same particle or in two close particles.

One should notice that the proposed coke formation kinetics is consistent with the view that at higher amounts of catalyst (elevated C/O values) or the equivalent higher catalyst density in the CREC Riser Simulator not only favor cracking of hydrocarbon species, but the interaction as well of coke precursor adsorbed species in close particles.

Given these findings, one should consider that the operation of an FCC unit, requires optimization of C/O ratios. This is equivalent to a careful selection of both catalyst mass flow and hydrocarbon mass flow in large-scale risers or downers. This optimum C/O ratio should be considered to achieve maximum feedstock conversion and both controlled coke-on-catalyst and gasoline benzene content.

One can note that this combined mechanism leads to increased coke selectivity at higher C/O ratios and this as reported consistently in CHAPTER 4 and 5 (refer to figure (4.15a-4.15c, and 5.7), the kinetic model of 1,3,5 TIPB over *E-CAT* base Y-Zeolite catalyst was established. This kinetic model was classified into two models a) model I, and Model II. As shown in upcoming section.

6.3 Kinetic Development- Model-I

6.3.1 Kinetic Model Assumptions

A new kinetics of 1,3,5-TIPB in the CREC Riser Simulator is proposed in the present PhD Dissertation based on the following assumptions:

- a) An ideal batch reactor model can be considered for the mini-fluidized bed in the CREC Riser Simulator. This is considered appropriate given the intense gas phase mixing and the expected fluidized conditions in the CREC Riser Simulator unit,
- b) Chemical changes of both 1,3,5-TIPB are hypothesized to be a contribution of catalytic cracking. The same assumption is adopted for the other species such as propylene and coke.
- c) Chemical changes in the 70 micron fluidizable particles are postulated, in principle, to be controlled by intrinsic chemical kinetics with both external and internal diffusional transport resistance being negligible.
- d) The ideal gas law applies to the various reactant and product species given total pressures are slightly above atmospheric.

6.3.2 Results Discussion - Model-I

6.3.2.1 System of Ordinary Differential Equations

A kinetic model can be developed based on chemical ordinary differential equations, using the rate of chemical reaction for every identified reaction step. In the present study, hydrocarbon catalytic cracking is developed in a mini-fluidized CREC Riser Simulator design. The CREC Riser Simulator operates as an ideal batch reactor model, with intense gas phase recirculation and gas-solid mixing, with catalyst particles being fluidized [103]. Under these conditions, and based on all of the above-mentioned steps and assumptions, the rate of consumption of 1,3,5-TIPB can be postulated as:

$$-\frac{dN_i}{dt} = \eta_i (-r_i)W \quad \text{Or alternatively} \quad \frac{dC_i}{dt} = \eta_i \frac{(r_i)W}{V_R} \quad (6.5)$$

with N_i representing the moles of “ i ” species, η_i being the effectiveness factor for species “ i ”, r_i is the reaction rate of i , V_R is the Riser Simulator volume (cm^3), W is the weight of the catalyst loaded in the reactor basket (g), C_i is the concentration of i (mol/cm^3), and t is time (s).

Furthermore, adsorption/ desorption processes for various species can be assumed at adsorption equilibrium with the following equation:

$$\theta_i = \frac{K_i C_i}{1 + \sum K_i C_i} \quad (6.6)$$

where i represents each one of the adsorbed hydrocarbon species and θ_i is the fraction of “i” species occupied sites.

Given the above considerations, 1,3,5-TIPB catalytic cracking kinetics can be described based on the following:

- a) Cracking reactions involving single sites (S1 or S2) with this leading to $r_i = \sum_1^n k_j \theta_j - \sum_1^m k_i \theta_i$ surface reaction kinetics.
- b) Cracking of 1,3,5-TIPB is affected by intracrystallite diffusional limitations ($\eta < 1$) with the η for all the other species (DIPB, IPB and benzene) being close to 1.
- c) $\sum K_i C_i$ in eqs (6.6) is smaller than 1.

Thus, and based on Figure 6.1, changes of various chemical species can be described as:

- For 1,3,5-TIPB or A species:

TIPB → Products (gas phase species and coke)

$$\frac{dC_A}{dt} = -(\eta_A (k_1 + k_4) K_A C_A) W / V_R \quad (6.7)$$

- For 1,3-DIPB or B species:

$$\frac{dC_B}{dt} = (\eta_A k_1 K_A C_A - (k_2 + k_5) K_B C_B) W / V_R \quad (6.8)$$

- For IPB or C species:

$$\frac{dC_C}{dt} = (k_2 K_B C_B - (k_3 + k_6) K_C C_C) W / V_R \quad (6.9)$$

- For Benzene or D species:

$$\frac{dC_D}{dt} = (k_3 K_C C_C)W/V_R \quad (6.10)$$

- For Propylene or E species:

$$\frac{dC_E}{dt} = (\eta_A k_1 K_A C_A + k_2 K_B C_B + k_3 K_C C_C)W/V_T \quad (6.11)$$

with the various k_i kinetic constants in eqs (6.7) to (6.11) defined as per of Figure 6.1 and thus,

$$k_i = k_{i0} \exp(-\alpha q_{coke}). \quad (6.12)$$

6.3.2.2 Kinetic Parameters Estimation-Assessing the Overall Kinetic 1,3,5-TIPB Conversion Constant

Figure 6.3 describes the observed 1,3,5-TIPB conversion with various Catoil ratios and contact time at fixed reaction temperature 550 °C. One should note the data of 530 °C and 510 °C are described in Appendix E (E1 and E2).

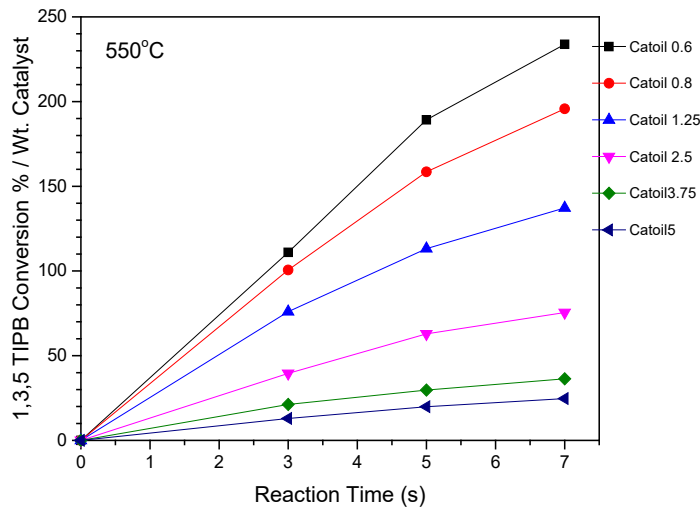


Figure 6.3 Changes of TIPB Conversion with Reaction Time at 550°C for Different C/O Ratios. Reported data represent average values for at least 5 repeat runs.

Thus, given the postulated kinetic model as given by Eq (6.7), and the kinetic data obtained at 550, 530, and 510 °C, various C/O and reaction times (refer to Figure 6.3) the $\frac{dC_A}{dt}$ was assessed at $t \rightarrow 0$ and for the lowest C/O of 0.6. This yielded the $\eta_A (k_{10}+k_{40}) K_A$ and designated as k'_{10} and reported in Table 6.1.

Table 6.1: Temperature Effect on $k'_{10} = \eta_A (k_{10}+k_{40}) K_A$

Reaction Temperature °C	$k'_{10}(\text{cm}^3/\text{g/s})$
550	34.15
530	32.79
510	28.04

Furthermore, and once k'_{10} constant calculated, the parameter α was adjusted for the entire reaction time period between 0 to 7 seconds and the three temperatures (510-550 °C). the results are reported in following Figure 6.4. One can also observe that the α parameter changes similarly at increases consistently with higher C/Os and these for the three thermal levels considered.

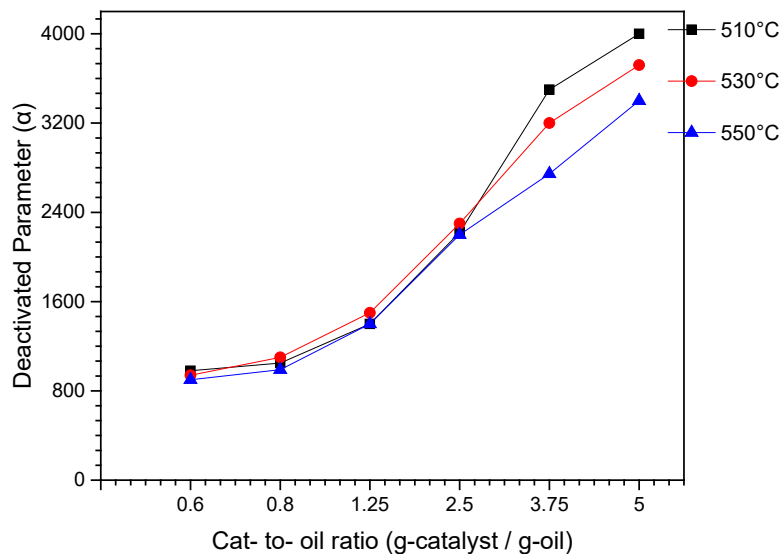


Figure 6.4: Deactivated Parameter (α) as a function of catalyst to oil ratio in the 550°C-510°C and 3-7 s ranges

Additionally, Figure 6.5 reports a parity plot, describing observed 1,3,5, TIPB conversions and model derived 1,3,5, TIPB conversions, showing a good fitting of the experimental data with the model proposed. This comparison was established at different reaction temperature, reaction time, and catalyst to oil ratio.

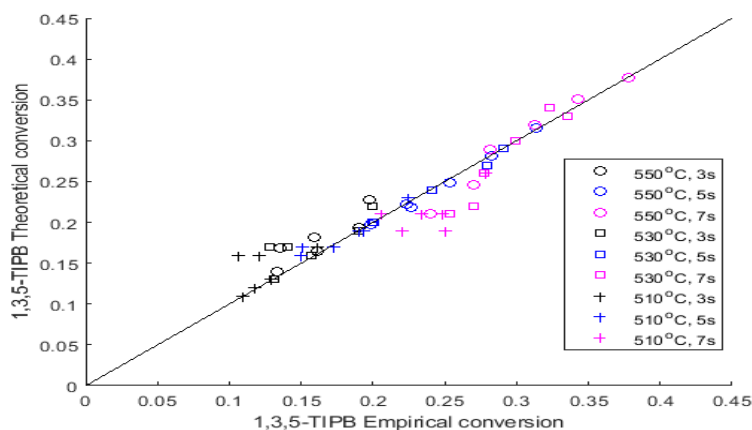


Figure 6.5 Parity Plot Comparison Theoretical Model Results with Experimental Data. Note: Relative Percentual Error: $\pm 6.5\%$.

6.4 Kinetic Development-Model II-Estimation of Reaction Step Intrinsic Parameters

Model-I was developed to determine a single kinetic parameter model for the TIPB consumption rate. This overall model can also be considered a good first estimate for the numerical calculations of various parameters involved in Model-II.

Furthermore, Model II was developed in order to calculate the various steps intrinsic kinetic parameters as described in Figure 6.1. Model assumptions for Model II were already described in Section (6.3.1) and are identical to the ones of Model I. One should also note that Model II accounts for catalytic cracking including all the detected chemical species as follows: a) 1,3,5-TIPB, b) 1,3 DIPB, c) cumene (IPB), d) benzene, e) propylene and f) coke.

Kinetic parameter estimation as considered for Model II, encompasses a concurrent evaluation of both frequency factors and energies of activation for the sets of Eqs (6.13) to (6.17), with the simplification $k_1 \gg k_4$, $k_2 \gg k_5$, $k_3 \gg k_6$

- For 1,3,5-TIPB or A species:

$$\frac{dC_A}{dt} = -\eta k_1 K_A C_A \exp(-\alpha' q_c^n) W/V_R \quad (6.13)$$

- For 1,3-DIPB or B species:

$$\frac{dC_B}{dt} = -(K_B k_2 C_B - k_1 C_A) \exp(-\alpha' q_c^n) W/V_R \quad (6.14)$$

- For IPB or C species:

$$\frac{dC_C}{dt} = -(k_3 K_C C_C - k_2 K_B C_B) \exp(-\alpha' q_c^n) W/V_R \quad (6.15)$$

- For Benzene or D species:

$$\frac{dC_E}{dt} = (k_3 K_C C_C) \exp(-\alpha' q_c^n) W/V_R \quad (6.16)$$

- For Propylene or E species:

$$\frac{dC_D}{dt} = (\eta_A k_1 K_A C_A + k_2 K_B C_B + k_3 K_C C_C) \exp(-\alpha' q_c^n) W/V_R \quad (6.17)$$

The data considered includes various hydrocarbon species changes with reaction time, using an extra “n” parameter in the deactivation exponent, in order to make “ α ” independent of the C/O ratio.

Furthermore, and considering apparent constants which lump chemical species reaction and adsorption: $k'_1 = \eta k_1 K_A$, $k'_2 = K_B k_2$, $k'_3 = K_C k_3$, thus the system of equations from Eqs (6.13) to (6.17) can be rewritten as,

- For 1,3,5-TIPB or A species:

$$\frac{dC_A}{dt} = -k'_1 C_A \exp(-\alpha q_c^n) W/V_R \quad (6.18)$$

- For 1,3-DIPB or B species:

$$\frac{dC_B}{dt} = -(k'_2 C_B - k'_1 C_A) \exp(-\alpha q_c^n) W/V_R \quad (6.19)$$

- For IPB or C species:

$$\frac{dC_C}{dt} = -(k'_3 C_C - k'_2 C_B) \exp(-\alpha q_c^n) W/V_R \quad (6.20)$$

- For Benzene or D species:

$$\frac{dC_E}{dt} = (k'_3 C_C) \exp(-\alpha q_c^n) W/V_R \quad (6.21)$$

- For Propylene or E species:

$$\frac{dC_D}{dt} = (k'_1 C_A + k'_2 C_B + k'_3 C_C) \exp(-\alpha q_c^n) W/V_R \quad (6.22)$$

6.5 Numerical Method Used

When reviewing Eqs (6.13) to (6.17), one can notice seven kinetic parameters, including 3 intrinsic/apparent parameters and 4 activation energies plus a “ α ” and a “ n ” deactivation parameter.

Given this, the following numerical method was adopted as follows: (a) First, initial values were assigned to various parameters, and the set of ordinary differential equations were solved using the “mode45” function of MATLAB. (b) Following this, the kinetic parameters were adjusted and optimized by using a nonlinear parameter optimization tool “lsqnonlin”, with the “trust-region reflective” algorithm minimizing the objective function (f_{obj}).

$$f_{obj} = \sqrt{\sum_i^{species} (C_{i,exp} - C_{i,pred})^2} \quad (6.23)$$

Where, C_i represents the “ i ” chemical species concentration (i = propylene, benzene, cumene, and 1,3 DIPB) obtained experimentally and predicted by the kinetic model.

During numerical regression, optimization parameter procedures were followed in order to obtain parameters that were all positive and displayed a low cross-correlation coefficient. In addition, and to assess numerical dependency between determined kinetic parameters, a cross correlation matrix was calculated.

One should note that in order to reduce parameter cross-correlation between frequency factors and activation energies, the recommended equation (6.18) was used in the Arrhenius equation:

$$k_i' = k_{i,o}' \exp\left[\frac{-E_i}{R} \left(\frac{1}{T} - \frac{1}{T_m}\right)\right] \quad (6.24)$$

Where, k_i^o is the pre-exponential factor (mol/g_{cat}.s), R is the universal gas constant, E_i is the activation energy (kJ/mol), T is the reaction temperature in Kelvin, and T_m is the average temperature (K).

Thus Eq (6.24) was employed in the numerical regression calculations to reduce the cross-correlation between kinetic parameters. This was obtained by centering the reaction temperature at the medium value of $T_m=783^{\circ}\text{K}$.

6.6 Discussion of Results-Model-II

6.6.1 Estimated Kinetic Parameters

The estimation of the proposed kinetic parameters was based on the catalytic runs with CAT-A. An ample range of operating conditions were covered as follows: a) Reaction temperatures: 510, 530 and 550°C, b) Contact times: 3, 5 and 7 seconds, c) Catalyst-to-oil ratios (C/O ratio): 0.6, 0.8, 1.25, 2.5, 3.75 and 5.

Figure 6.6 reports the parity plot for 270 experimental data points including at least 3-5 repeat runs for each condition. Thus, the DOF (degrees of freedom analysis) for the Model II was 262: $\text{DOF}=\text{Data Points}-\text{Parameters}$. This figure reports a parity plot, showing the observed product species concentrations and the derived model product species. This was the case for the three thermal levels considered (510°C, 530°C, 550°C). It is thus shown that the proposed model with the calculated parameters is able to correlate well with measured species distributions, with deviations being confined to $\pm 7\%$.

As well, one should note that in the case of DIPB and cumene (IPB) intermediates, these chemical species remain at relatively low concentrations, while on the other hand 1,3,5-TIPB, benzene and propylene are present at much higher concentrations. This inequality in concentration values significantly challenges the kinetic parameter fitting via nonlinear regression

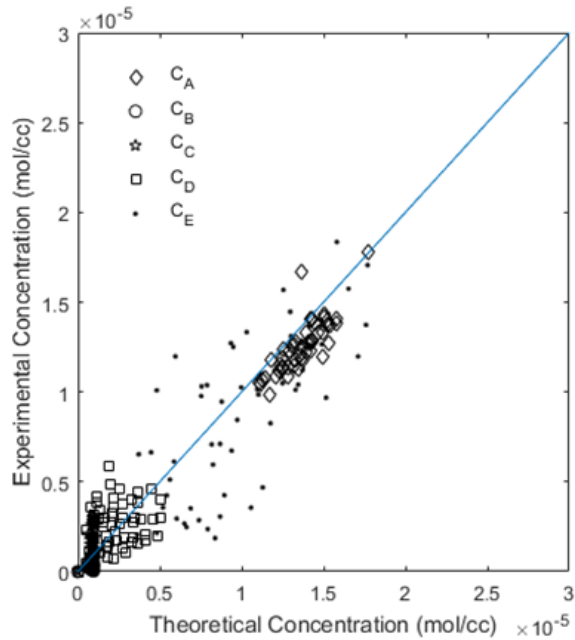


Figure 6.6 Parity Plot Comparing Experimental Observed Chemical Species Concentrations with Model Predicted Concentrations in the 510- 550 oC and 3-7s ranges. Data: 270 average data points involved including at least 3-5 repeats per experimental condition.

Table 6.2 shows the 7 estimated kinetic parameters with their respective 95% confidence spans. One can see that all calculated spans are positive with a satisfactory low level of parameter correlation.

Table 6.2: Optimized Intrinsic Kinetic Parameters for Model II and Cross-Correlation Coefficients

Apparent Parameters	Value	Correlation matrix							
		$k'_{0,1}{}^a$	$k'_{0,2}$	$k'_{0,3}$	β_0	$E_a{}^b$	E_b	E_c	E_α
$k'_{0,1}{}^a$	17.9	1							
$k'_{0,2}$	196.9	-0.38	1						
$k'_{0,3}$	187.9	-0.07	-0.34	1					
β_0	7.11	0.63	0.14	0.13	1				
$E_a{}^b$	11.8	-0.79	0.30	0.05	-0.49	1			
E_b	13.34	0.28	-0.74	0.25	-0.11	-0.37	1		
E_c	12.88	0.05	0.26	-0.76	-0.10	-0.08	-0.34	1	
E_α	12.28	-0.49	-0.12	-0.11	-0.80	0.60	0.17	0.12	1
m	270	${}^a\text{cm}^3\text{g}^{-1}\text{s}^{-1}$; ${}^b\text{kJmol}^{-1}$; $T_c=783\text{K}$; Degree of freedom (DOF)= data points (m) – parameters (p)= 270 – 8= 262							
DOF	260								

Figure 6.6 reports the predicted chemical species concentrations and compares them with the observed concentrations taking place within the 3-7 s reaction times and 0.6-5 C/O range. Similar data for 550 and 510 °C are reported in Appendix F (F1 and F2). On this basis, one can thus consider that the determined kinetic parameters are adequate.

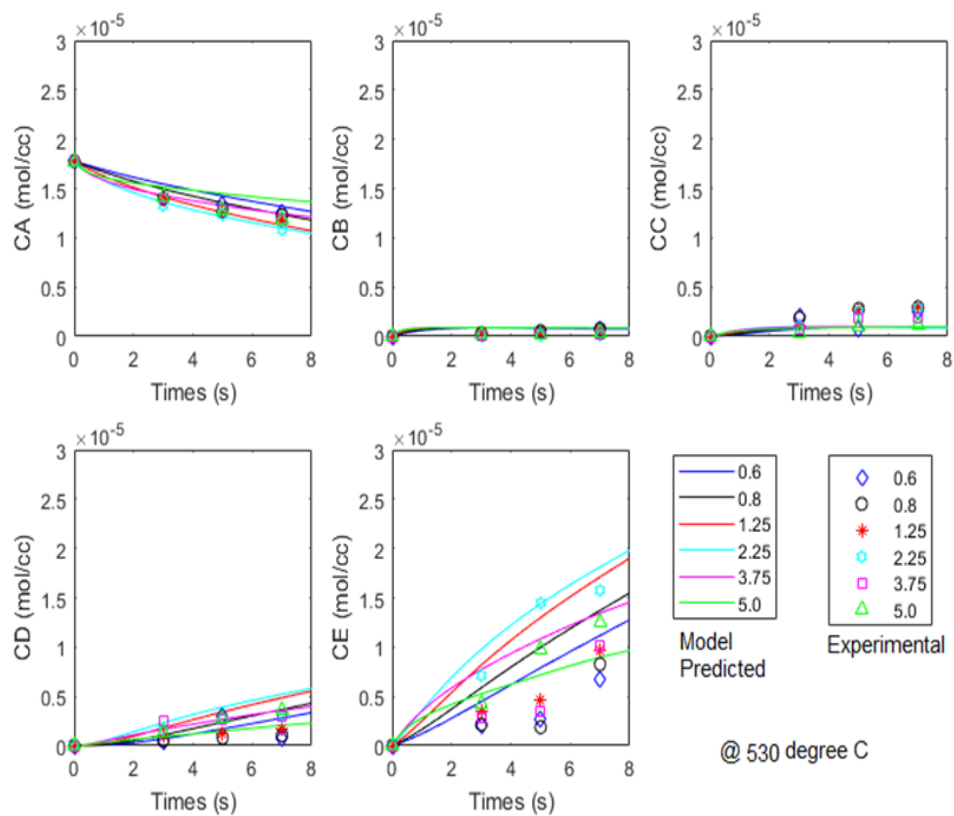


Figure 6.7 Comparison of Experimental and Model Predicted Chemical Species Concentrations during the 1,3,5-TIPB Catalytic Cracking. Operating Conditions: Contact times: 3-7s, C/O= 0.6-5, Temperature: 550 °C: Data: 270 average data points including at least 3-5 repeats.

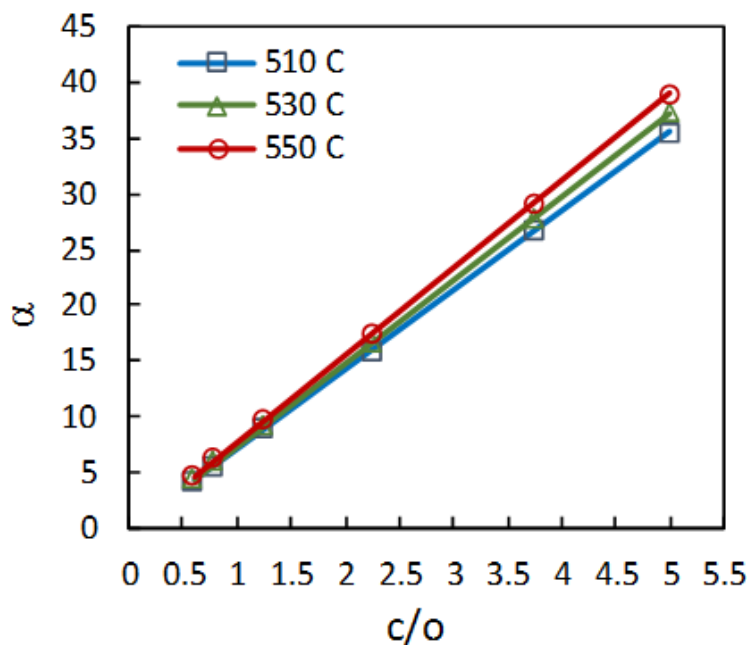


Figure 6.8 Deactivated Parameter (α) as a Function of the Catalyst to Oil Ratio in the 510°C-550°C and 3-7 s Ranges

Furthermore, Figure 6. reports the calculated “ α ” deactivation factor as a function of the C/O ratios at the three temperatures studies. One can observe the consistent change of the α deactivation constant with C/O ratio. Thus, and as hypothesized in Figure 6.2, a higher catalyst density boosts the cracking of the hydrocarbon species, but also promotes the coke precursor species interaction in close catalyst sites either in the same particle or close particles.

Thus, regarding the significant increase of the “ α ” with the augmentation of the C/O, as reported in Figures 6.3 and 6.7 (Model-I and Model-II), the following can be concluded:

- a. There is a growing influence of the C/O on the total coke formed.
- b. The amount of total coke becomes greater at higher catalyst loadings. This can be assigned to the fact that larger catalyst densities increase the ability to capture coke precursors.
- c. The formed (q_c) coke-on-catalyst at higher catalyst density becomes progressively non-uniform across the FCC particles, and thus promotes 1,3,5 TIPB diffusional transport limitations or lower effectiveness factors, with this leading to an increased “ α ” parameter.

- d. The role of the solid particles of catalyst as “coke collectors” is increased, given the higher influence of bimolecular coke precursor reactions.

6.7 Conclusions

- a) It is hypothesized that a coke formation mechanism allows one to explain the observed changes of TIPB conversion with C/O ratios as reported in CHAPTER 4 and 5.
- b) It is assumed that a mechanistic based explanation, leads to a coke formation mechanism involving the contribution of both coke precursor species adsorbed in two sites in the same particle and two sites in close but different particles.
- c) It is shown that a reaction network involving observable chemical species allows one to establish two kinetic models (Model I and Model II) with different degrees of complexity. In both cases, model parameters were determined using nonlinear least square regression with low cross correlation. This was done at three thermal levels and for various operating conditions, including temperature, contact time, and C/O ratios.
- d) It is proven that the proposed kinetic model evaluated with a large degree of freedom (DOF), yields both positive kinetic constants and good fittings of the observed chemical species concentrations.
- e) It is shown that catalytic cracking is influenced by catalyst density. Thus, an optimum C/O ratio can be anticipated for other feedstocks, with this fact being of major importance while selecting operating conditions for FCC industrial units.

CHAPTER 7

7 CONCLUSIONS AND RECOMMENDATIONS

7.1 Conclusions

The major contributions and findings of the present PhD research can be summarized as follows:

- e) It is shown, that by using the BET specific surface area and the N₂-adsorption isotherm, the influence of the C/O ratios on the structural properties of the FCC catalyst can be demonstrated. The results obtained showed coke selectivity steadily increasing as the C/O ratio augmented.
- f) It is documented that by employing NH₃-TPD adsorption and pyridine desorption analysis, that changes in total catalyst acidity and Brönsted and Lewis acid site ratios can be monitors. This was valuable to establish the influence of operating conditions and especially C/O ratio on the FCC catalyst physiochemical properties.
- g) It is shown that the fluidized CREC Riser Simulator is a reliable experimental simulation device. The CREC Riser Simulator provides valuable catalytic cracking information concerning 1,3,5 -TIPB hydrocarbon conversion and product selectivity, in the 510-550 °C and 3-7s ranges.
- h) It is demonstrated that both 1,3,5-TIPB conversion and coke yields are influenced by the reduced acidity and diminished micropore volume observed at C/O s higher than 5.
- i) It is shown that the 1,3,5-TIPB catalytic cracking products are propylene, benzene, cumene (IPB), 1,3-DIPB and coke. Based on those chemical species, product selectivities were calculated, showing the highest coke levels and undesirable benzene selectivities at the highest studied C/O ration of 5.
- j) It is proven that the three-based Y-zeolite catalysts (CAT-A, CAT-B and CAT-C) studied, having different acidities and crystallinities, display a consistent activity change when C/O ratio is increased. This trend exhibits a maximum 1,3,5-TIPB conversion at C/O ratios of 2.5, while decreasing gradually until reaching the highest studied C/O ratios of 5.

- k) It is postulated that coke formation allows one to explain the observed changes of TIPB conversion as a function of catalyst density. This was elucidated using a coke formation mechanism involving the additive contribution of coke precursor species adsorbed in two sites in the same particle and close sites in different particles. These findings were strong indicators of the significant influence of the C/O ratio on the total coke deposited on the catalyst, as the quantity of catalyst increases for a set amount of feedstock.
- l) It is proven that a reaction network involving observable chemical species allows one to establish two kinetics models with different degrees of complexity. In both cases, parameter models were determined using nonlinear least square regression and cross correlation among estimated parameters.
- m) It is anticipated that the postulated catalytic cracking reaction network influenced by catalyst density, leads to an optimum C/O ratio. Accounting for the optimum C/O allows achieving maximum feedstock conversion, controlled coke-on-catalyst and gasoline benzene content.

7.2 Recommendations

Given the originality and valuable results obtained in this PhD study, the following are recommended:

- I. It would be valuable to investigate the developed catalyst activity decay model using VGOs. This would allow demonstrating the value of the proposed catalytic cracking kinetics and of the existence of an optimum C/O ratio using typical FCC unit feedstocks.
- II. It would be important to use the developed catalyst decay model in the numerical simulation of FCC industrial scale units. This would allow establishing the value of the new proposed catalyst decay model versus the current available ones in large scale FCC unit operations.

REFERENCES

1. Corma, A.; Sauvanaud, L. FCC testing at bench scale : New units , new processes , new feeds. *Catal. Today* **2013**, *218–219*, 107–114.
2. Vogt, E.T.C, B. M. weckhuysen. Fluid catalytic cracking: recent development on the grand and old lady of zeolite catalysis. *Chem. Soc. Rev* **2015**, *44*, 7342.
3. Passamonti, F.; de la Puente, G.; Gilbert, W.; Morgado, E.; Sedran, U. Comparison between fixed fluidized bed (FFB) and batch fluidized bed reactors in the evaluation of FCC catalysts. *Chem. Eng. J.* **2012**, *183*, 433–447.
4. Harding, R. H.; Peters, A. W.; Nee, J. R. D. New developments in FCC catalyst technology. *Appl. Catal. A Gen.* **2001**, *221*, 389–396.
5. Xiong, K.; Lu, C.; Wang, Z.; Gao, X. Kinetic study of catalytic cracking of heavy oil over an in-situ crystallized FCC catalyst. *Fuel* **2015**, *142*, 65–72.
6. Awayssa, O.; Al-Yassir, N.; Aitani, A.; Al-Khattaf, S. Modified HZSM-5 as FCC additive for enhancing light olefins yield from catalytic cracking of VGO. *Appl. Catal. A Gen.* **2014**, *477*, 172–183.
7. Dupain, X.; Makkee, M.; Moulijn, J. A. Optimal conditions in fluid catalytic cracking: A mechanistic approach. *Appl. Catal. A Gen.* **2006**, *297*, 198–219.
8. Hollander, M. A. Den; Makkee, M.; Moulijn, J. A. Coke formation in fluid catalytic cracking studied with the microriser. *Catal. Today* **1998**, *46*, 27–35.
9. Corma, A.; González-Alfaro, V.; Orchillés, A. V. The role of pore topology on the behaviour of FCC zeolite additives. *Appl. Catal. A Gen.* **1999**, *187*, 245–254.
10. Quintana-Solórzano, R.; Rodríguez-Hernández, A.; García-de-León, R. Study of the performance of catalysts for catalytic cracking by applying a lump-based kinetic model. *Ind. Eng. Chem. Res.* **2009**, *48*, 1163–1171.
11. Moustafa, T. M.; Froment, G. F. Kinetic Modeling of Coke Formation and Deactivation in the Catalytic Cracking of Vacuum Gas Oil. *Ind. Eng. Chem. Res.* **2003**, *42*, 14–25, doi:10.1021/ie0204538.
12. Martignoni, P.; Science, E. Modeling and Simulation of FCC Riser reactors: An Heterogeneous Approach, University of Western Ontario, 1998.
13. Xiong, K.; Lu, C.; Wang, Z.; Gao, X. Quantitative correlations of cracking performance

- with physiochemical properties of FCC catalysts by a novel lump kinetic modelling method. *Fuel* **2015**, *161*, 113–119.
14. Jesus A, Atias. Tonetto, Gabriela M. de Lasa, H. Modeling Fluid Catalytic Cracking in a Novel CREC Riser Simulator: Adsorption Parameters under Reaction Conditions. *Int. J. Chem. React. Eng.* **2003**, *1*, 1–23.
 15. Quintana-solorzano, Roberto. Thybaut, Joris. Marin, Guy B. Lodeng, Rune. Holmen, A. Single-Event MicroKinetics for coke formation in catalytic cracking. *Catal. Today* **2005**, *108*, 619–629, doi:10.1016/j.cattod.2005.07.036.
 16. Du, S.; Gamliel, D. P.; Giotto, M. V; Valla, J. A.; Bollas, G. M. Coke formation of model compounds relevant to pyrolysis bio-oil over ZSM-5. *Applied Catal. A, Gen.* **2016**, *513*, 67–81, doi:10.1016/j.apcata.2015.12.022.
 17. Cerqueira, H. S.; Caeiro, G.; Costa, L.; Ribeiro, F. R. Deactivation of FCC catalysts. *J. Mol. Catal. A Chem.* **2008**, *292*, 1–13.
 18. Guisnet, M.; Magnoux, P. Coking and Deactivation of Zeolites Influence of the Pore Structure. *Appl. Catal.* **1989**, *54*, 1–27.
 19. Guisnet, M.; Magnoux, P. Organic chemistry of coke formation. *Appl. Catal. A Gen.* **2001**, *212*, 83–96.
 20. Corella, José. Bilbao, Rafael, Molina, José A. Artigas, A. Variation with Time of the Mechanism, Observable Order, and Activation Energy of the Catalyst Deactivation by Coke in the FCC Process. *Ind. Eng. Chem. Process Des. Dev.* **1985**, *24*, 625–636, doi:10.1021/i200030a018.
 21. Delattre, C.; Forissier, M.; Pitault, I.; Schweich, D.; Bernard, J. R. Improvement of the microactivity test for kinetic and deactivation studies involved in catalytic cracking. *Chem. Eng. Sci.* **2001**, *56*, 1337–1345.
 22. Shan, H.; Dong, H.; Zhang, J.; Niu, G. Experimental study of two-stage riser FCC reactions. *Fuel*. **2001**, *80*, 1179–1185.
 23. Collyer, R. Larocca, M. de Lasa, H. Modelling the Kinetics of Fast Catalytic Cracking Reactions. *Can. J. Chem. Eng.* **1989**, *67*, 955–962.
 24. Dupain, X.; Makkee, M.; Moulijn, J. A. Optimal conditions in fluid catalytic cracking : A mechanistic approach. *Appl. Catal. A Gen.* **2006**, *297*, 198–219.
 25. Pinheiro Carla. I. C, Joana L. Fernandes, Luis Domingues, Alexander J. S. Chambel,

- Ines Grace, N. M. C.; Oliveira; Cerqueira, H. S.; Fernando Ramoa Ribeiro Fluid Catalytic Cracking (FCC) Process Modeling , Simulation , and Control. *Ind. Eng. Chem. Res.* **2012**, *51*, 1–29.
26. Fernandes, J. L.; Domingues, L. H.; Pinheiro, C. I. C.; Oliveira, N. M. C.; Ramôa, F. Influence of different catalyst deactivation models in a validated simulator of an industrial UOP FCC unit with high-efficiency regenerator. *Fuel* **2012**, *97*, 97–108, doi:10.1016/j.fuel.2012.03.009.
 27. Lappas, A. A.; Iatridis, D. K.; Papapetrou, M. C.; Kopalidou, E. P.; Vasalos, I. A. Feedstock and catalyst effects in fluid catalytic cracking - Comparative yields in bench scale and pilot plant reactors. *Chem. Eng. J.* **2015**, *278*, 140–149.
 28. Bartholomew, C. H.; Argyle, M. D. Advances in Catalyst Deactivation and Regeneration. *Catalysts.* **2015**, *5*, 949–954.
 29. Jarullah, A. T.; Awad, N. A.; Mujtaba, I. M. Optimal design and operation of an industrial fluidized catalytic cracking reactor. *Fuel* **2017**, *206*, 657–674.
 30. Al-Sabawi, M.; Atias, J. A.; de Lasa, H. Kinetic modeling of catalytic cracking of gas oil feedstocks: Reaction and diffusion phenomena. *Ind. Eng. Chem. Res.* **2006**, *45*, 1583–1593.
 31. Usman, A.; Bari, M. A.; Hussain, A.; Aitani, A.; Al-khattaf, S. catalytic cracking of crude oil to light olefins and naphtha : Experimental and kinetic modeling. *Chem. Eng. Res. Des.* **2017**, *120*, 121–137.
 32. Guang- fu, Y.; Gang, W.; Jin sen, G.; Chun ming, X. Coke formation and olefins conversion in FCC naphthaolefin reformulation at low reaction temperature. *J. Fuel Chem. Technol.* **2007**, *35*, 572–577.
 33. Li, X.; Li, C.; Zhang, J.; Yang, C. Effects of Temperature and Catalyst to Oil Weight Ratio on the Catalytic Conversion of Heavy Oil to Propylene Using ZSM-5 and USY Catalysts Xiaohong. *J. Nat. Gas Chem.* **2007**, *16*, 92–99.
 34. Abul-Hamayel, M. A.; Aitani, A. M.; Saeed, M. R. Enhancement of propylene production in a downer FCC operation using a ZSM-5 additive. *Chem. Eng. Technol.* **2005**, *28*, 923–929.
 35. Sotelo-Salazar, D.; Maya-Yescas, R.; Mariaca Dominguez, E.; Rodriguez Salomon, S.; aguiler Lopez, M. Effect of hydrotreating FCC feedstock on product distribution.

- Catal. Today* **2004**, *98*, 273–280, doi:10.1016/j.cattod.2004.07.040.
36. Al-Khattaf, S.; Atias, J. A.; Jarosch, K.; de Lasa, H. Diffusion and catalytic cracking of 1,3,5 tri-iso-propyl-benzene in FCC catalysts. *Chem. Eng. Sci.* **2002**, *57*, 4909–4920.
 37. Al-khattaf, S.; Lasa, H. I. De Diffusion and Reactivity of Gas Oil in FCC Catalysts. *Can. J. Chemical Eng.* **2001**, *79*, 341–348.
 38. Javaid, R.; Urata, K.; Furukawa, S.; Komatsu, T. Factors affecting coke formation on H-ZSM-5 in naphtha cracking. *Applied Catal. A, Gen.* **2015**, *491*, 100–105, doi:10.1016/j.apcata.2014.12.002.
 39. Cheng, W-C. Rajagopalan, K. Conversion of Cyclohexene over Y-Zeolites : A Model Reaction for Hydrogen Transfer. *J. Catal.* **1989**, *358*, 354–358.
 40. Hussain, A. I.; Palani, A.; Aitani, A. M.; Shamzhy, M.; Kub, M.; Al-khattaf, S. S. Catalytic cracking of vacuum gasoil over -SVR , ITH , and MFI zeolites as FCC catalyst additives. *Fuel Process. Technol. J.* **2017**, *161*, 23–32, doi:10.1016/j.fuproc.2017.01.050.
 41. Corma, A. Planelles, J. J. S.-Mar. F. T. The Role of Different Types of Acid Site in the Cracking of Alkanes on Zeolite Catalysts. *J. Catal.* **1985**, *37*, 30–37.
 42. Al-bogami, S. A. Catalytic Conversion of Benzothiophene Over a H-ZSM5 Catalyst , Reactivity and a Kinetic Model, The University of Western Ontario, 2013.
 43. Jiménez-garcía, G.; Aguilar-lópez, R.; Maya-yescas, R. The fluidized-bed catalytic cracking unit building its future environment. *Fuel* **2011**, *90*, 3531–3541, doi:10.1016/j.fuel.2011.03.045.
 44. Corella, J. On the modeling of the kinetics of the selective deactivation of catalysts. Application to the fluidized catalytic cracking process. *Ind. Eng. Chem. Res.* **2004**, *43*, 4080–4086.
 45. Olah, George.A, Molnar, A. *Hydrocarbon Chemistry*; Second Edi.; WILEY-INTERSCIENCE, A John Wiley & sons, Inc.,: New Jersey, 2003;
 46. Greensfelder, B. S.; Voge, H. H.; Good, G. M. CATALYTIC CRACKING OF PURE Aromatics and Comparison of Hydrocarbon Classes. *Ind. Eng. Chem.* **1945**, 1168–1176, doi:10.1021/ie50432a012.
 47. Maya-Yescas, R.; Villafuerte-Macias, E. F.; Aguilar, R.; Salazar-Sotelo, D. Sulphur oxides emission during fluidised-bed catalytic cracking. *Chem. Eng. J.* **2005**, *106*, 145–

152.

48. Kraemer, D. W. Modelling Catalytic Cracking In A Novel Riser Simulator (volumes I And Ii), Western University, Digitized Theses, 1991.
49. Müller, S.; Liu, Y.; Vishnuvarthan, M.; Sun, X.; Veen, A. C. Van; Haller, G. L.; Sanchez-sanchez, M.; Lercher, J. A. Coke formation and deactivation pathways on H-ZSM-5 in the conversion of methanol to olefins. *J. Catal.* **2015**, *325*, 48–59, doi:10.1016/j.jcat.2015.02.013.
50. Arandes, Jose M. Azkoiti, Miren J. Bilbao, J. H. de L. Modelling FCC Units under Steady and Unsteady State Conditions. *Can. J. Chem. Eng.* **2000**, *78*, 111–123.
51. Bai, T.; Zhang, X.; Wang, F.; Qu, W.; Liu, X.; Duan, C. Coking behaviors and kinetics on HZSM-5 / SAPO-34 catalysts for conversion of ethanol to propylene. *J. Energy Chem.* **2016**, *25*, 545–552.
52. Marin, G. B.; Beeckman, J. W.; Froment, G. F. Rigorous Kinetic Models for Catalyst Deactivation by Coke Deposition : Application to Butene Dehydrogenation '. *J. Catal.* **1986**, *426*, 416–426.
53. Han, I.; Riggs, J. B.; Chung, C. Modeling and optimization of a fluidized catalytic cracking process under full and partial combustion modes. *Chem. Eng. Process.* **2004**, *43*, 1063–1084.
54. Gupta, R. K.; Kumar, V.; Srivastava, V. K. Modeling of Fluid Catalytic Cracking Riser Reactor: A Review. *Int. J. Chem. React. Eng.* **2010**, *8*.
55. Kemp, R. R. D.; Wojciechowski, B. W. The Kinetics of Mixed Feed Reactions. *Ind. Eng. Chem., Fundam.* **1974**, *13*, 332–335, doi:10.1021/i160052a006.
56. Wojciechowski, W. . B. The Reaction Mechanism of Catalytic Cracking : The Reaction Mechanism of Catalytic Cracking : Quantifying Activity . Selectivity . and. *Catal. Rev.* **1998**, *40*, 209–328, doi:10.1080/01614949808007110.
57. Gupta, R. K.; Kumar, V.; Srivastava, V. K. Modeling of Fluid Catalytic Cracking Riser Reactor: A Review. *Int. J. Chem. React. Eng.* **2010**, *8*.
58. Olah, G. A. The General Concept and Structure of Carbocations Based on Differentiation of Trivalent (' Classical') Carbenium Ions from Three-center Bound Penta- or Tetracoordinated(' Nonclassical'') Carbonium Ions. The Role of Carbocations in Electrophilic Reaction. *J. Am. Soc.* **1972**, *94*, 808.

59. Olah, A, G. Carbocation and Electrophilic Reactions. *Int. Ed. English* **1973**, *12*, 173–254.
60. Mariaca dominguez, Ernesto. Rodrigues Salmon, S.; Rafael, M. Y. Reactive Hydrogen Content: A Tool to Predict FCC Yields Ern. *Int. J. Chem. React. Eng.* **2003**, *1*, 1–11.
61. Al-khattaf, S.; Ali, S. A.; Aitani, A. M.; Žilková, N.; Čejka, J.; Al-khattaf, S.; Ali, S. A.; Aitani, A. M. Recent Advances in Reactions of Alkylbenzenes Over Novel Zeolites : The Effects of Zeolite Structure and Morphology Recent Advances in Reactions of Alkylbenzenes Over Novel Zeolites : The Effects of Zeolite. *Catal. Rev. Sci. Eng.* **2014**, *4940*, 333–402, doi:10.1080/01614940.2014.946846.
62. Zhang, J.; Xu, L.; Zhang, Y.; Huang, Z.; Zhang, X.; Zhang, X. Hydrogen transfer versus olefins methylation : On the formation trend of propene in the methanol-to-hydrocarbons reaction over Beta zeolites. *J. Catal.* **2018**, *368*, 248–260, doi:10.1016/j.jcat.2018.10.015.
63. Kotrel, S.; Kno, H.; Gates, B. C. The Haag – Dessau mechanism of protolytic cracking of alkanes. *Microporous Mesoporous Mater.* **2000**, *36*, 11–20.
64. Rahimi, N.; Karimzadeh, R. Catalytic cracking of hydrocarbons over modified ZSM-5 zeolites to produce light olefins : A review. *Applied Catal. A, Gen.* **2011**, *398*, 1–17, doi:10.1016/j.apcata.2011.03.009.
65. Corma, A. Orchilles, A. V. Current views on the mechanism of catalytic cracking A. *Microporous Mesoporous Mater.* **2000**, *36*, 21–30.
66. Sanchez, Astrid, Ramirez, s, Silva, W. Espinal, J. F. Prediction of 1,3,5-triisopropylbenzene cracking pattern through thermodynamic evaluation of products and protonation intermediates. *Mol. catalysis* **2019**, *466*, 13–18.
67. Haw, J. F.; Nicholas, J. B.; Xu, T.; Beck, L. W.; Ferguson, D. B. Physical Organic Chemistry of Solid Acids : Lessons from in Situ NMR and Theoretical Chemistry. *Acc. Chem. Res.* **1996**, *29*, doi:10.1021/ar950105k.
68. Farag, H. I. Catalytic Cracking Of Hydrocarbons With Novel Metal Traps, The University of Western Ontario, 1993.
69. Hussain, A. I.; Aitani, A. M.; Kubů, M.; Čejka, J.; Al-Khattaf, S. Catalytic cracking of Arabian Light VGO over novel zeolites as FCC catalyst additives for maximizing propylene yield. *Fuel* **2016**, *167*, 226–239.

70. García-Dopico, M.; García, A.; Santos García, A. Modelling coke formation and deactivation in a FCCU. *Appl. Catal. A Gen.* **2006**, *303*, 245–250, doi:10.1016/j.apcata.2006.02.026.
71. Francis Omotola, O.; Paul, O. C. Prediction of the Optimal Reaction Temperature of the Riser of an Industrial Fluid Catalytic Cracking (FCC) Unit. *Chem. Process Eng. Res.* **2015**, *30*, 34–46.
72. Ino Takashi, A.-K. S. Effect of unit cell size on the activity and coke selectivity of FCC catalysts. *Appl. Catal. A Gen.* **1996**, *142*, 5–17.
73. Al-khattaf, S.; Saeed, M. R.; Aitani, A.; Klein, M. T. Catalytic cracking of light crude oil to Light Olefins and naphtha over E-Cat and MFI : Microactivity Test versus Advanced cracking evaluation and the effect of high reaction temperature. *Energy & Fuels* **2018**, *32*, 6189–6199.
74. Wallensteln, D. Harding, R. Witzler, J. Zhao, X. Rational assessment of FCC catalyst performance by utilization of micro-activity testing. *Appl. Catal. A Gen.* **1998**, *167*, 141–155.
75. Du, Y.; Zhao, H.; Ma, A.; Yang, C. Equivalent Reactor Network Model for the Modeling of Fluid Catalytic Cracking Riser Reactor. *Ind. Eng. Chem. Res* **2015**, *54*, 8732–8742, doi:10.1021/acs.iecr.5b02109.
76. Tonetto, G.; Atias, J.; Lasa, H. De FCC catalysts with different zeolite crystallite sizes : acidity , structural properties and reactivity. *Appl. Catal. A Gen.* **2004**, *270*, 9–25, doi:10.1016/j.apcata.2004.03.042.
77. Jiménez-García, G.; Quintana-Solórzano, R.; Maya-Yescas, R. Improving accuracy in the estimation of kinetic frequency factors from laboratory data to model industrial catalytic cracking risers. *Ind. Eng. Chem. Res.* **2011**, *50*, 2736–2745.
78. Wallenstein, D.; Alkemade, U. Modelling of selectivity data obtained from microactivity testing of FCC catalysts. *Appl. Catal. A Gen.* **1996**, *137*, 37–54.
79. Jiménez-García, G.; de Lasa, H.; Quintana-Solórzano, R.; Maya-Yescas, R. Catalyst activity decay due to pore blockage during catalytic cracking of hydrocarbons. *Fuel* **2013**, *110*, 89–98.
80. Atias, J. A.; de Lasa, H. Adsorption, diffusion, and reaction phenomena on FCC catalysts in the CREC riser simulator. *Ind. Eng. Chem. Res.* **2004**, *43*, 4709–4720.

81. Al-Khattaf, S.; de Lasa, H. Catalytic cracking of cumene in a riser simulator: A catalyst activity decay model. *Ind. Eng. Chem. Res.* **2001**, *40*, 5398–5404.
82. Spretz, R.; Sedran, U. Operation of FCC with mixtures of regenerated and deactivated catalyst. *Appl. Catal. A Gen.* **2001**, *215*, 199–209.
83. de Lasa, H. Riser Simulator. *United States Pat.* **1992**, U.S. Patent No. 5,102,628.
84. Passamonti, F. J.; Puente, G. de La; Sedran, U. Comparison between MAT flow fixed bed and batch fluidized bed reactors in the evaluation of FCC catalysts. 2. Naphtha composition. *Energy and Fuels* **2009**, *23*, 3510–3516.
85. Wang, B. Zeolite Deactivation During Hydrocarbon Reactions: Characterisation of Coke Precursors and Acidity, Product Distribution, University College London, 2007.
86. Torrealba, Y. Y. A. Sulfur Species Selective Adsorption Using A New Offretite Based Additive, The University of Western Ontario, 2016.
87. John, Y. M.; Patel, R.; Mujtaba, I. M. Modelling and simulation of an industrial riser in fluid catalytic cracking process. *Comput. Chem. Eng. j* **2017**, *106*, 730–743.
88. Ng, S.; Yang, H.; Wang, J.; Zhu, Y.; Fairbridge, C. Comparison of Catalytic Cracking Performance between Riser Reactor and Microactivity Test (MAT) Unit. *Energy & Fuels* **2001**, *96*, 783–785, doi:10.1021/ef000115o.
89. Sadrameli, S. M. Thermal / catalytic cracking of liquid hydrocarbons for the production of olefins : A state-of-the-art review II : Catalytic cracking review. *Fuel* **2016**, *173*, 285–297, doi:10.1016/j.fuel.2016.01.047.
90. Chen Liew, S. Impacts of Vanadium and Coke Deposition on CO₂ Gasification of Nickel Catalysts Supported on Activated Carbon from Petroleum Coke, UNIVERSITY OF CALGARY Impacts, 2014.
91. Jimenez -Garcia., G.; Aguilar-lopez, R.; Quintana-solorzano, R.; Maya-yescas, R. Modelling Catalyst Deactivation by External Coke Deposition during Fluid Catalytic Cracking. *Int. J. Chem. React. Eng.* **2010**, *8*.
92. Al-Khattaf, S. and de Lasa, H. Activity and Selectivity of Fluidized Catalytic Cracking Catalysts in a Riser Simulator : The Role of Y-Zeolite Crystal Size. *Ind. Eng. Chem. Res* **1999**, 1350–1356, doi:10.1021/ie980433z.
93. Errazu, A. F.; de Lasa, H.; SARTZ, F. A Fluidized Bed Catalytic Cracking, Regenerator Model. *Can. J. Chem. Eng.* **1979**, *57*, 191–197.

94. Moulijn, J. A.; Diepen, A. E. Van; Kapteijn, F. Catalyst deactivation : is it predictable ? What to do ? *Appl. Catal. A Gen.* **2001**, *212*, 3–16.
95. Cerqueira, H. S.; Sievers, C.; Joly, G.; Magnoux, P.; Lercher, J. A. Multitechnique Characterization of Coke Produced during Commercial Resid FCC Operation. *Ind. Eng. Chem. Res* **2005**, *44*, 2069–2077.
96. Argyle, M. D.; Bartholomew, C. H. Heterogeneous Catalyst Deactivation and Regeneration: A Review. *Catalysis* **2015**, *5*, 145–269, doi:10.3390/catal5010145.
97. Bazyari, A.; Khodadadi, A. A.; Hosseinpour, N.; Mortazavi, Y. Effects of steaming-made changes in physicochemical properties of Y-zeolite on cracking of bulky 1, 3, 5-triisopropylbenzene and coke formation. *Fuel Process. Technol.* **2009**, *90*, 1226–1233, doi:10.1016/j.fuproc.2009.06.002.
98. Mathieu, Y.; Corma, A.; Echard, M.; Bories, M. Single and combined Fluidized Catalytic Cracking (FCC) catalyst deactivation by iron and calcium metal–organic contaminants. *Appl. Catal. A Gen.* **2014**, *469*, 451–465.
99. Etim, U. J.; Bai, P.; Liu, X.; Subhan, F.; Ullah, R.; Yan, Z. Vanadium and nickel deposition on FCC catalyst: Influence of residual catalyst acidity on catalytic products. *Microporous Mesoporous Mater.* **2019**, *273*, 276–285, doi:10.1016/j.micromeso.2018.07.011.
100. Escobar, A. S.; Pereira, M. M.; Cerqueira, H. S. Effect of iron and calcium over USY coke formation. *Appl. Catal. A Gen.* **2008**, *339*, 61–67, doi:10.1016/j.apcata.2008.01.008.
101. Du, X.; Zhang, H.; Cao, G.; Wang, L.; Zhang, C.; Gao, X. Effects of La₂O₃, CeO₂ and LaPO₄ introduction on vanadium tolerance of USY zeolites. *Microporous Mesoporous Mater.* **2015**, *206*, 17–22, doi:10.1016/j.micromeso.2014.12.010.
102. Gulsnet, M. , Magnoux, P. Deactivation by coking of zeolite catalysts . Prevention of deactivation . Optimal conditions for regeneration. *Catal. Today* **1997**, *36*, 477–483.
103. Brillis, A. A.; Manos, G. Coke Formation during Catalytic Cracking of C₈ Aliphatic Hydrocarbons over Ultrastable Y Zeolite. *Ind. Eng. Chem. Res* **2003**, *42*, 2292–2298, doi:10.1021/ie020460w.
104. Kemp, R. R.; Wojciechowski, B. The Kinetics of Mixed Feed Reactions. *Ind. Eng. Chem., Fundam.* **1974**, *13*, doi:10.1021/i160052a006.

105. Voltz, Sterling E. Nace, Donald M. Weekman, V. W. Application of a Kinetic Model for Catalytic Cracking Some Correlations of Rate Constants. *Ind. Eng. Chem. Process Des. Dev.* **1971**, *507*, 1969–1972, doi:10.1021/i260040a019.
106. Froment, G. F.; Bischoff, K. B. Kinetic data and product distributions from fixed bed catalytic reactors subject to catalyst fouling. *Chem. Eng. Sci.* **1962**, *17*.
107. Voorhies, Alexis, J. Carbon Formation in Catalytic Cracking. *Ind. Eng. Chem.* **1945**, *37*, 318–322, doi:10.1021/ie50424a010.
108. Voltz, Sterling E. Nace, Donald M. Weekman, V. W. Application of a Kinetic Model for Catalytic Cracking. *Ind. Eng. Chem. Process Des. Dev.* **1971**, *10*, 1969–1972, doi:10.1021/i260040a019.
109. Yates, J. G. *Fundamentals of Fluidized Bed Chemical processes.*; Butterworth Monographs in Chemical Engineering: London, England, 1982, 121.
110. Meng, X.; Xu, C.; Gao, J. Coking behavior and catalyst deactivation for catalytic pyrolysis of heavy oil. *Fuel* **2007**, *86*, 1720–1726, doi:10.1016/j.fuel.2006.12.023.
111. Al-khattaf, S.; de Lasa, H. The role of diffusion in alkyl-benzenes catalytic cracking. *Appl. Catal. A Gen.* **2002**, *226*, 139–153.
112. Zaman, S. F.; Loughlin, K. F.; Al-khattaf, S. A. Kinetics of Desorption of 1,3-Diisopropylbenzene and 1,3,5 Triisopropylbenzene. 2. Diffusion in FCC catalyst Particles by Zero Length Column Method. *Ind. Eng. Chem. Res* **2015**, *54*, 4572–4580, doi:10.1021/ie504963e.
113. Mi, S.; Wei, T.; Sun, J.; Liu, P.; Li, X.; Zheng, Q.; Gong, K.; Liu, X. Catalytic function of boron to creating interconnected mesoporosity in microporous Y zeolites and its high performance in hydrocarbon cracking. *J. Catal.* **2017**, *347*, 116–126.
114. Qin, Z.; Shen, B.; Gao, X.; Lin, F.; Wang, B.; Xu, C. Mesoporous y zeolite with homogeneous aluminum distribution obtained by sequential desilication-dealumination and its performance in the catalytic cracking of cumene and 1,3,5-triisopropylbenzene. *J. Catal.* **2011**, *278*, 266–275.
115. Varshney, P.; Kunzru, D.; Gupta, S. K. A multigrain catalyst model for unifunctional multicomponent catalysts. *Chem. Eng. Res. Des.* **2010**, *88*, 455–464.
116. Alkhattaf, S. Odedario, T. B. R. . Kinetic and Catalytic Performance of a Bi-Porous Composite Material in Catalytic Cracking and Isomerisation Reactions. *Can. J. Chem.*

- Eng.* **2013**, *91*, 607–617.
117. Etim, U. J.; Xu, B.; Bai, P.; Ullah, R.; Subhan, F.; Yan, Z. Role of nickel on vanadium poisoned FCC catalyst : A study of physiochemical properties. *J. Energy Chem.* **2016**, *25*, 667–676.
 118. Corella, José. Bilbao, Rafael. Molina, J. A. A. A. Variation with Time of the Mechanism, Observable Order, and Activation Energy of the Catalyst Deactivation by Coke in the FCC Process. *Ind. Eng. Chem. Process Des. Dev.* **1985**, *24*, 625–636, doi:10.1021/i200030a018.
 119. Wang, Huai-Ping. Wang, F.-Z. W.-R. W. Effect of vanadium poisoning and vanadium passivation on the structure and properties of REHY Zeolite and FCC catalyst 623–628.
 120. Wang, B.; Han, C.; Zhang, Q.; Li, C.; Yang, C.; Shan, H. Studies on the Preliminary Cracking of Heavy Oils : The Effect of Matrix Acidity and a Proposal of a New Reaction Route. *Energy & Fuels* **2015**, *29*, 5701–5713.
 121. Sahu, R.; Song, B.; Pyo, Y.; Wee, C. Upgrading of vacuum residue in batch type reactor using Ni – Mo supported on goethite catalyst. *J. Ind. Eng. Chem.* **2016**, *35*, 115–122, doi:10.1016/j.jiec.2015.12.017.
 122. Gueudré, L.; Thegarid, N.; Burel, L.; Jouguet, B.; Meunier, F.; Schuurman, Y.; Mirodatos, C. Coke chemistry under vacuum gasoil / bio-oil FCC co-processing conditions. *Catal. Today* **2015**, *257*, 200–212.
 123. White, M. G. *Heterogeneous Catalysis*; Prentice Hall: New Jersey, .;
 124. Quddus, M. R. A Novel Mixed Metallic Oxygen Carrier for Chemical Looping Combustion : Preparation , Characterization & Kinetic Modeling, University of Western Ontario, 2013.
 125. Aponte, Y.; Che-galicia, G.; Lasa, H. De A fluidizable Zn-offretite for selective thiophenic species adsorption . Additive performance under FCC conditions. *Fuel* **2016**, *186*, 222–234, doi:10.1016/j.fuel.2016.08.020.
 126. Gianetto, A. Novel Cracking Catalyst for the Production of Reformulated Gasolines, University of Western Ontario, 1993.
 127. Bauer, F.; Karge, H. G. Characterization of Coke on Zeolites. *Mol Sieves* **2007**, 249–364, doi:DOI 10.1007/3829_005.
 128. Epelde, E.; Ibañez, M.; Aguayo, A. T.; Gayubo, A. G.; Bilbao, J.; Castaño, P.

Differences among the deactivation pathway of HZSM-5 zeolite and SAPO-34 in the transformation of ethylene or 1-butene to propylene. *Microporous Mesoporous Mater.* **2014**, *195*, 284–293, doi:10.1016/j.micromeso.2014.04.040.

129. Jiménez-garcía, G.; de Lasa, H.; Maya-yescas, R. Simultaneous estimation of kinetics and catalysts activity during cracking of 1, 3, 5-tri-isopropyl benzene on FCC catalyst. *Catal. Today* **2014**, *222*, 178–185.
130. Gianetto, A.; Farag, H. I.; Blasetti, A. P.; de Lasa, H. Fluid Catalytic Cracking Catalyst for Reformulated Gasolines . Kinetic Modeling. *Ind. Eng. Chem. Res.* **1994**, *33*, 3053–3062.

Appendices

Appendix A: – Mass Balance closure

This appendix reports the calculation method for mass balance closure. This method was consistently applied to all the experimental runs of this report.

Data were obtained via FID chromatographic peak areas, which involved all chemical species fed to the reactor (TIPB) and evacuated from the riser. For instance, DIPB, Cumen, Benzene and propylene. It has to be mentioned that the mass balance closures were in the range ± 2 .

The mass balance closure was calculated as:

$$MB_C = \frac{m_{out}}{m_{in}} * 100 \quad (A.1)$$

Where

MB_C = Mass balance closure, wt/wt %

m_{in} = total mass of reactants injected, g (total amount of reactants injected was determined from the difference between the mass of syringe prior and after the TIPB was being injected)

m_{out} = total mass of reactants produced, g

$$m_{out} = Np_r * Mw_{ave} + M_{coked} \quad (A.2)$$

$$Np_r = \frac{(P_{fr} - P_{ir}) V_r}{RT_r} \quad (A.3)$$

Where

Np_r = total moles of product in the reactor, mole

Mw_i = average molecular weight of the product mixture, was calculated by using an individual specie molecular weight and weight fraction as follow:

$$Mw_{ave} = \frac{1}{\sum \frac{w_i}{Mw_i}} \quad (A.4)$$

P_{fr} = final reactor pressure, psia

P_{ir} = initial reactor pressure, psia (Both pressures were taken from pressure profile)

R = Ideal gas constant, 1205.91 cm³psia/g_{mole}K

T_r = Reactor temperature, K

V_r = volume of the reactor, 55.06 cm³

M_{coked} Was measured by TOC equipment for each reaction run.

Table A.1. Reports a Typical Mass Balance Closure for the Catalytic Cracking of 1,3,5, TIPB at C/O=5, 550°C and 5s reaction time.

C/O	$m_{ACT.}$	$m_{INJ.}$	P_{fr}	P_{ir}	T_r	M_{coked}	V_r	M_{wave}	N_{pr}	m_{out}	MB_C
	g	g	psia	psia	K	g	cm ³	g/mole	moles	g	%wt/wt
5	0.2	0.199	34.55	14.7	823	0.00024	55.06	177.489	0.00110	0.195	98.097

One should mention that for all experiments mass balance closure calculations were in the 95%-98% range.

Appendix B – Coke -on Catalyst Formed $q_c (g_{coke} \setminus g_{cat})$

Figure B1 and B2 report coke formed per gram of CAT-A at various C/O ratio (coke-on- catalyst) at different reaction temperatures 530°C, 510°C, and fixed reaction time at 7s respectively, showing a consistent trend of increase coke-on-catalyst formed with augmenting reaction time and C/O ratio.

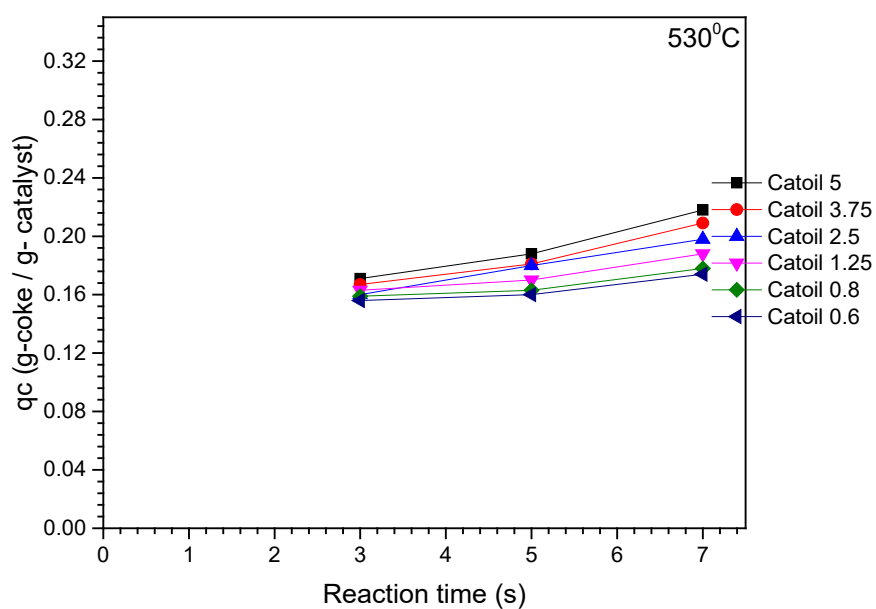


Figure B1 reports at a 530°C the effect of reaction time on the amount of coke formed per gram of catalyst at various C/O ratios.

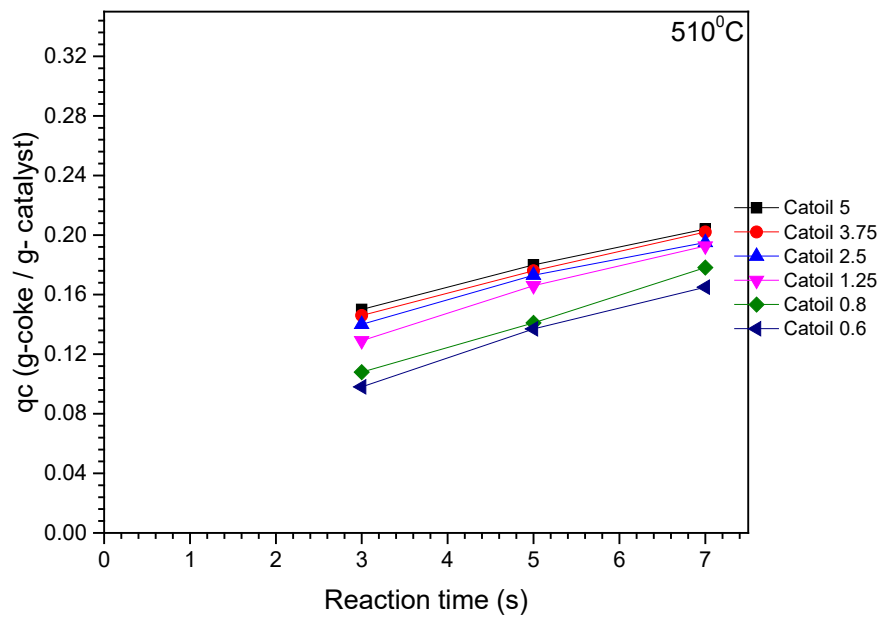


Figure B2 reports at a 510°C the effect of reaction time on the amount of coke formed per gram of catalyst at various C/O ratios.

Appendix C - Catalyst Characterization

C1: X- Ray Diffraction

Figure C1. Reports XRD Diffractograms for a CAT-B Sample mixed with pure Silicon. Characteristic bands for silicon are shown at 28, 47 and 56 degrees in the 2θ scale.

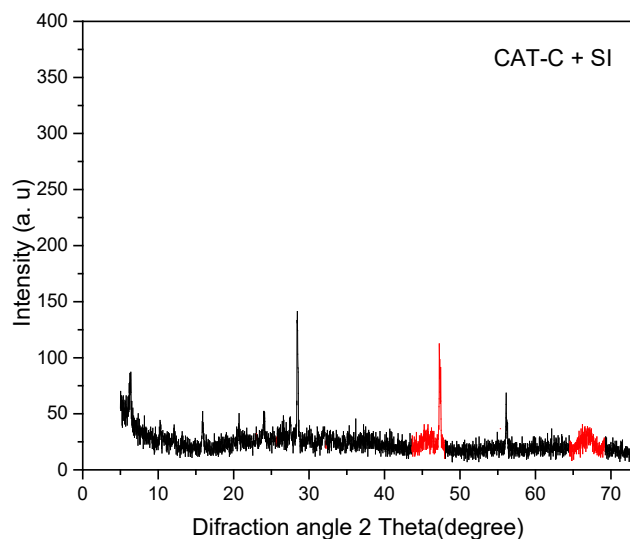


Figure C1. XRD Diffractograms for a CAT-C Sample of the Present Study Mixed with pure Silicon. Characteristic bands for silicon are shown at 28, 47 and 56 degrees in the 2θ scale.

C2: X-Ray Fluorescence (XRF) Analysis

All the catalysts studied are of the equilibrium type, which means that they were involved in FCC refinery usage include steaming. It is expected that such an FCC sample may contain various metal contaminants, including nickel and vanadium. Metals may potentially reduce the density and strength of acid sites affecting catalyst activity. Table C2 summarizes the observed metal content in the catalyst samples studied.

Table C2: Metal Content of Different Catalysts

Catalyst	NiO (ppm)	V ₂ O ₅ (ppm)	Fe (ppm)	Ca (ppm)
CAT-A	1880	7180	12700	1200
CAT-B	2030	3730	7200	1100
CAT-C	6320	9700	7000	3000

C3: NH₃-TPD (Temperature Programmed Desorption)

Figure C3 reports NH₃-TPD analyses for six CAT-C samples at different C/O ratios.

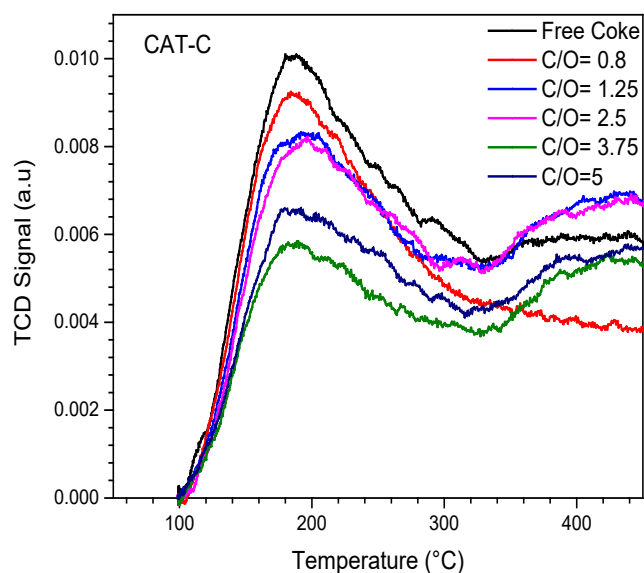


Figure C3. NH₃-TPD Analyses for CAT-C. Notes: Continuous black line: FCC catalyst free of coke; continuous red line: C/O= 0.8; continuous blue line: C/O=1.25; continuous violet line: C/O=2.5; continuous green line: C/O=5; continuous blue line: experiment baseline.

Samples with coke were analyzed following catalytic cracking runs at 550°C and 7 s.

C4: N₂ Adsorption-Desorption Isotherms

Figure C4.1 and Table C4.2 report the N₂ Adsorption-Desorption Isotherms for CAT-C and determined catalyst specific surface area (SSA) and catalyst pore volume (PV), respectively.

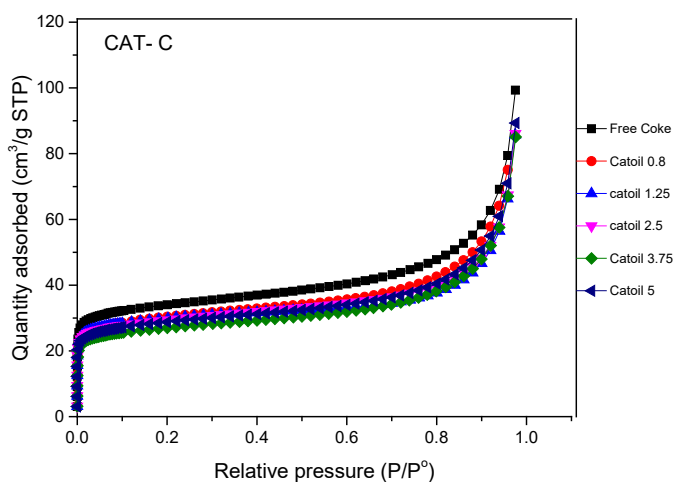


Figure C4.1: BET-Nitrogen Adsorption Plot. N₂ Adsorption-Desorption Isotherms Obtained from Different Samples of CAT-C after a Run at 550°C and 7 s Contact Time.

Table C4.2. Specific Surface Areas [SSA] (m²/g) and Pore Volumes [PV] (cm³/g) for *CAT-B*. Mesopore Volumes (cm³/g) for *CAT-B* were determined following catalytic cracking runs at 550°C and 7 s, using different C/O ratios. SD on repeats: +/- 3 m²/g.

CAT-C Catalyst Samples						
	Free Coke	C/O=0.6	C/O=0.8	C/O=1.25	C/O=3.75	C/O=3.75
BET (SSA)	118.5	97.8	91.9	90.2	86	92.9
Pore Volume (PV)	0.196	0.136	0.137	0.135	0.128	0.131
Macropores Volume	0.142	0.0898	0.0935	0.0930	0.0868	0.0870
Micropores Volume	0.0540	0.0463	0.0439	0.0426	0.0412	0.0440

Appendix D- Product Selectivity

Figure D1 describes the selectivity changes of various dealkylation products as a function of the 1,3,5- TIPB conversion.

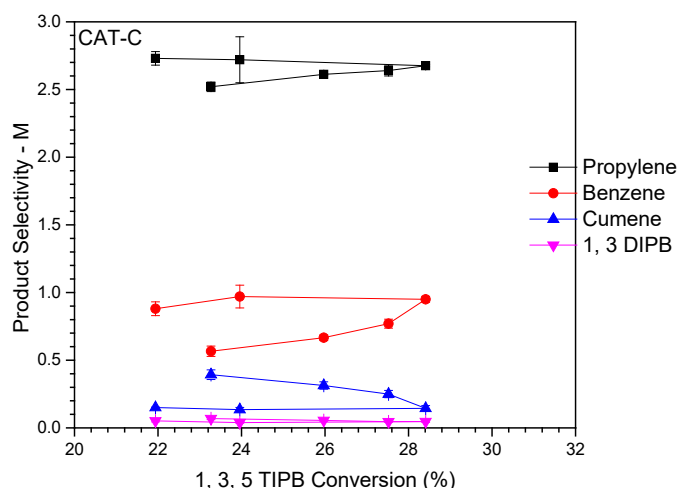


Figure D1. Effect of C/O on the Product Selectivity Using 1,3,5-TIPB and CAT-C. The temperature and contact time were kept constant at 550°C and 7s, respectively. Notes: Reported data and standard deviations (vertical bars) represent average values from at least 4-7 repeat runs.

Appendix E - 1,3,5-TIPB Conversion Changes with Reaction Time at Various C/O Ratios.

Figure E1 and E2 describes the observed 1,3,5-TIPB conversion with various C/O ratios and contact time 3, 5, and 7s at fixed reaction temperature 510 °C and 530 °C as described respectively in follows:

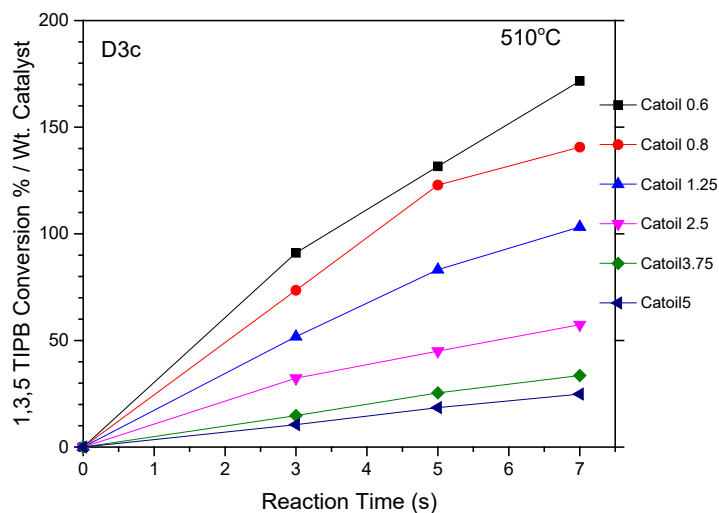


Figure E1. Changes of TIPB Conversion with Reaction Time at 510°C for Different C/O Ratios. Reported data represent average values for at least 5 repeat runs.

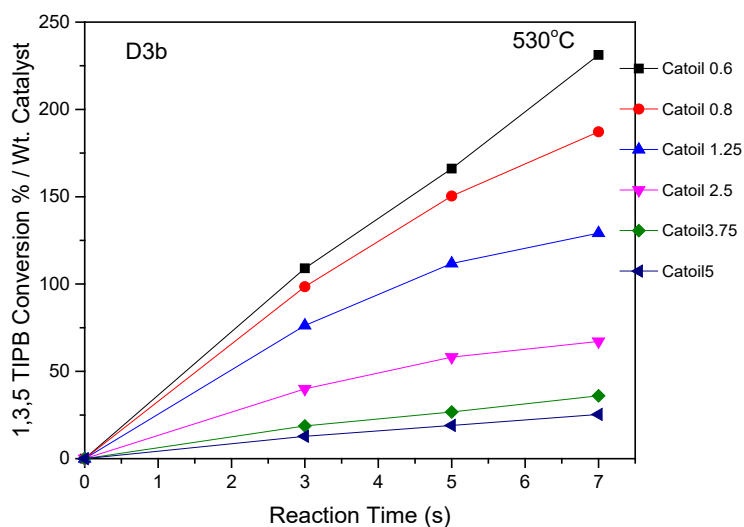


Figure E2. Changes of TIPB Conversion with Reaction Time at 530°C for Different C/O Ratios. Reported data represent average values for at least 5 repeat runs.

Appendix F- predicted chemical species concentrations

Figure F1 and F2 report the predicted chemical species concentrations and compares them with the observed concentrations taking place within the 3-7s reaction times and 0.6-5 C/O range.

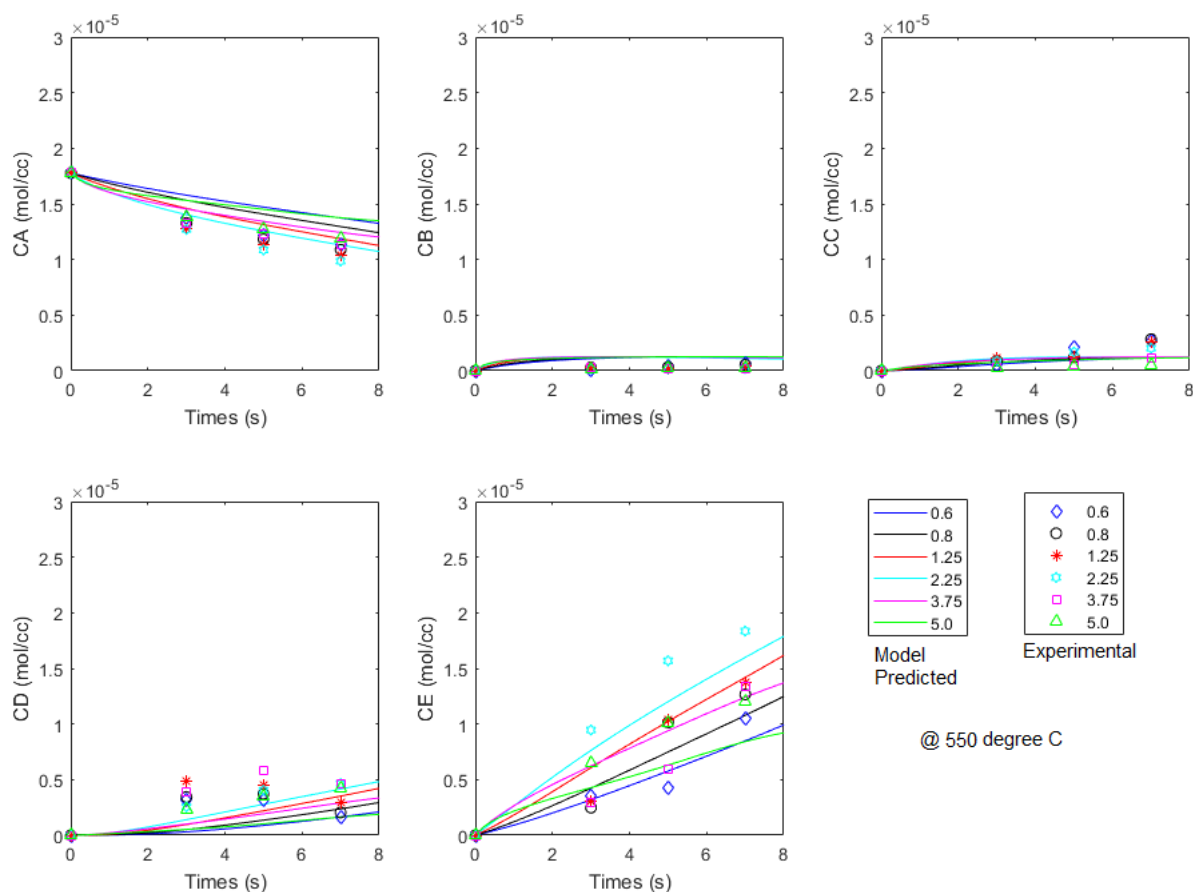


Figure F1: Comparison of Experimental and Model Predicted Chemical Species Concentrations during the 1,3,5-TIPB Catalytic. Operating Conditions: Contact times: 3-7s, C/O= 0.6-5, Temperature: 530 °C: Data: 270 average data points including at least 3-5 repeats.

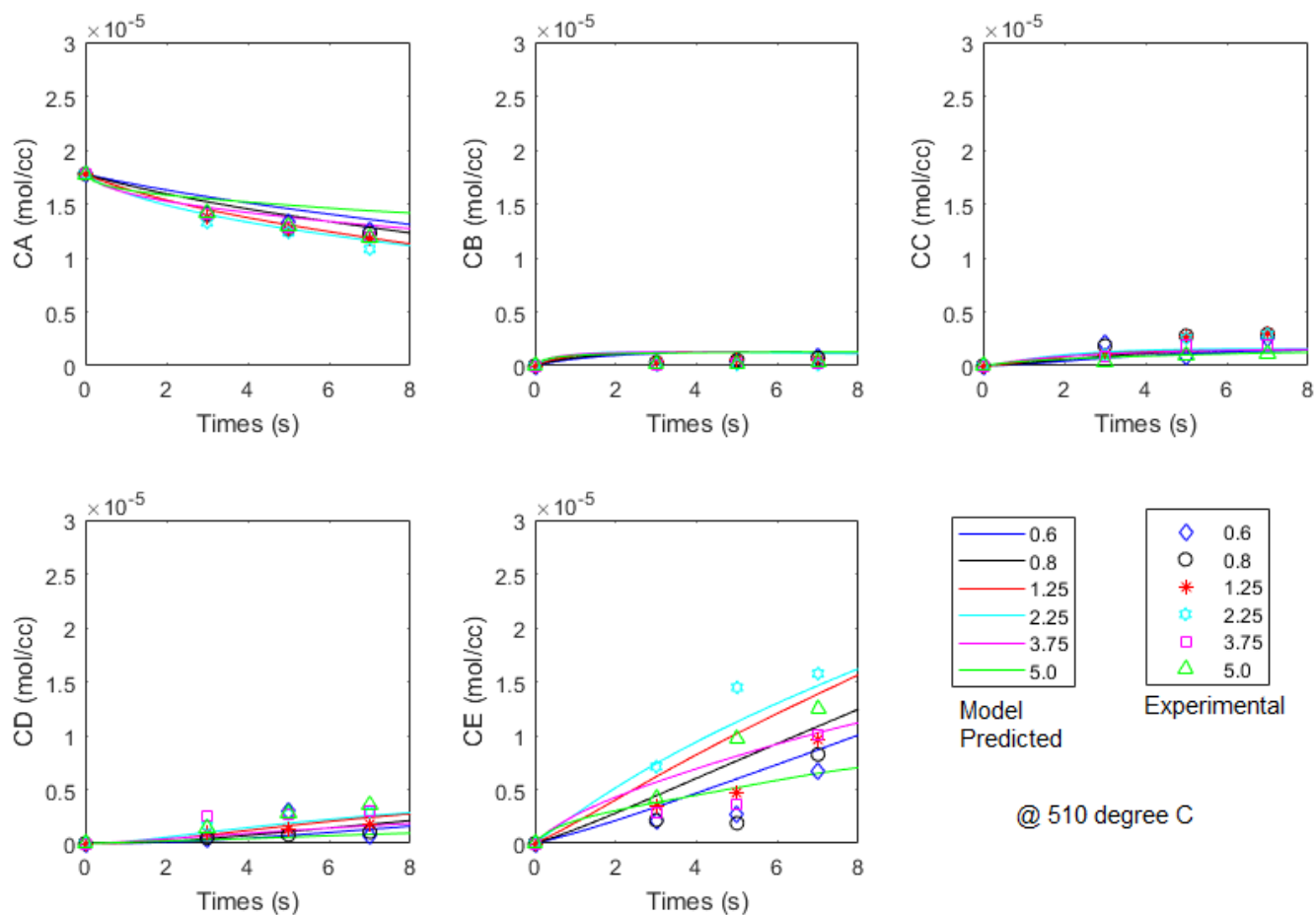


Figure F2: Comparison of Experimental and Model Predicted Chemical Species Concentrations during the 1,3,5-TIPB Catalytic. Operating Conditions: Contact times: 3-7s, C/O= 0.6-5, Temperature: 510 °C: Data: 270 average data points including at least 3-5 repeats.

1 Curriculum Vitae

Name: Abdualkaber Alkhlel

Post-secondary University of Sirt
Libya
1996-2001 B.Sc. in Chemical Engineering

The University of UKM.
Malaysia
2006-2008 M.E.Sc. in Chemical and Biochemical Engineering.

The University of Western Ontario
London, Ontario, Canada
2014-2019 Ph.D. in Chemical and Biochemical Engineering

Honors and Awards: Libyan Government Technical Scholarship 2013-2019

Related Work Experience the University of Western Ontario, London, Ontario.
Teaching Assistant in the Chemical and Biochemical Engineering Department
2015-2019.
Delivered lectures, and conducted tutorials
September 2009 – August 2013
Assistant lecture at Sebha University, Libya.

JOURNAL PUBLICATIONS AND CONFERENCES ATTENDED

- I. Conference Presentation 1: A. Alkhlel, H. de Lasa, “Catalytic Cracking of Hydrocarbons in a CREC Riser Simulator Using a Y-Zeolite Based Catalyst. Assessing the Catalyst/Oil(C/O) Ratio Effect”, CSCHE Conference Toronto, October 29, 2018.

- II. Manuscript 1: S. Lopez-Zamora, A. Alkhlel, H. de Lasa. Monitoring the progress of catalytic cracking for model compounds in the mid-infrared (MIR) 3200–2800cm⁻¹ range. *Chemical Engineering Science* 192 (2018) 788–802. <https://doi.org/10.1016/j.ces.2018.08.021>

- III. Manuscript 2: A. Alkhlel, H. de Lasa, “Catalytic Cracking of Hydrocarbons in a CREC Riser Simulator Using a Y-Zeolite Based Catalyst. Assessing the Catalyst/Oil(C/O) Ratio Effect”. *Industrial & Engineering Chemistry Research*. 2018, 57, 41, 13627-13638. <https://doi.org/10.1021/acs.iecr.8b02427>

- IV. Manuscript 3: Abdulkaber Alkhlel, Hugo de Lasa, “Catalyst/Feedstock Ratio Effect on FCC Using Different Catalysts Samples”. *Catalysts* 2019, 9(6), 542; <https://doi.org/10.3390/catal9060542>